**Advanced Control and Energy Management Schemes for Power Grids with High Proliferation of Renewables and Electric Vehicles**

by Bo Wang

B.S. in Automation, May 2013, Jilin University
M.S. in Electrical Power and Energy, May 2015, The George Washington University

A Dissertation submitted to

The Faculty of
The School of Engineering and Applied Science
of The George Washington University
in partial satisfaction of the requirements
for the degree of Doctor of Philosophy

August 31, 2020

Dissertation directed by

Payman Dehghanian
Assistant Professor of Engineering and Applied Science

The School of Engineering and Applied Science of The George Washington University certifies that Bo Wang has passed the Final Examination for the degree of Doctor of Philosophy as of May 11, 2020. This is the final and approved form of the dissertation.

**Advanced Control and Energy Management Schemes for Power Grids with High Proliferation of Renewables and Electric Vehicles**

Bo Wang

Dissertation Research Committee:

Payman Dehghanian, Assistant Professor of Engineering and Applied Science, Dissertation Director

Robert Harrington, Professor of Engineering and Applied Science, Committee Member

Milos Doroslovacki, Associate Professor of Engineering and Applied Science, Committee Member

Gina Adam, Assistant Professor of Engineering and Applied Science, Committee Member

Shahrokh Ahmadi, Teaching Professor of Engineering and Applied Science, Committee Member

**Acknowledgments**

First and foremost, I would like to express my sincere gratitude to my advisor Prof. Payman Dehghanian for the continuous support of my Ph.D study and related research, for his patience, motivation, and immense knowledge. His insight and wisdom has made remarkable contributions to our publications and writing of this dissertation. I could not have imagined having a better advisor and mentor for my Ph.D study.

Many thanks to my committee members, Prof. Robert Harrington, Prof. Milos Doroslovacki, Prof. Gina Adam and Prof. Shahrokh Ahmadi for their encouragement, great efforts and valuable feedback on my research. I would also like to thank Dr. Dongbo Zhao at Argonne National Laboratory and Jorge Camacho at the Public Service Commission of the District of Columbia for their support and guidance in my research internship projects, their valuable time, insightful comments on my Ph.D. study and research. My sincere thanks also goes to Prof. Amir Etemadi, who provided me the stimulating discussions and precious suggestions on my work. I also want to thank my colleagues and friends in Smart Grid Laboratory at the George Washington University , and all the friends I met during my two internships. All of our discussions about study and life are the most precious memories to me.

Last but not the least, I would like to thank my family: my parents, my brother and my girlfriend for supporting me spiritually throughout writing this dissertation and my life in general. I could not have achieved my goal without their love and sacrifices. They are always my strong backing.

## Abstract

### Advanced Control and Energy Management Schemes for Power Grids with High Proliferation of Renewables and Electric Vehicles

A power grid transformation is needed to integrate large-scale variable renewable energies (VREs) and electric vehicles (EVs), in order to address the environmental concerns. Organizations and governments have set ambitious targets for the integration of these emerging resources into the modern power grids to build, plan, and operate a clean and sustainable energy landscape. This dissertation proposes an integrated control and energy management scheme for power grids with massive integration of VREs and EVs.

We firstly propose new EV charging station (EVCS) control scheme and a holistic approach to evaluate the electrical safety of the large-scale EVCSs. Our approach mainly focuses on several topics on the operational safety of EVCS primarily concerning: (1) the facility degradation which could potentially result in a compromised EVSE reliability performance and EVCS protection failure; (2) the cyber-attack challenges when the smart charging and the communication between EVCSs and electric utilities are enabled; and (3) the potential mismatch between the renewable output and EVCS demand, which could trigger the system stability challenges during normal operation and inability to supply the critical EV loads during outages.

A two-stage energy management system (EMS) for power grids is proposed. The first stage economic dispatch determines the optimal operating points of charging stations and battery swapping stations (BSS) for EVs under plug-in and battery swapping modes, respectively. The proposed stochastic model predictive control (SMPC) problem in this stage is characterized through a chance-constrained optimization formulation that can effectively capture the system and the forecast uncertainties. A distributed algorithm, the alternating direction method of multipliers (ADMM), is applied to accelerate the optimization computation through parallel computing. The second stage is aimed in coordinating the EV charging mechanisms to continuously follow the first-stage solutions, i.e., the target operating points,

and meeting the EV customers' charging demands captured via the Advanced Metering Infrastructure (AMI). The proposed solution offers a holistic control strategy for large-scale centralized power grids in which the aggregated individual parameters are predictable and the system dynamics do not vary sharply within a short time-interval.

Based on this new control and energy management schemes, we propose a new data-driven approach for EV charging load modeling. We first introduce a mathematical model that characterizes the flexibility of EV charging demand. Advanced simulation procedures are then proposed to identify the parameters of different EV load models and simulate EV charging demand under different electricity market realizations. The proposed EV load modeling approach can simulate different EV operation schedules, charging levels, and customer participation as a benchmark system.

Eventually, a restoration approach for EVCSs is also proposed to utilize the flexibility of the aggregated EV loads to enhance the power grid resilience against extremes. A framework is also introduced to offer adaptive operation strategies for the EVCS operators. As a result, the system can effectively manage the EVCS under different penetration levels of EVs, considering both normal operating conditions and restoration processes during interruptions and emergencies. The proposed adaptive operation mechanism could bring significant advantages to the operation and control of smart power grids with high penetration of renewables and EVs when facing different operating conditions.

## Table of Contents

## List of Figures

## List of Tables

## Nomenclature

### A. Indices

| | |
|---|---|
| $i$ | Index for state variables (1,...,$n$). |
| $j$ | Index for EV numbers. |
| $m$ | Index for stochastic scenarios (1,...,$M$). |
| $k$ | Index for time-steps (1,...,$K$). |
| $s$ | Index for EV groups (1,...,$S$). |
| $t$ | Index for time. |

### B. Parameters

| | |
|---|---|
| $\alpha_c, \alpha_d$ | Charge/discharge efficiency of the battery. |
| $\alpha_r$ | Ratio of regulation capacity to regulation limits. |
| $\beta_p$ | Percentage of the total energy. |
| $\beta_r$ | Ratio of regulation capacity that the energy storage units can provide to the total regulation capacity needed in the system. |
| $\varepsilon$ | Probability of constraint violation. |
| $\gamma$ | Penalty factor for deviations from daily consumption of the PEVs. |
| $\rho$ | Ratio of spinning reserve to load demand. |
| $\Delta t$ | Length of the time step. |
| $\lambda_p$ | Locational marginal price of the electricity ($/MWh). |
| $\Lambda_R$ | Total power output of renewables. |
| $\varsigma$ | The maximum flexibility of PEV loads. |
| $c_d$ | Battery degradation cost per MWh. |
| $E_C$ | Forecasted energy consumption of EVCSs in the next 24 hours. |
| $E_{dep}$ | EV's energy demand upon departure. |
| $E_{ini}$ | Energy state of the plug-in EVs at the initial time interval. |
| $E_s$ | Energy consumption of EVs by swapping the batteries. |
| $f_c^{max}$ | Maximum frequency regulation capacity needed in the system. |

| | |
|---|---|
| $k_1, k_2$ | Current and departure time intervals for EVs under plug-in mode. |
| $L_1, L_2$ | Look-ahead time windows for SED and OPF, respectively. |
| $L_F$ | Electricity demand for EV fast charging. |
| $L_O$ | Original customer electricity demand. |
| $t_{dep}$ | EV departure time. |
| $V_C$ | Value of renewable energy curtailment. |
| $V_F$ | Value of frequency regulation provided by the storage units. |
| $V_S$ | Value of PHEV load shedding (i.e., gas price). |

## C. Variables

| | |
|---|---|
| $\alpha$ | Auxiliary variable for convex approximation. |
| $\lambda$ | Scaled dual variable in ADMM. |
| $\Delta P_{G,i}$ | Ramp rate of generating unit $i$. |
| $B_s$ | Energy stored in battery swapping station. |
| $C_i(P_{G,i})$ | Operating cost function of generating unit $i$. |
| $E_p$ | Energy state of the plug-in EVs. |
| $f_c$ | Frequency regulation capacity of the aggregated EV load demand. |
| $f_l$ | Frequency regulation limit of the aggregated EV load demand. |
| $L_c$ | Total energy allocated to EVCSs. |
| $P_C$ | Curtailed power of renewables. |
| $P_E$ | Active power from the external grid. |
| $P_G$ | Active power of generating units. |
| $P_{net}$ | Vector of the net generation. |
| $P_R$ | Effective active power of renewables integrated into the power grid. |
| $R_{G,i}$ | Reserve of power generating unit $i$. |
| $TU$ | Auxiliary variable. |
| $u$ | System control variable. |
| $u_c$ | Supplied power from the grid to BSS. |
| $u_d$ | Delivered power from BSS to the grid. |

| | |
|---|---|
| $u_l$ | Charging power to EVCSs. |
| $u_{ls}$ | The PHEV load shed by EVCS but met by the gas station. |
| $u_p$ | Power allocated to plug-in EVs. |
| $w$ | System disturbance. |
| $x$ | System state variable. |
| $z$ | Common global variable in ADMM. |

# Chapter 1: Introduction

## 1.1 Background

Fossil fuels, consisting of coal, petroleum, and natural gas, are currently the main energy source for our society as they are relatively inexpensive to extract and can be directly used. In addition, converting fossil fuels to electricity is a mature technology at low cost. With the high inertia of the large conventional generators, they can also secure power network stability and withstand small deviations from the desired frequency even under a relatively large imbalance between mechanical power supply and electrical power demand [1].

The aforementioned three types of fossil fuels account for 80% of the energy consumption by energy source in the United States in year 2018 [2]. Figure 1.1 shows the types and amounts of primary energy sources consumed in the United States, the amounts of primary energy used by the electric power sector and the energy end-use sectors, and the sales of retail electricity by the electric power sector to the end-use energy sectors. Each energy source is measured in different physical units and converted to common British thermal unit (Btu). Based on Figure 1.1, the primary energy consumption by source includes fossil fuels, renewable and nuclear. The electric power sector includes electricity-only and combined-heat-and-power (CHP) plants whose primary business is to sell electricity, or electricity and heat, to the public. The end-use consumption sector consists of primary energy and electricity retail sales, excluding electrical system energy losses from electricity retail sales. The electric power sector accounts for about 96% of the total U.S. electricity generation, nearly all of which was sold to other sectors, i.e., industrial, residential and commercial sectors. The remaining 4% of the total electricity generation are produced by the three end-use sectors in 2018. Less than 1% of the electric power sector's primary energy is used by the transportation sector, about 92% of which is provided by petroleum.

However, using fossil fuels as the main source of energy has caused a series of chal-

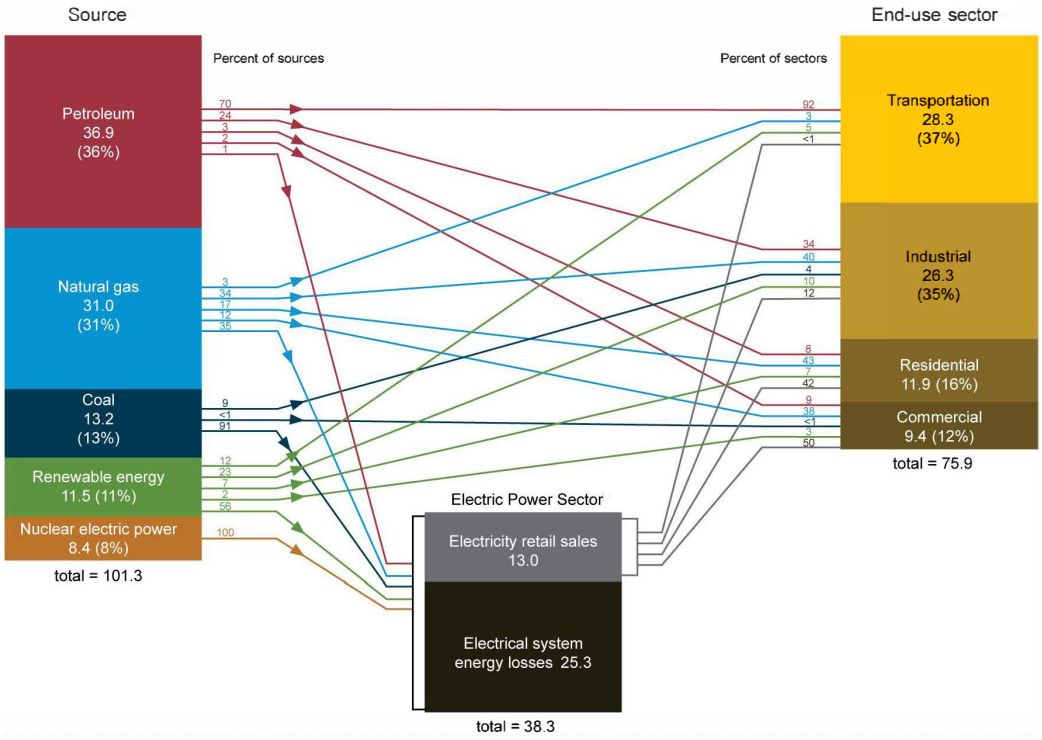


Figure 1.1: U.S. energy consumption by source and sector in 2018 [3].

lenging concerns [4]. Fossil fuels, which are non-renewable sources of energy, will run out and cause energy crisis to the society if they are continually being used as the main energy source in the future. Burning fossil fuels is also harmful for the environment. When coal and oil are burned, they release particles that can pollute the air, water, and land. Moreover, burning fossil fuels also upsets the Earth's "carbon budget," which balances the carbon in the ocean, earth, and air. When fossil fuels are combusted (heated), they release carbon dioxide into the atmosphere, a gas that keeps the heat in the Earth's atmosphere. The massive carbon dioxide emission has caused global warming issues in recent decades.

In response, the Paris Agreement's central aim is to strengthen the global response to the threat of climate change by keeping a global temperature rise in this century well below 2 degrees Celsius above the pre-industrial levels, and to pursue efforts to limit the temperature increase even further to 1.5 degrees Celsius [5]. The production of low-carbon energy technologies, such as solar panels, wind turbines, and lithium-ion batteries, are the key factors to replace the fossil fuel as the main source of energy provision and for effective

decarbonization emissions [6].

The International Renewable Energy Agency (IRENA) published a road-map to year 2050. This report makes clear that an energy transition is urgently required, and that renewable energy, energy efficiency and electrification are the three cornerstones of this transition [7]. As illustrated in Figure 1.2, in order to limit the rise in global temperature to well below 2 degrees Celsius above pre-industrial levels, electrification of heat and transport with renewable power is the key, together making up 60% of the emission mitigation potentials; if the additional reductions from direct use of renewables are considered, the share increases to 75%. When adding energy efficiency, that share increases to over 90%. The share of electricity in final energy (total energy consumed by the end users) would increase from just 20% today to almost 50% by 2050. Renewable share in electricity should reach to 86%, and 60% would come from solar and wind. The transport sector sees the largest transformation. The light-duty vehicles and heavy-duty vehicles together account for nearly 80% of the transport sector's energy use in United States in 2018 [8]. Electrification of these vehicles will result in a structural change in the transport energy use. Electrification of transport is showing early signs of disruptive acceleration, and key enabling technologies such as batteries are experiencing rapid reductions in costs. It is estimated that by 2050, around 70% of all vehicles would be powered by electricity [7].

With the above plans enforced and followed globally, there will be a high proliferation of renewables and electric vehicles (EVs) in the near future. There will also be massive integration of renewables and EVs into the modern power systems of the future by 2050. Maintaining the balance between the electricity supply and demand in presence of significant variable renewable energy (VRE) will require an increasingly smart, digitalized and flexible power system. While aggregated EV loads can provide some flexibility to facilitate integration of VREs in power grids, the challenges on EV load uncertainty and EV charging infrastructure expansion planning should be addressed holistically by the power system planners and operators.

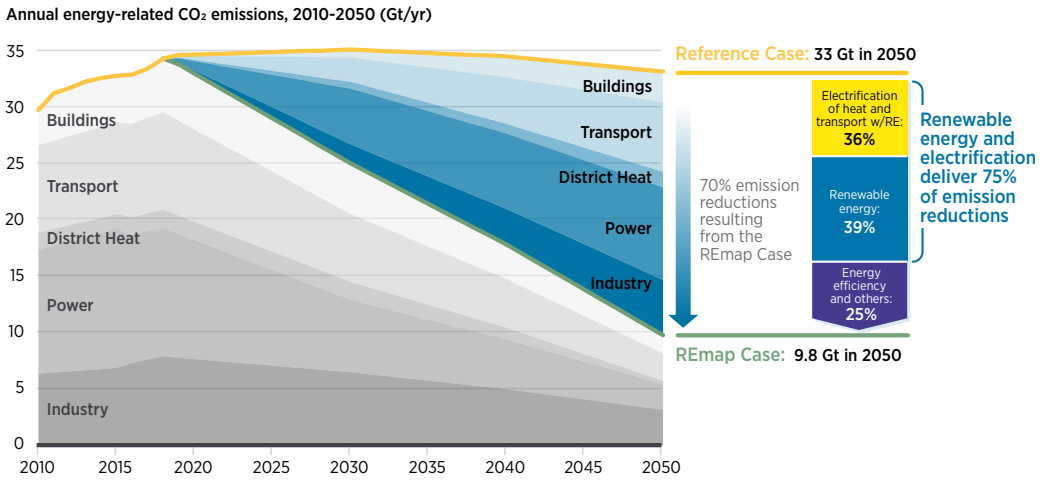


Figure 1.2: Renewables and energy efficiency, boosted by substantial electrification, can provide over 90% of the necessary reductions in energy-related carbon emissions [7].

The rest of this chapter is organized as follows. Section 1.2 reviews the existing literature concerning the EV charging methods, charging scheduling strategies and load models, and identifies their merits and drawbacks. Section 1.3 points out the existing technical issues and the research objectives. The dissertation organization is presented in Section 1.4.

## 1.2 Literature Review

### 1.2.1 EV Charging Methods

With the emerging advancements in the EV charging technologies, there are three main methods [9] widely used to charge an EV: (i) conductive charging, where the battery is connected by a cable and plugged directly into an EV supply equipment (EVSE); (ii) inductive charging, also called wireless charging, where the electricity is transferred through an air gap from one magnetic coil in the charger to a second magnetic coil fitted into the car; and (iii) battery exchange, by swapping the EV battery with fresh ones in a battery swapping station (BSS). The conductive charging is currently preferred by the EV operators due to its lower cost, higher efficiency, and simpler business model. Some testbeds based on the conductive charging mechanism have been built to test the operation of large EV

| Charging level | AC Level 1 | AC Level 2 | DC level 1 | DC level 2 |
|---|---|---|---|---|
| Voltage level | 120 V | 208-240 V | 50-1000 V | 50-1000 V |
| Maximum Power | 1.92 kW | 19.2 kW | 80 kW | 400 kW |
| Charging topology | On-board | On-board | Off-board | Off-board |
| Phase | 1-phase | 1-phase | 1 or 3-phase | 1 or 3-phase |

Table 1.1: EV charging power levels in SAE J1772-2017.

charging stations (EVCSs), for instance, the EVCS at the Argonne National Laboratory with 7 EVSEs [10] and the EVCS in Caltech with 54 EVSEs [11].

The charging level describes the power level of a charging outlet using conductive charging mechanisms. The Society of Automotive Engineering (SAE) has published its recommended practices for charging the plug-in EVs (PEVs). Based on the SAE J1772 in 2017 [12], there are two AC and two DC charging levels as shown in Table 1.1. While both AC levels require the EV with an on-board charger to receive the single-phase AC power from the EVSE, the DC levels charge the EV battery directly with DC power using off-board charging, where the DC power can be converted from both single and three phase AC power supply of the utility. In contrast to the SAE J1772, SAE J3068 in 2018 is a recommended practice for conductive charging that utilizes three-phase AC power. Presenting a symmetric three-phase load enhances the grid stability, especially at high power levels. The SAE J3068 standardizes an AC three-phase capable charging coupler and digital control protocols, offering sufficient power and reliability for the commercial vehicle market with heavy-duty vehicles [13]. The charging voltage and power levels are illustrated in Table 1.2. The plugs and connectors, and the EVSE with electrical safety protection features have also been addressed in the standards from a safety standpoint.

While the SAE standards addressed the safety considerations of the plugs and connectors as well as the EVSEs, many other standards and regulation policies related to safely operating an EV have been published, the primary focuses in most of which are on the battery pack [14].

| Charging level | AC | AC | AC |
|---|---|---|---|
| Voltage level | 120/208 V | 277/480 V | 347/600 V |
| Maximum Power | 57.6 kW | 133 kW | 166 kW |
| Charging topology | On-board | On-board | On-board |
| Phase | 3-phase | 3-phase | 3-phase |

Table 1.2: EV charging power levels in SAE J3068-2018.

EV battery performance and safety are considered by the vehicle manufacturers to prevent the battery from combustion, explosion, and other potential accidents resulted from the failure and miss-operation of the battery itself [15]. The electrical safety considerations of EVCSs from the perspective of an EVCS operator are also investigated by policy and research communities. Guidelines are introduced requiring the EVCS design to meet the aforementioned standards requirements, and the EVCSs are also required to be subject to periodic safety assessments [16]. Fire safety when charging EVs is discussed in [17]. The transformer loss-of-life due to the uncoordinated PEV charging in a parking garage has been analyzed in [18]. The integration of photovoltaic (PV) system and the use of smart charging algorithms can avoid the transformer aging and early replacements. An advanced communication system for EVCSs brings about additional opportunities for the EVCS operator, where a communication assisted protection strategy can alleviate the faults and ensure a safe charging of the EVCS [19]. In [20], the cloud has been used as a platform for online monitoring and analysis of the EVCS data and power quality assessments.

With bidirectional digital communications between the EV and the EVSE via single-wire base-band signaling for local control, a large three-phase EVCS provides low-cost, less-complex, and highly-reliable charging of EVs. It can also supply both AC and DC power based on the customer preferences. Furthermore, large three-phase EVCSs using conductive charging can operate as DERs to support the grid. The IEEE Standard 1547 in 2018 provides requirements relevant to the performance, operation, testing, safety considerations, and

maintenance of the interconnection between utility electric power systems (EPSs) and the DERs. The requirements are universally needed for interconnection of different types of DERs [21], where inability to address such requirements may lead to cascading failures in power systems [22–24]. For instance, tripping of wind farms during a storm resulted in a major blackout in South Australia in 2016, affecting 650,000 customers [25]. Thus, it requires the EVCS operators to not only account for the traditional considerations of the EVSEs, but also capturing the safety of the EVCS cyber-physical system and their interactions with the grid.

### 1.2.2 EV Charging Scheduling Strategies

The uncontrolled charging, which assumes EVs to begin charging immediately after arrival with continued charging until the battery is full or the next trip starts, may enforce EVs to charge during daytime with higher electricity prices. This, in turn, may increase the system peak load [26]. With the proliferation of EVs, the aggregated EV charging load imposes a significant impact on the power system load profile. In response, different charging strategies have been used to optimize the EV charging schedule.

Many literature propose locally optimal charging and discharging schedules to maximize the benefits of particular stakeholders. A cyber-physical energy management system for networked nanogrids with battery swapping stations (BSSs) is introduced in [27]. Optimal day-ahead operation and service scheduling of the BSS is investigated in [28]. In the decentralized EV charging strategies, every EV aggregator makes a decision for it's own behaviour and the resulting system behaviour is the aggregate response. Therefore, no single EV aggregator will have the complete system information. Pricing signals are widely utilized in decentralized charging strategies to coordinate the aggregators and avoid the locally optimal solutions. Scheduling of the plug-in EVs with co-optimized customer and system objectives is addressed in [29] where the battery degradation, customer costs, and system load profiles are taken into account. However, the scheduling scheme presented

in [29] is centered on the electricity market price, the real-time dynamics of which are prominently affected by the high penetration of EVs. In response, dynamic pricing scheme and optimal charging scheduling of the BSS is studied in [30]. Efforts have also been made in [31] to structure a dynamic charging mechanism that is able to adjust and update the EV charging prices according to the tracked demand portfolios. The proposed method in [31] is to incentivize the customers to meet the charging station demand requirements, which may not be an effective assumption in practice considering the random behaviours of EV customers.

Centralized EV charging strategies can use complete system knowledge to optimize the EV charging schedule and reduce the system operation cost [32]. However, to date, centralized EMS architectures able to globally optimize EV charging schedules are either applicable to power distribution systems with small-scale EV penetrations or tailored to specific EV customers with certain behaviors. EV charging management for commercial buildings with PV generation is studied in [33]. In [34], a chance-constrained control strategy is proposed for EV-integrated microgrids in which each EV is modeled as a variable making it a computationally-intensive optimization problem with large numbers of EVs. A centralized power dispatch strategy considering an aggregate model of EV fleet with certain customer behavior is approached in [35]. Regional EV charging capacity is proposed in [36] to evaluate their energy demand assuming a certain charging requirement upon arrival. EV fleets are considered as stationary storage services in [37] to reduce the transmission system operation cost.

Distributed EV charging systems can use either decentralized charging strategies or centralized charging strategies with complete system knowledge, but distributed architectures require computations to be made across all nodes instead of the aggregator nodes or in one center [38]. Alternating direction method of multipliers (ADMM) is widely used for distributed computations in two different application categories:

- Computations are done in all the buses, and each bus or node can communicate

only the coupling information with the neighborhood nodes. One major benefit is that it could protect the privacy of the customers as no node could have access to the system-level information. This distributed method requires high communication investments as all nodes should have communications with their neighborhoods. It also requires distributed control in power systems of the future, as power systems are currently operated in a centralized manner, maintained by the independent system operators (e.g., PJM);

- ADMM is employed to distribute the large optimization problems into multiple CPUs or just one CPU: to decrease the computation time, it is implemented only in the central node. Here, the term "distributed" here is interpreted as a distributed algorithm to solve large-scale optimization problems. The reduction in computation time relies on the implementation in particular problems.

### 1.2.3 Aggregated EV Load Modeling

Lithium-ion batteries are typically employed as the power source for EVs. Constant current constant voltage (CC-CV) and constant power constant voltage (CP-CV) charging mechanisms are frequently employed to charge the EV batteries. Both charging strategies characterize a linear state of charge (SOC) profile until about 95% of the battery is charged [39]. As illustrated in Fig. 1.3, during the discharge process, the voltage would drop rapidly when the SOC is less than 5% (after roughly 95% of the capacity is spent). From the EV aggregators' perspective, battery operation in the nonlinear SOC region, i.e., CV region during the charging period, cannot be included in the EV charging coordination schemes. Therefore, the SOC of the batteries is limited from 5% to 95% considering both battery operation and lifetime. In the common practice, several EV manufacturers recommend the SOC to be in the range of 20% to 90% considering the SOC impacts on the battery lifetime. Hence, charging load of a single EV is typically considered as a constant power load during the steady-state power grid operation [40].

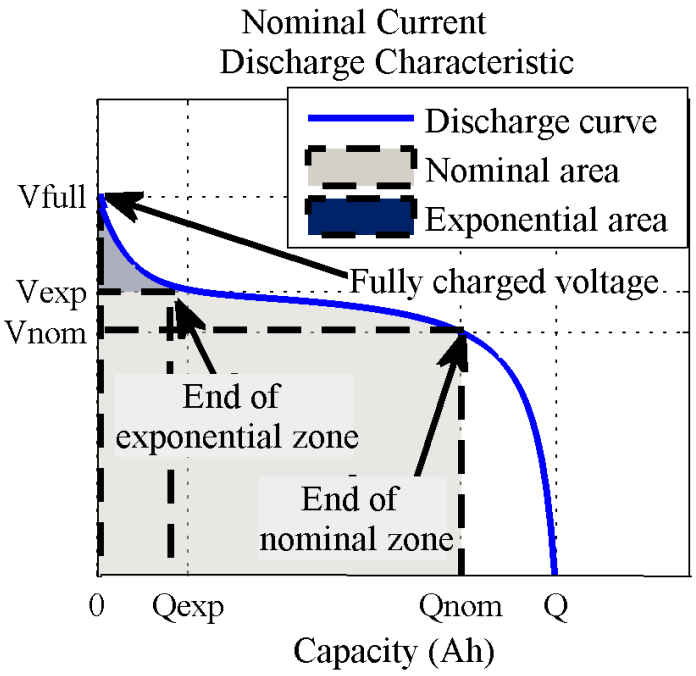


Figure 1.3: Typical discharge curve [41].

The importance of EV load management has been recognized by the industry and different regulatory mechanisms have been proposed to manage the EV load. Currently, EV load models that the industry uses are based on the EV charging through rate design or demand response programs [42]. One approach to rate design for EVs is time-varying pricing, which includes time-of-use (TOU) and dynamic pricing. TOU is the simplest form of time-varying pricing and has been widely used in the utilities. It features low communication requirements and is easy to be applied in practice. However, the TOU rates can change the charging behavior and may result in spikes in the load curve as EV customers may simultaneously charge their EVs during the lowest price period. Hence, this mechanism is suitable only when there is a very low EV penetration in the system. Dynamic pricing, which is another form of time-varying pricing, can be applied to scenarios with higher levels of EV penetration. However, it requires the PEV owners to be responsive to the price signals, while customers may not be conformable with its complexity. Demand response programs have been deployed to make EV charging load partially dispatchable. The EV load

can be responsive to system needs with appropriate communication system. However, the partial control and decentralized scheduling of EVs is still unable to further optimize the EV charging schedules and the system objectives and performance requirements. Hence, the EV load models utilized in the industry are suitable for power grids with lower EV penetration and could not ensure robustness to the inherent uncertainties in customer behavior [43].

With wide deployment of advanced metering infrastructure (AMI) in the power distribution system [44] and direct load control implementation in the EV charging stations (EVCSs) [45], both the transient and steady-state characteristics of the aggregated EV loads are primarily driven by the EVCSs' control and operation strategies. The flexibility of the EV loads can also be harnessed during the day-to-day normal operating conditions, particularly in systems with high penetration of variable renewables such as wind and solar [46].

Power system operation flexibility is the system ability to respond to changes in demand and supply [47]. VRE can increase the need for flexibility such as steeper ramps, deeper turn downs, and shorter peaks in system operations. As power systems evolve to incorporate more renewable energy and responsive demand, flexibility across all power system elements must be addressed by ensuring: flexible generation, flexible transmission, flexible demand-side resources, and flexible system operations [46]. The demand-side flexibility includes [48] (i) the daily load demand variation accounting for the shortage or surplus in renewable energies, (ii) inter-day load dispatch to smoothen the load profile, (iii) intra-hour flexibility such as frequency regulation, etc. While the flexibility of an energy storage unit [49] can be simply defined as the energy, power and ramp-rate it provides, the flexibility of the aggregated EV load has to take into account many factors such as the EV customer behaviors, different charging methods and strategies [50–52]. The EV loads using conductive charging —including level 1 and level 2 charging—can be regarded as the *deferrable loads* when the smart charging algorithms are employed. Based on the conductive charging principles, fast charging (FC) EV loads are assumed to be *inelastic* and the EV load should be charged once the EV is connected to the EV supply equipment (EVSE) [53]. The inductive charging,

also called wireless charging, reveals similar load characteristics as conductive charging and the load flexibility is mainly driven by the charging power rates. The battery swapping station (BSS) can swap the EV batteries with fresh batteries and the flexibility of EV load is further enhanced with the deployment of large BSSs. Detailed models for different charging methods and charging levels are discussed in [54–57].

## 1.3 Problem Statement and Research Objectives

As it was discussed in the previous section, the existing EV charging methods for EVCSs in the literature suffers from one or more of the following limitations.

- lack of interconnections and interoperability in design with associated electric power system interfaces.
- lack of electrical safety considerations of the EVCS cyber-physical systems.

Furthermore, it has remained a challenge to schedule the EV charging through a global scheduling optimization problem [58]. The main obstacles to achieve a centralized charging strategy with large numbers of EVs [59] at the transmission level are: (i) perfect knowledge of the system parameters and EV customer driving profiles is not available and is hard to characterize; (ii) high computation burdens; and (iii) high communication infrastructure investment requirements. Existing literature related to the EV charging scheduling strategy fails to fill the knowledge gap, and the methods are typically suitable for power grids with lower EV penetration and could not ensure robustness to the inherent uncertainties in customer behavior. Specifically, they suffer from one or more of the following defects:

- relying on strong assumptions of customer behavior: (i) EV customer has a certain behavior and EV demands can be precisely forecasted, (ii) EVs are assumed to be charged upon arriving home, (iii) the customers' main priority is their payments.
- lack of global optimization algorithm with high penetration of EVs.

As a result, research on the aggregated EV load modeling to analyze the impacts of different combinations of EV charging methods on the grid and the EV charging infrastructure expansion planning is found rare and missing in the literature.

In an attempt to address the aforementioned issues, this dissertation research aims at developing integrated control and energy management schemes for large-scale electric power systems with higher penetration of renewables and electric vehicles. The research objectives are listed as follows:

- introduce a new EVCS architecture, address the EVCS safety considerations in its cyber-physical system and its interactions with the power grid, and develop a risk assessment framework to evaluate its electrical safety.

- design a two-stage EMS architecture that accounts for DER forecast uncertainties and stochastic randomness of the EV customer behaviors.

- proposed a model that can optimize the EV charging schedules and reduce the system operation cost at the transmission level by providing a nearly-optimal solution to the global EV charging scheduling optimization problem.

- quantify the flexibility of the aggregated EV loads and simulate the impacts of aggregated EV loads on the power grid considering different communication scenarios (delays, etc.).

- introduce simulation procedures to numerically identify the model parameters and provide guidelines for the system operators to integrate large numbers of EVs to the power grids of the future.

- develop an adaptive operation framework including four strategies for EVCS operators to handle various operating conditions and EV penetration levels.

## 1.4 Dissertation Organization

The rest of the dissertation is organized as as follows:

- **Chapter 2** presents the suggested EVCS architecture and control scheme. Then, electrical safety considerations and the risk assessment model for EVCSs are introduced.

- **Chapter 3** presents the suggested 2-stage EMS architecture. The proposed first-stage optimization problem and the corresponding mathematical formulations for the SED are introduced. The second-stage EV charging strategies under both plug-in and battery swapping modes are also presented.

- **Chapter 4** presents the suggested EV load models and associated flexibility metrics. The mathematical model formulated to consider different charging mechanisms and communication delay scenarios between EVs and the power system is introduced. The interactions between the EV charging loads and the power grid are then simulated through a two-stage energy management system (EMS), where the model parameter identification is accomplished through simulations.

- **Chapter 5** presents the charging strategies of EVCSs under normal operating conditions. Then, the different restoration processes for EVCSs considering various interruptions are introduced.

- **Chapter 6** summarizes the contributions of the proposed dissertation research and introduces the publications from this research effort. Recommendations for the future work are provided as well.

# Chapter 2: EVCS Control Scheme and Associated Electrical Safety Considerations

## 2.1 Abstract

Several safety regulations particularly concerning the charging electric vehicles (EVs) are developed to ensure the electric safety and prevent the hazardous accidents, in which safety requirements for electric vehicle supply equipment (EVSE) and the EV battery are the two main driving factors. At present, quantitative assessment of electrical safety considering the operation conditions of large-scale electric vehicle charging stations (EVCSs) has still remained a challenge. The EVCS and low level control scheme is firstly introduced in this chapter. Driven by the hierarchy of hazard control mechanisms, this chapter then proposes a holistic approach to evaluate the electrical safety of the large-scale EVCSs based on the EVCS control scheme. We eventually present the numerical case studies and simulation results, followed by the concluding remarks.

## 2.2 Proposed EVCS Architecture

The proposed EVCS architecture considering the EVCS cyber-physical system is shown in Fig. 2.1. We aim at large-scale EVCSs, corresponding to the long-term-parking locations, such as parking garages and parking lots. These EVCSs typically offer 5 kW to 25 kW charging capacity through EVSEs (some of them may also offer charging power of 26–60 kW). This is because the EVSEs with very high charging capacity (more than 60 kW) come at higher installation costs [60], higher degradation of the battery life cycle, and higher charging cost as they may get charged during peak load hours with premium electricity prices. An EVCS with several EVSEs are typically comprised of three parts: (i) the physical system that provides the EV charging services, (ii) the communication system, and (iii) the

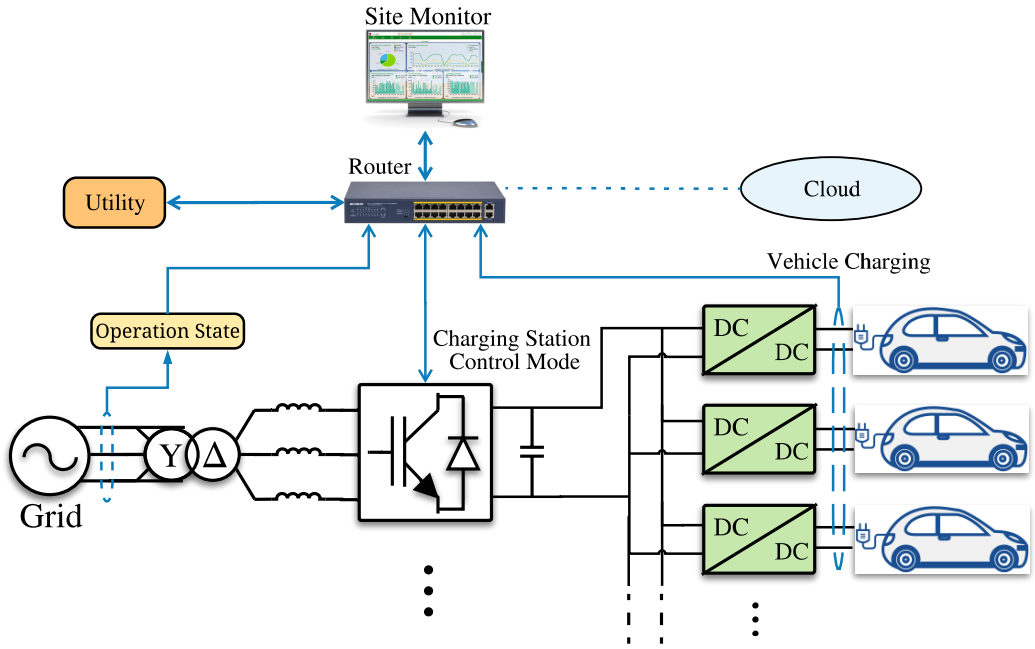


Figure 2.1: The overall architecture of an EVCS.

control center. The architecture for a large EVCS is proposed to manage charging of tens to hundreds of EVs that also act as DERs in the grid, in order to compliance with the recent recommended practices and standards.

The EVCS's physical system is demonstrated in black in Fig. 2.1 and is connected to the distribution grid through a step down transformer. An LC filter is used to filter out harmonics and a voltage source converter (VSC) is used as the AC/DC converter to maintain the dc-link voltage of the capacitor and control the reactive power. The VSC can operate in four-quadrant, and the reactive power injection/absorption is accomplished with the dc-link capacitor. Bi-directional DC/DC converter is used to control the active power. While most current EVSEs have independent AC/DC converters and connect separately to the AC busbar, the EVSEs can share the same AC/DC converter and have multiple parallel DC/DC converters on the DC busbar when EVs are charged with DC power.

The communication system is illustrated in blue in Fig. 2.1. The cyber system transmits the signals between the physical system and the control center. Direct load control can be achieved by enabling and disabling the EV charging, or through proportional adjustments in

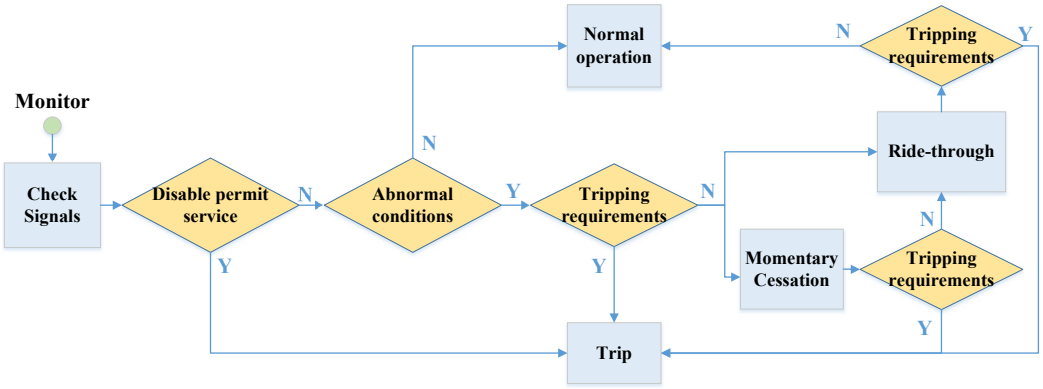


Figure 2.2: The EVCS operation states and priority diagram as a DER.

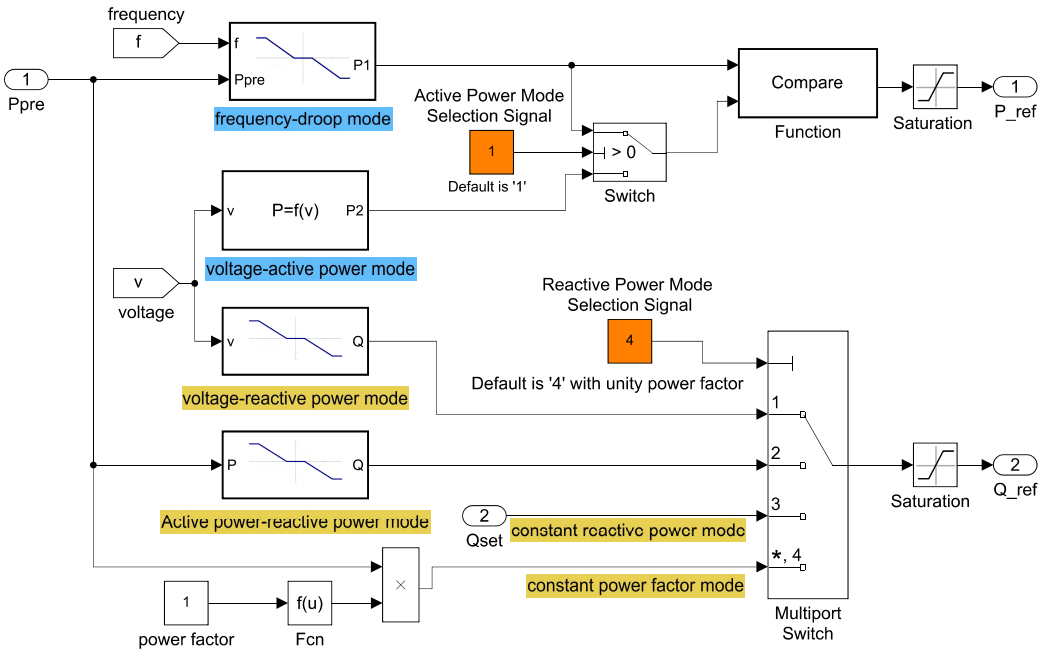


Figure 2.3: A recommended ride-through priority and mode selection diagram.

the duty cycle of the DC/DC converter. The control center can coordinate the load control of EVs to enable smart charging, and the EVCS can participate into the utility demand side management programs as a DER. The control center will also communicate other signals with the utility. Many EVCS operators analyze the data and run the EV scheduling algorithms on the cloud [10, 11], and thus, the communication between the EVCS and the cloud is also enabled.

The control center with a site monitor and the operation and control platform can

monitor and control the EVCS directly or implement the signals sent from the utility and the cloud. Based on the IEEE Std. 1547-2018, a DER shall change the operation state based on the DER response priorities. Different operation states of the DER are illustrated in Fig. 2.2. The EVCS operator checks the communication signals and grid conditions to decide on the operating states. For instance, the EVCS should trip in no more than 2 seconds when it receives the signals from the utility to disable *permit service*. The control center can also adjust the active/reactive power management modes based on the operation requirements. According to the standard, there are two active power management modes and four reactive power management modes for DERs. The DER can select different control modes during normal operating conditions and ride-through based on the ride-through priority. A recommended ride-through priority and mode selection diagram is shown in Fig. 2.3. The *voltage-active power* mode is disabled in default. Once the mode is on, e.g., if the *Active Power Mode Selection Signal* '-1' is sent from Area electric power system (EPS) to the DER operator, a *Switch* will select the second data signal and the *Compare* function will then select the lesser of the power value between the frequency-droop mode and voltage-active power mode. Reactive power control functions include Constant power factor mode, Voltage-reactive power mode, Active power-reactive power mode and Constant reactive power mode. The DER needs to be capable of activating each mode one at a time. Multi-port Switch is used to achieve this selection, e.g., if *Reactive Power Mode Selection Signal* '1' is sent from Area EPS to the DER operator, port 1 is selected, and then the voltage-reactive power mode is activated. Constant power factor mode with unity power factor setting is the default mode of the installed DER, thus Signal '4' is selected in the default mode.

## 2.3 Proposed Risk Management Model for EVCSs

The proposed risk management framework of the EVCS is shown in Fig. 2.4 and includes three layers: (i) safety considerations of EVCS, (ii) risk assessment, and (iii) risk control.

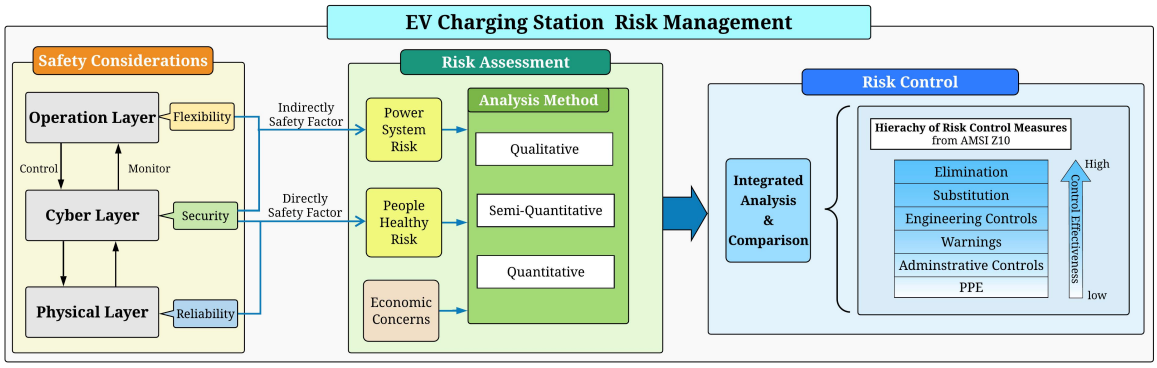


Figure 2.4: The risk management framework for the EVCSs.

The safety considerations in different layers of EVCS are explored, risk assessment analytics are suggested, and finally the integrated analysis and comparisons are done in the design and planning procedures to meet the requirements of the hierarchy of risk control measures.

### 2.3.1 Safety Considerations and Mitigation Methods

The electrical safety offered by the EVSE can be defined as the probability that it will continue to properly carry out its duties without causing a dangerous voltage to appear on a touchable surface due to random faults. Some faults may compromise safety, but not the functionality of the charger, which may keep working. This very hazardous situation is even more crucial in large-scale EVCSs, which are publicly exposed. Because electrical safety of the EVCS decays in time, it should be assessed to prevent the hazardous situations such as people injury, device damage, unstable operation of the grid, and the discontinuity of power supply to EV load. Safety considerations in Fig. 2.4 include all three layers of the EVCS. The reliability of the EVCS components, cyber security of communications, and flexibility of EVCS operation should be considered to reduce the risk and mitigate the impacts of the potential hazards.

The conductive charging requires the customers to plug-in their EVs to the EVSEs, and thus, the EVSE design should protect the customer against electric shock when the EV is being charged. The protection against electric shock is achieved by implementing two

"layers" of protection: the basic protection (i.e., preventing persons from being in contact with energized parts) and fault protection (i.e., protection in the event of failure of the basic insulation), which is generally obtained via disconnection of the supply. The International Electrotechnical Commission (IEC) defines different charging modes and describes the safety communication protocol between EV and EVSE [61]. Charging mode 3 should be used for AC charging, and charging mode 4 should be used for the fast DC charging in large-scale EVCSs. The two charging modes have control and protection functions installed permanently. The reliability of the EVSE components with electrical safety protection features should also be monitored by the control center and assessed by periodic safety inspections. For instance, the potential failure of Ground Fault Circuit Interrupter breaker or charging circuit interrupting devices due to environmental factors (e.g., humidity and aging), or vandalism activities like copper theft, can create a dangerous situation for EV customers when they are in touch with the EVSE. The cyber reliability is also very important to the EVCS: if the router is down, the EV load management signals could not be implemented, and the communication between the utility and the EVCS also fails. Hence, a very large EVCS should have backup router and battery resources to support the EVCS communication system at minimum cost.

A well-designed protection system in EVCS to have a swift fault clearance is also one main factor to ensure the EV charging safety and protect the EVCS equipment. Over current protection is a major protection function for EVCSs. Adaptive protection with the communication assistance is recommended to coordinate the protection devices and to change the protection algorithms of circuit breakers when necessary [19, 62]. However, performance of the adaptive protection primarily relies on the EVCS cyber layer. In cases of delays in signal communications (or cyber system) and protection device failure, the risk will increase significantly. Hence, hierarchical protection design, in which the upper layer acts as the backup protection for the lower layer, should still be featured and embedded in the adaptive protection to account for communication failure. The use of communication

also makes the EVCS protection vulnerable to cyber attacks. The attacker may disable the protective devices which may potentially compromise the electric safety. Corrective protection should be used to safeguard the EVCS if the adaptive protection devices fail to trip. For example, the power devices like IGBTs can switch off when they reach their current limits. In addition, with the EVCS cyber-physical system, the circuit breaker conditions can be uploaded to the EVCS control center, which can guide necessary maintenance and life-cycle management using condition monitoring data [63]. Algorithms to detect the device malfunction and cyber attacks can also be developed to enable the EVCS control center to monitor its performance at all times. Suitable fire detection and warning systems should be installed to detect fire scenarios during the charging, which may also be contributed by other factors (e.g., high temperature in summer).

The cyber attack to the internal communication system of EVCSs or the advanced metering infrastructure (AMI)—that enables the communication between utility and EVCSs—could also affect the power grid stability. For example, the attacker can send the disabling permit service signal to trip the EVCS from the grid. This may cause cascading failures when the grid operates in a marginal operating condition. The attacks targeting the EVCS internal communication system and AMI may have limited impact, and the likelihood of manipulating the communication between the utility and the EVCS may be low when the utility connects the DERs using isolated optical fiber systems. However, the EV load management and control employing cloud services expose the EVCS and the grid with additional vulnerabilities to cyber threats and outside intruders. Particularly, the great exposure and interactions of the EVCS energy management systems and the public internet will change the communication system in power grids from isolated systems to the attack and defend mode, giving birth to a myriad of cyber threats. For example, the distributed denial-of-service (DDoS) attack can coordinate the DoS attacks to cause serious delays or failures in the data transmission between EVCSs and clouds. As a result, the EVCSs may not respond to the frequency disturbances and fail to coordinate with the main grid services during the

ride-through operation. The attacker can also send signals to EVCSs to continuously switch on/off the EV load and thereby can cause grid oscillations. With massive integration of EVCSs in the coming future, the consequences arisen from any of the above disruptions may be far higher than before, potentially leading to cascading failures and major blackouts in bulk power grids. Hence, the large EVCSs should run the EV load management and control algorithm on their own computer or the utility server, while other data can be uploaded to the public cloud so that the cloud can only read/store the EVCS data.

EVCSs are allowed to over subscribe the EV charging if the total load at any time is within the supply system safety limits. Smart charging considering the EVCS and grid constraints can be implemented to achieve this and avoid the possible overload and temperature rise of the transformer connected to the EVCS (which will otherwise result in an accelerated transformer loss-of-life). The smart charging assisted by EVCS communication system can also facilitate the EV load recovery following interruptions. The interrupted EV load during the outages can be charged back to the required state of charge (SOC) as long as the EVSE is able to supply the remaining EV load demand before the EV departure time. Although the cold start status—that asks the EVs to start charging within a random time up to 15 minutes following the interruption—will not allow a simultaneous charging of the EVs and causes the transient stability problem in the grid, the uncoordinated charging still allows all EVs to charge after a short time period and may violate the grid operation constraints. On the contrary, smart charging with communication can estimate the EV load and schedule the charging considering both the transient stability of the grid and steady-state grid operation constraints. Hence, the EVCS communication should be supplied by the backup batteries during the interruption or in the recovery process before EVs start to charge. Large EVCSs with major charging power between 26 kW–60 kW, or more than 60 kW are most suitable for areas where drivers park for less than half an hour, such as restaurants. These EV loads are usually regarded as critical loads and may charge during the premium electricity price periods. Distributed generators and storage units can be used to mitigate the increased peak

loads in such EVCSs and supply the load during the interruption. It is worth mentioning that continuous supply of some critical EV loads (such as hospital EV fleet) is very important as failure in doing so may cause catastrophic consequences. One approach is to build or increase the capacity of the uninterrupted power supply system considering the EV loads. Other alternatives can be to use the plug-in hybrid EV (PHEV) fleet or build the BSSs which reserve the fully-charged batteries for the fleet and locate the BSS within short distances.

Note that the safety distance to prevent the EVCS workers from arc flash hazards should also be considered by the EVCS operators. The arc flash boundary for the EVCSs with AC busbar can be calculated by the IEEE Std. 1584-2018 [64]. Additional research needs to be done to address the arc flash boundary for the EVCSs with DC busbar. RF hazards [65] need to be considered for large EVCSs with the inductive charging that may be built in the future. To the large BSSs using robotic arms to swap the EV batteries and automated factory to manage and charge the batteries, several issues mentioned earlier (e.g., EVCS cyber-physical system) should still be complied to ensure an electrically-safe BSS operation.

### 2.3.2 Risk Assessment Metric

A hazard is defined as the potential for harm, and includes all aspects of technology and activity that produce risk. A risk is the likelihood that a hazard will cause harm. In response to the identified hazardous situations for the proposed EVCS architecture and the corresponding safety considerations, we here provide a systematic tool to analyze the risk of EVCSs and guidelines to take a promising risk control action.

#### 2.3.2.1 Risk of Injury or Health Damages

The risk score $R_i$ related to an identified hazard is a function of the likelihood of occurrence of the injury or health damage $Po_i$ and the subsequent impacts and severity $Se_i$ of the event $i$, calculated using (2.1). The total risk score, $Rt$, which is assessed in (2.2), is the sum of the

risk scores $R_i$ over all potential risk scenarios.

$$R_i = Po_i \times Se_i \tag{2.1}$$

$$Rt = \sum_i R_i \tag{2.2}$$

*Rt* includes the risk of exposing customers to dangerous voltages during the EV charging, and workers to potential arc flash during the maintenance, etc. It varies with time, and is affected by the effectiveness of site inspection and maintenance actions. While *Rt* can be used to estimate the total risk of an EVCS, a heat map of the $R_i$ can be generated with *Po* and *Se* identified in order to prioritize the safety bottlenecks and to take additional controls for events with higher $R_i$. Note that although the risk score approach is a semi-quantitative mechanism and could not quantify an accurate risk measure, it is a widely used risk assessment method to estimate the risk and can help an effective decision making and risk control to hazards including, but not limited to, shocks and electrocution, burns, etc. [66, 67]. The estimated total risk score *Rt* reflects the current state of risk for the EVCS, and can be calibrated by real-world operation data.

#### 2.3.2.2 Risk to Power System Operation

Another risk index is the energy not supplied factor, $ENSF$. Firstly, the expected energy not supplied $EENS$ is calculated using (2.3) and reflects the grid reliability status and its ability to continuously serve the demands. $EENS$ and $EENS'$ are the sum of the energy not supplied with and without EVCS during each outage event $j$. The contribution of the EVCS to the changes in the $EENS$ of the system is then assessed via (2.4).

$$EENS = \sum_j EENS_j \tag{2.3}$$

$$ENSF = \alpha_f (EENS - EENS') \tag{2.4}$$

where $\alpha_f$ indicates the contribution factor of an EVCS to the *EENS*, and is calculated as the ratio of the EVCS rated capacity to the total capacity of EVCSs that contribute to the interruption. The EV load interruption may not contribute to a large increase of the *EENS* if the mobility and flexibility of the EV load is taken into account and utilized during feeder-level interruption recovery. Some utility-level interruptions can also be mitigated when the EVs are charged and ready to supply the grid several hours earlier than potential disruptions. Hence, EVCS can contribute to a decrease in *EENS*. However, EVCS failure to ride-through and respond to the grid disturbance may lead to transient stability problems that may finally affect the system reliability and increase the *EENS*. Hence, *ENSF* is proposed to reflect the risk of the EVCS cyber and operation layers that contribute to the interruptions. Approaches on power flow [68] and Monte Carlo Simulation analysis are typically employed to evaluate the system *EENS*. The state-of-the-art methods could not quantify the impact of communication systems and the flexibility in the EVCS smart charging on *EENS*. The cyber-physical system impact of the EVCS on the grid and computation of *EENS* requires a co-simulation framework of the cyber-physical power system, and integrated evaluation of system stability and reliability. Future work needs to be done to address these research topics. Here, we limit the discussion on power system stability and reliability risk that cyber layer brings as the indirect safety factor to power system operation.

Maintaining the system stability is the necessary condition to guarantee a safe operation of the power grid. The proposed EVCS architecture features voltage and frequency support during the system transient state to facilitate maintaining the system stability when disturbances happen. We introduce the stability risk index *Sr* to qualitatively reflect the risk imposed by the EVCS cyber layer to the system stability and reliability performance. Qualitative risk assessment is a simple, yet fast and effective, approach commonly used when numerical data are inadequate or unavailable [69]. The risk levels of *Sr* are here classified as 'Very low', 'Low', 'Medium', 'High' and 'Very high'.

### 2.3.3 Discussions on Risk Control

We have discussed several mitigation methods against several hazards facing the EVCS operation. Most mitigation approaches are for the earlier stages in the hierarchy of risk control and should be considered during the EVCS design procedures which are less impacted by the supervision performance and human error. However, a large EVCS with several electrical safety challenges and concerns may require sophisticated design and high investments focused on its cyber-physical system. The EVCS operator may wish to maintain a certain level of electrical safety at minimum cost. For example, the EVSEs with safety features are mandatory for all EVCSs considering that the generality of users has minimum knowledge on the electricity, but other EVCS designs are selected based on the EV load characteristics and load demand. The storage or the uninterrupted power system needs to be considered when the EVCS supply critical EV load routinely. Cyber security of EVCSs with high power capacity and with a DER role to support the grid need to be rigorously checked.

We here define the EVCS cost per unit of power ($/kW) as an index to indicate the economics of the investments:

$$Cu = \frac{Capital\ Cost + Operational\ Cost}{Rated\ Capacity} \tag{2.5}$$

*Cu* reflects the life-cycle cost of the EVCS. As shown in Fig. 2.4, the EVCS design and operation need to consider all indices and do the trade-off among all of them (*Rt*, *Sr* or *Cu*) when necessary. For instance, an EVCS with a few EVSEs can maintain the basic communication function and use the cloud to manage the EV charging, as it has little impacts on the grid. With the same features, a large EVCS with hundreds of EVSEs will have higher *Rt* and *Sr*. However, large EVCS might simultaneously reduce the three indices when adding the cyber security enhanced monitoring and control system. For instance, the predictive maintenance can be done based on an advanced monitoring system in order to minimize the risk of load interruption. This in turn may reduce the operation cost due to

reduced inspection frequency and economic losses. To simplify the process and show the effectiveness of the proposed risk assessment model, we also use the qualitative method to represent the $Cu$ values.

## 2.4 Numerical Case Studies

This section compares the performance of the EVCSs with different designs using the proposed risk assessment model and the two indices of $Rt$ and $Sr$. All EVCSs are assumed to have the total capacity of 1 MW, and the EVSEs in the EVCS are the same type with the charging capacity of 20 kW. Hence, the EVCS can use up to 50 EVSEs to charge the EVs simultaneously. The following four cases are discussed:

- **Case 1:** An EVCS with no communication and uncoordinated charging.
- **Case 2:** An EVCS with smart charging using public communication system, but no grid support as a DER.
- **Case 3:** An EVCS with smart charging using public communication, and also working as a DER.
- **Case 4:** An EVCS with smart charging, also working as a DER to provide grid support, but using isolated utility AMI and server to communicate signals.

### 2.4.1 Risk of Injury

A large EVCS may have several situations that can cause electrical hazards. We classify the electrical hazards into the following categories: (1) electrical shock to EV customers, (2) electrical shock and arc flash hazards to workers, and (3) fire hazard caused by the EV charging that may affect the personnel's safety. It is important to note that the electric shock hazard during the charging process greatly depends on the electrical characteristics of the charger (e.g., Class II chargers equipped with an isolation transformer) [70]. We evaluate the

Table 2.1: The Total Risk Score for the EVCS in Case 1

| Hazard Category | Severity | Probability of Occurrence of Harm $Po = (Fr + Pr + Av)$ | | | | Risk Score (R) |
|---|---|---|---|---|---|---|
| | $Se$ | $Fr$ | $Pr$ | $Av$ | Total | $Se \times Po$ |
| 1 | 5 | 5 | 3 | 1 | 9 | 45 |
| 2 | 7 | 3 | 3 | 3 | 9 | 63 |
| 3 | 6 | 2 | 2 | 1 | 5 | 30 |

severity of the possible injury or damage to health $Se$, and likelihood of occurrence of such incidents $Po$ in EVCS based on the risk assessment process criteria of [66]. We assume the EVCS in Case 1 has the $Se_i$ and $Po_i$ values as shown in Table 2.1. Therefore, the total risk score $Rt$ is the summation of $R_i$ for all hazard categories and equals to 138. The $Se$ values are similar in all studied cases. The $Po$ includes the frequency and duration of exposure $Fr$, the likelihood of occurrence of a hazardous event $Pr$ and the likelihood of avoiding or limiting injury or damage to health $Av$. The $Fr$ and $Av$ values will also be similar in different cases where EVCSs have similar number of customers and physical facilities. With the enhanced cyber layer in EVCS, the $Pr$ decreases. The $Pr$ with a value of 3 indicates that a hazardous event is likely to happen, the $Pr$ with a value of 2 means the hazard has a rare chance to happen and $Pr$ value of 1 reflects a negligible possibility of the hazard. We assume the EVCS in Case 2 and Case 3 will decrease the $Pr$ values of three hazard categories to 2, 2, and 1, respectively. And the EVCS in Case 4 with further considerations of cyber reliability and security will decrease the $Pr$ value to 1, 1, and 1, respectively. The $Rt$ values in all cases are tabulated in Table 2.2.

### 2.4.2 Impacts on Power Grid Stability and Reliability

We assume that the EVCSs oversubscribe 20 EVSEs for Case 2 to 4 so that the individual EV customer behavior has a little impact on the EVCS charging capacity. We also assume the EVCSs as DERs in the grid in Case 3 and Case 4, following the grid code of IEEE Std.

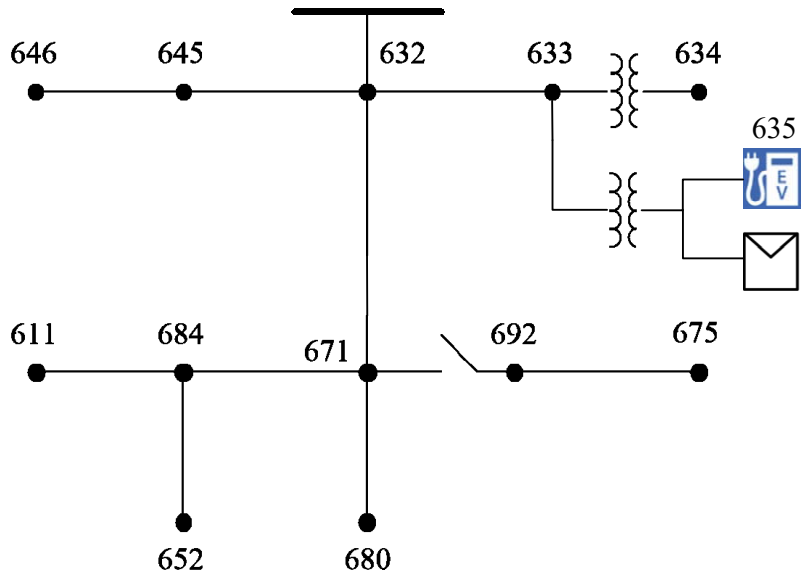


Figure 2.5: The modified IEEE 13-node test feeder.

1547-2018. The DER ride-through priority and mode selection is based on Fig 2.3. The voltage-reactive power setting of the EVCS follow the default setting of the Category B DER requirements and the response time is set to 1 second. The frequency-droop operation of the EVCS during an abnormal condition in the Area EPS follows the Category III DER requirements, the frequency dead-band is set to 0.2 Hz, and the response time is set to 0.2s.

The IEEE 13-node test feeder [71] is modified to test the interconnection impact of the EVCS to the power grid, the one-line diagram of which is shown in Fig. 2.5. The total load is 3.58 MW. We assume that there are 3 same EVCSs with the rated power of 1 MW located at node 635. Hence, the aggregated EVCS capacity is 3 MW. The PV system is also located at node 635 with the capacity of 4 MW and the maximum power point tracking technology with the power factor of 1. We assume a steady-state initial operation of the feeder during a typical summer day, when the EVCSs are charging the EVs with 0.2 MW, and the PV output is 2.17 MW. The nominal line-to-line voltage rating of the feeder is 4160V and the grid supply 1.01 per unit at node 632. The Matlab/Simulink software package is used to run the electromagnetic transient (EMT) simulations and illustrate the EVCS response as DERs. The simulation step is $2.5 \times 10^{-7}$s.

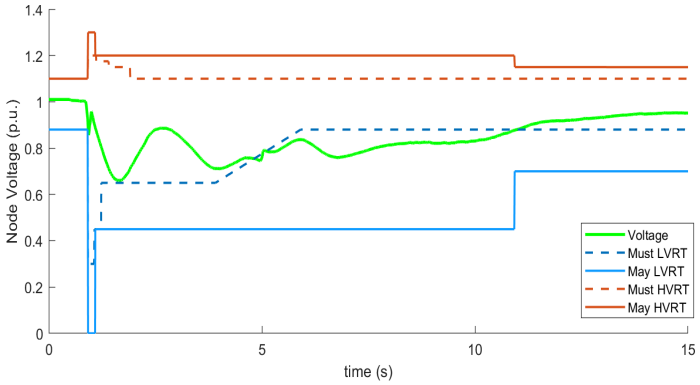


Figure 2.6: Low voltage ride through of the EVCS.

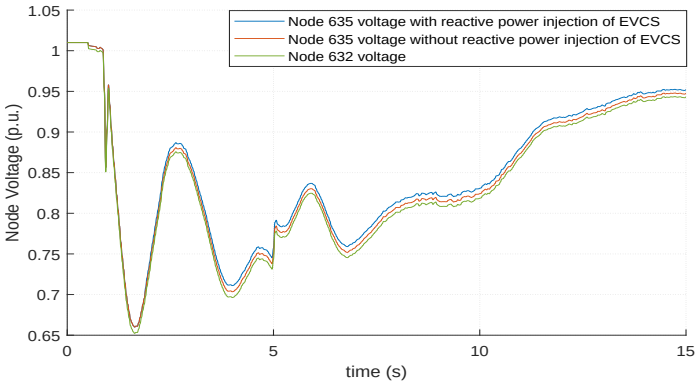


Figure 2.7: Comparisons of the EVCSs voltage response during the transients.

Three-phase programmable voltage source is used as the grid supply at node 632 to generate the *voltage event*, where the EVCSs operate under the voltage-reactive power mode. The EVCS voltage curve is shown in Fig. 2.6. The EVCS can ride through the voltage event and avoid a trip if its design allows for a May Ride Through ranges of the grid voltage. Hence, the EVCSs should be designed and built to withstand specified abnormal conditions and support the grid stability and reliability while still protecting the equipment from damage and ensuring personnel safety. Figure 2.7 shows different voltage responses during the generated voltage event. Compared to the grid voltage at node 632, the voltage at node 635 without reactive power injection of EVCS but with PV power output, is found higher in Case 2. The voltage at node 635 with reactive power injection of EVCS and PV power output in Case 3 and Case 4 is higher than both voltage curves after the required voltage-reactive

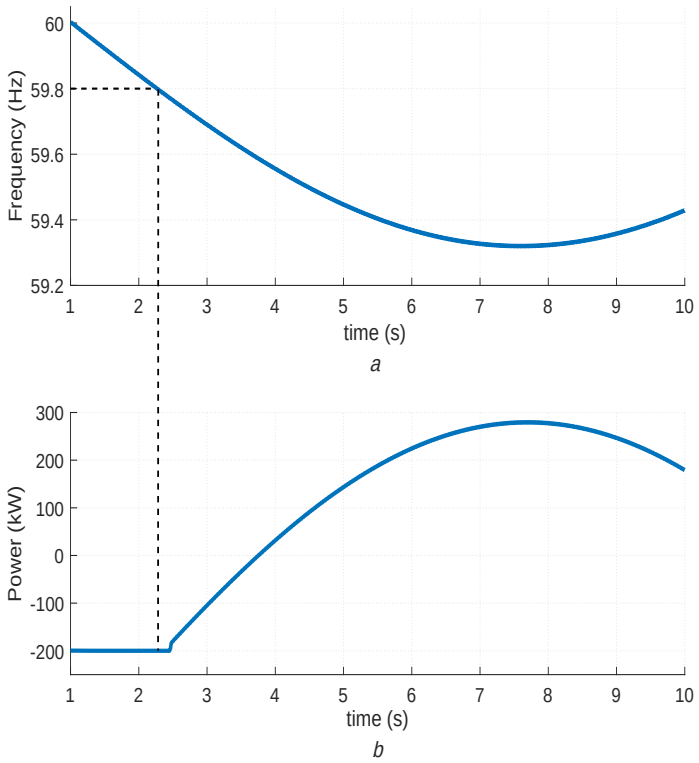


Figure 2.8: Frequency response performance. (a) Frequency of the grid, (b) Frequency response of the EVCS.

power response time. This is because the R and X values of distribution overhead lines in the medium voltage distribution network are similar, where an increase in both nodal active and reactive power will increase the voltage. The reactive power injection to the grid during the low voltage event will bring more benefits when there are induction loads such as air conditioners. However, the EVCSs in Case 3 employing public communication system to select the control mode and monitor the station is more vulnerable than that in Case 4 due to potential communication delays and failures.

A *frequency event* is also generated by the grid supply at node 632 to test the frequency response of the EVSEs. The grid frequency drops starting from 60 Hz at 1 s to 59.3 Hz and then recovers back, as illustrated in Fig. 2.8a. The EVCS responses to the frequency event after 0.2s when the grid frequency reaches its low-frequency dead-band of 59.8 Hz. It can be seen in Fig. 2.8b that instead of charging 0.2 MW before the frequency event, the EVCS

Table 2.2: Index Comparisons in Different Case Studies

| TC | *Rt* | *Sr* | *Cu* |
|---|---|---|---|
| 1 | 138 | high | low to medium |
| 2 | 120 | high | medium |
| 3 | 120 | medium | medium |
| 4 | 108 | low | medium to high |

reduces the charging power and starts to supply power to the grid when the grid frequency declines. Different from the controllable reactive power output that can provide local voltage support, the active power output of all resources can impact the system frequency and wide-area system stability [72]. EVCS frequency support with the frequency-droop design in Case 3 and Case 4 will be more beneficial when the number of EVCSs in the system increases, and is highly effective when the system integrates more intermittent renewable sources such as solar and wind. However, the EVCSs frequency support in Case 3 is more vulnerable to the communication delay and malfunctions as the EV power schedule is managed by the public cloud. In case of successful information acquisition and a cyber attack to public network or cloud, the bulk power system safety is threatened and system wide blackout may happen due to inability to preserve the system stability thresholds.

Based on the above analyses, the EVCS in Case 2 has higher stability risk due to the cyber vulnerability. The EVCS in Case 3 has 'medium' *Sr* value as the EVCS can ride-through the gird disturbance when no cyber hazard occurs. The EVCS in Case 4 has 'low' *Sr* value as the cyber attack probability is low. The EVCS without communication with the utility and cloud in Case 1 will not be affected by the cyber system performance, but the uncoordinated charging increases the chance that the grid operates near marginal conditions, thereby the *Sr* value is 'high'. The *Sr* values for all cases are also included in Table 2.2.

### 2.4.3 Comparisons

As the EVCS in all four test cases use the same facilities in the physical layer, the EVCS in Case 1 features little investment cost for cyber layer and the *Cu* is 'low'. The *Cu* values for EVCS using public communication system in Case 2 and Case 3 are 'medium'. The *Cu* value for EVCSs using isolated communication system is 'high' considering the extra investments in the communication system. However, the EVCS using uncoordinated charging in Case 1 may not over-subscribe the EVSE and require transformer and distribution line upgrades with a higher operation cost. The *Cu* value in Case 1 may then increase. The *Cu* value for the EVCS using the isolated communication system may decrease if the utility has built the AMI with isolated communication system for gird modernization. According to Table 2.2, the EVCS configuration in Case 4 has the lowest risk. While the isolated communication system for EVCSs in Case 4 needs extra investment, it may be preferred by electric utilities.

## 2.5 Conclusion

This chapter discussed several safety considerations around large EVCS [73]. In order to ensure a safe operation environment of the EVCSs, they need to not only follow the safety requirements for EVSEs [74], but also comply with other existing standards and guidelines such as the arc flash boundary [64], grid interoperability [21], periodic inspection [16], fire safety [17], and maintenance related to the EVCS facilities discussed in National Fire Protection Association (NFPA) 70B and Canadian Standards Association (CSA) Z463 [75] etc. We have also analyzed the safety considerations of the proposed EVCS cyber-physical system in different layers. Furthermore, a risk assessment model for large EVCSs is proposed, enabling the EVCS operators to evaluate the electrical safety using the hierarchy of hazard control methods. Numerical case studies demonstrated that the risk assessment model for EVCSs can effectively evaluate the safety considerations of large EVCSs and help informative planning and operation decisions.

# Chapter 3: New Energy Management Scheme Considering Renewables and EVs

## 3.1 Abstract

The proposed EVCS architecture in the previous chapter ensures power system stability during the power grid transients when a disturbance occurs. A centralized energy management system (EMS) architecture is proposed in this chapter to achieve economic operation during the grid steady-state under system normal operating conditions considering large-scale integration of EVs. The philosophy of the proposed two-stage EMS is similar as a double closed-loop control system used for motor speed control, in which the outer loop can handle the system level disturbance and the inner loop enables fast response of the system. The proposed method can be used for optimization of large-scale complex systems in general once the system satisfy the following three conditions (i) established communication system, (ii) the aggregated individual parameters are predictable, (iii) the system dynamics do not vary sharply within a short time-interval.

We first presents the suggested 2-stage EMS architecture. Then we introduces the proposed first-stage optimization problem and the corresponding mathematical formulations for the stochastic economic dispatch (SED). The next section presents the second-stage EV charging strategies under both plug-in and battery swapping modes. Numerical case studies and simulation results are presented, the scalability and optimality of the proposed models are also discussed, followed by the conclusions.

## 3.2 The Proposed Chance-Constrained EMS Architecture

The proposed EMS architecture is illustrated in Fig. 3.1. We assume that both EV operation modes, plug-in or battery exchange, are viable options and customers who prefer exchanging the batteries through the BSS can subscribe in this service. The customers who charge

their EVs under the plug-in mode and do not subscribe in the BSS service can still swap their depleted EV batteries with a higher price. The AMI is utilized to manage the EV energy demand by analyzing the data from smart meters connected to EVs. The EMS design in [34, 76] is modified to integrate the EVs and DERs in modern power grids. The proposed control framework is composed of two stages. The first stage is centered on a SED optimization to determine the hour-ahead dispatch target ($\Delta t_1 = 1$ h) capturing the system uncertainties. The second stage shrinks the control horizon to 5 minutes ($\Delta t_2 = 1/12$ h) and is tailored to an optimal power flow (OPF) mechanism to dispatch the available resources including the controllable loads and storage units with respect to system dynamics and the first-stage targets. In particular,

1. In Stage 1, the SED is solved at time $t$ with an $L_1$-hour look-ahead rolling horizon based on the stochastic model predictive control (SMPC). We assume $L_1$ to be equal to 24 hours. Stochastic forecast of renewable and load profiles, estimated EV energy demand and availability (representing customer behavior), as well as system-wide battery swapping rates are effectively employed in the decision making process. If we assume an OPF look-ahead time window of $L_2$, the states of controllable loads and storage units at time step $t + L_2$ are employed as the boundary conditions in Stage 2, i.e., SED sets a short-term target for the OPF, updated hourly based on the macro system information.

2. In Stage 2, the OPF is solved with an $L_2$-hour look-ahead time window using the certainty-equivalent MPC. The charging constraint for the EVs under plug-in operation mode is updated by the aggregators through the AMI system (Section 3.4.1). The control mechanism of the BSS is discussed in Section 3.4.2. The look-ahead time window starts with $L_2/\Delta t_2$ time steps, and shrinks as time progresses to the next hour. The look-ahead time window will be changed to $L_2/\Delta t_2$ as the next hour starts. Ensuring both system and EV customer behavior constraints, the OPF engine sends the next-time-step dispatch signals to controllable loads, EV aggregators and storage

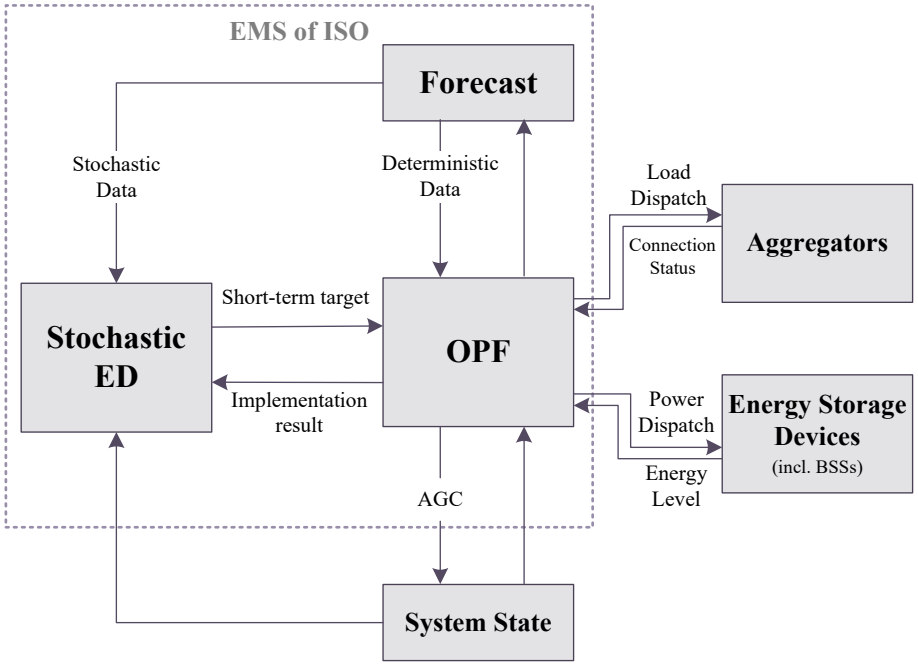


Figure 3.1: Logical view of the proposed chance-constrained EMS architecture

units. Since the OPF engine will first try to meet the system dynamics and then to follow the SED dispatch target, its outcome may be different from the short-term plan in Stage 1. $L_2$ should be set longer than 1 hour so that the OPF does not have to follow exactly the SED dispatch signals. Deterministic forecasts are used in this stage to (i) ignore small deviations between the predicted and the realized data during a short time interval, (ii) compensate possible communication delays, and (iii) enable a fast response to system dynamics. The information and plan asymmetry in the mid-term and short-term stages are compensated periodically.

The forecast errors and dispatch delays of 5 minutes at the second-stage are addressed by the grid primary generation control and automatic generation control (AGC) mechanisms. Once the EVs' dispatch signal is acquired, it will last for 5 minutes and EVs can be regarded as constant power loads. The proposed AMI architecture to achieve the second-stage EV dispatch communication is demonstrated in Fig. 3.2. It is a hierarchical system including smart meters, neighborhood area networks (NANs), and the local area network (LAN) within

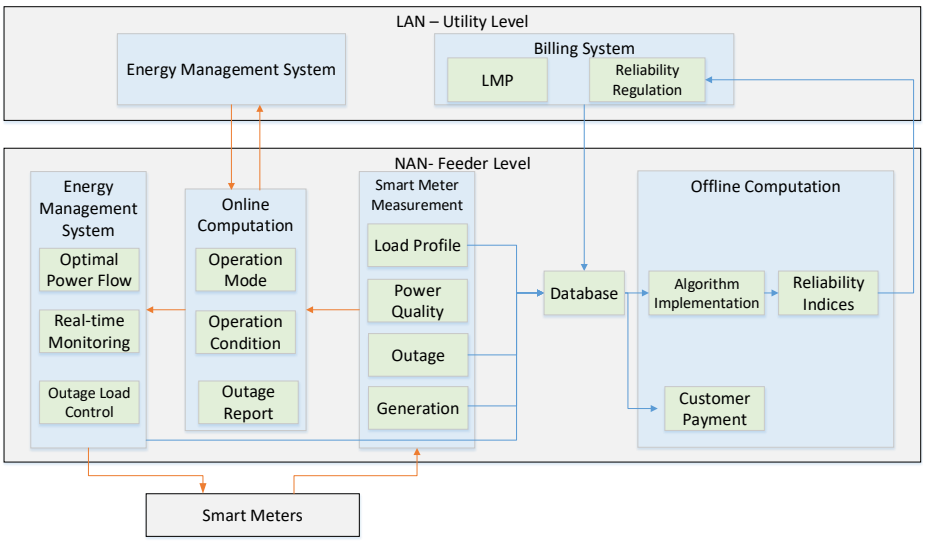


Figure 3.2: Logical view of the proposed advanced meter infrastructure.

the utility domain. In contrast with the conventional AMI structures through which meter data is directly uploaded to MDMS, the proposed architecture contains 2 inter-connected loops: (i) the *online loop* represented by red lines is mainly focusing on grid monitoring and power flow controls. Since the main concerns for the LAN are system operational states and power flow constraints, this online computational platform can swiftly classify and process the measurements and upload the necessary information. The online loop normally transmits data every 2 seconds to 5 minutes; (ii) the *offline loop* represented by blue lines stores all data in the NAN-level database and calculates the reliability indices and upload the results to LAN. The LAN-level billing system then maps different reliability performance levels of system feeders and analyzes the overall reliability of the distribution system. The utility can also send the Locational Marginal Prices (LMP) to the NAN and calculate the electricity pricing at the NAN-level billing system.

This new architecture is suitable for prosumer-oriented smart grids with highly-dense penetration of DERs and can be employed even by electric utilities with high-speed data transfer requirements. The primary advantages of the suggested AMI architecture can be summarized as follows:

- it preserves and protects customer privacy in the physical layer of communication network systems. The customer load profiles are actually to be stored in the NAN networks and will not require to be uploaded into a centralized data center.

- it shrinks the volume of data uploaded into the utility meter data management system (MDMS) platform. With the envisioned online and offline computation loops, the measured data is classified and processed before an upload process starts. All the information can be recorded in the NAN and, hence, the communication capacity requirement from NAN to LAN significantly decreases.

- it brings about potentials for more accurate load forecast and feeder health diagnosis with local weather and temperature information as well as feeder-level data analytics.

- it offers opportunities for fast and efficient energy management in distribution systems. With the suggested online computation loop, Wide Area Networks (WANs) can acquire robust real-time system operational conditions from distribution feeders. Through a system-wide optimal power flow mechanism, the feeder-level energy management signal can be sent to NANs. As NANs gather smart meters data and monitor the feeder in real time, they can determine the operation points of each DER and load control signals for each connected node.

## 3.3 The First-Stage SED Optimization Formulation and Solution Technique

### 3.3.1 Deterministic ED Optimization Model

Focusing on PEVs, let $L_c$ denote the cumulative energy that is expected to be allocated to the PEVs in EVCSs; equation (3.1a) states that the $L_c(k+1)$ during the next time step $k+1$ is the sum of $L_c(k)$ and the actual charging power allocated to PEVs ($u_l$) at the current time step $k$. Equation (3.1b) restricts the PEV demand, and $\varsigma$ reflects the maximum flexibility of

the PEV demand. $u_l$ is limited to the lower and upper bound capacities in (3.1c).

$$L_c(k+1) = L_c(k) + (\alpha_c \Delta t) u_l(k) \qquad \forall k \tag{3.1a}$$

$$0 \ \leq \ L_c(k) \ \leq (1+\varsigma) E_C \qquad \forall k \tag{3.1b}$$

$$u_l^{min}(k) \ \leq \ u_l(k) \ \leq u_l^{max}(k) \qquad \forall k \tag{3.1c}$$

While $E_C$ for the aggregated EVCSs can be predicted and is stable over a day, the charging power constraints are time-dependent and are affected by the charging capacity, number of connected EVs, and charging algorithms. AMI is employed to enable the communication between the utilities and EVCSs. The control and coordination of EV charging by the EVCS is also activated. Therefore, the actual aggregated constraints for EV charging can be calculated and provided to the system operator by EVCSs, and the charging power sent from the system operator to each EVCS can also be implemented through direct load control. The estimated aggregated constraints are based on the day-ahead forecast values. The difference between the estimation and actual implementation can be acquired via AMI and compensated periodically. The online computation loop for the centralized EMS requires an established AMI which can communicate bidirectional signals every 5 minutes.

Focusing on the BSSs, it can be regarded as a storage unit with fixed battery capacity but varying battery swapping demand during each time period. The energy stored in the BSS ($B_s$) and the charging and discharging power ($u_c$ and $u_d$) should be within the corresponding limits. The battery swapping load can be regarded as an additive disturbance to the BSS. Note that $E_s$ includes both the battery swapping load by the subscribed customer and the additive EV load by BEV customers who prefer plug-in charging but their charging demand cannot be met by using the plug-in charging mechanism.

$$B_s(k+1) = B_s(k) + (\alpha_c u_c(k) - (\alpha_d)^{-1} u_d(k)) \Delta t - E_s(k) \qquad \forall k \tag{3.2a}$$

$$B_s^{min} \leq B_s(k) \leq B_s^{max} \qquad \forall k \tag{3.2b}$$

$$0 \leq u_c(k) \leq u_c^{max} \qquad \forall k \tag{3.2c}$$

$$0 \leq u_d(k) \leq u_d^{max} \qquad \forall k \tag{3.2d}$$

It is assumed that the vehicle to grid (V2G) function is enabled in the BSS. So, it can discharge the power to the grid acting as a storage unit. $u_c$ and $u_d$ are power variables observed in the grid side. The multiplication of the two variables is 0 so that the BSS does not charge and discharge simultaneously. However, this constraint is not included in (3.2). The convex problem (3.2) will yield the same results as the non-convex problem with this constraint when the charging efficiency and battery degradation cost are considered. The self-discharge of the batteries is here ignored.

If the communication network latency is high and the AMI only supports the 5-minute bi-directional communication, the aggregated EV load could not provide the frequency regulation services to the system. The proposed first-stage deterministic ED model for the system operator considering the EV load with both plug-in and battery swapping charging mechanisms is presented as follows:

$$\text{minimize} \quad \gamma(L_c(K+1) - E_C)^2 + \sum_{k=1}^{K}(\sum_{i=1}^{n} C_i(P_{G,i}(k)) + 2c_d u_d(k)) \tag{3.3a}$$

subject to

$$\sum_{i=1}^{n}(\Lambda_{R,i}(k) + P_{G,i}(k)) + u_d(k) - u_c(k) - u_l(k) = L_O(k) \qquad \forall k \tag{3.3b}$$

$$P_{G,i}(k+1) = P_{G,i}(k) + \Delta P_{G,i}(k) \qquad \forall k \; \forall i \tag{3.3c}$$

$$P_{G,i}^{min} \leq P_{G,i}(k) \leq P_{G,i}^{max} \qquad \forall k \; \forall i \tag{3.3d}$$

$$\Delta P_{G,i}^{min} \leq \Delta P_{G,i}(k) \leq \Delta P_{G,i}^{max} \qquad \forall k \; \forall i \tag{3.3e}$$

$$\boldsymbol{H} \cdot \boldsymbol{P}_{net}(k) \leq \boldsymbol{F} \qquad \forall k \tag{3.3f}$$

$$(3.1), (3.2)$$

where the objective function (3.3a) minimizes the total dispatch cost by allocating both generation and EV loads. The objective function (3.3a) consists of (i) the penalty cost for the deviations from daily energy consumption of the PEVs, (ii) the quadratic generation cost of conventional generating units, and (iii) the cost for discharging EVs—the degradation cost of EVs are considered when the vehicle to grid (V2G) operating mode results in extra battery cycles to EV customers. Equation (3.1) and (3.2) represent the state and input constraints of EVCS and BSS, respectively. Equation (3.3b) enforces the power balance constraint. Equations (3.3c)–(3.3e) are the state equations for the conventional generating units. Transmission line constraints are expressed in (3.3f). $\boldsymbol{F}$ is the vector of the transmission line flow limits. $\boldsymbol{H}$ is the power transfer distribution factor (PTDF) matrix. $\boldsymbol{P}_{net}$ is the vector storing intermediate calculation of the net generation at buses.

### 3.3.2 Stochastic Chance-Constrained ED Optimization Model

In the first-stage SED problem, the hourly energy consumption by the swapping batteries can be forecasted as a disturbance to the optimization model. Load, wind, and solar forecasts can be also incorporated as additive uncertainties and modeled via probability distributions using weather and historical datasets. We assume the disturbance to be a sequence of independent, identically distributed random variables. Let $w_1$ be the battery swapping energy, and $w_2$ be the net load—the total renewable energy generation minus the total load. We assume that there are enough number of chargers for EVs to connect to. The availability of EVs under a plug-in operation mode depends on the total number of EVs parked, modeled as the charging upper constraint. The estimated daily EV energy consumption in the plug-in mode is modeled as the total controllable load $E_C$ during the next 24-hour interval. The first stage is implemented in a central node, sample-based SMPC method is used to solve the

look-ahead SED problem in a receding-horizon manner, and distributed algorithm ADMM is used to manage the computation time.

The deterministic ED optimization model is reformulated with chance constraints. In other words, (3.3) is re-written to (3.4), which is similar to the general formulation of the SMPC problem [77]. Monte Carlo sampling approach is employed to approximate the SED problem. A finite number of $M$ scenarios are generated, each assigned a probability of $\pi_m = 1/M$. Chance constraints are utilized so that the objective function can minimize the expected cost over all scenarios with the optimization constraints satisfied in most scenarios. Let $x(k) = \{P_{G,1}(k), ..., L_{c,i}(k), B_{s,n}(k)\}$ denote the state vector $x$ at time step $k$, including the real power output of conventional generating units $P_G$, controllable loads $L_c$, and the storage devices $B_s$. The input vector is denoted by $u(k) = \{\Delta P_{G,1}(k), ..., u_{l,i}(k), u_{c,n}(k), u_{d,n}(k)\}$ and the additive uncertainty vector is represented by $w(k) = \{w_1(k), w_2(k)\}$. Instead of the dispatch decisions following the load, we allocate both generation and load to satisfy the power balance constraints and minimize the total economic dispatch cost. The optimization problem is formulated in (3.4):

$$\text{minimize} \quad \sum_{m=1}^{M} \frac{1}{M} \left[\gamma (L_{c,i}^m(K+1) - E_C)^2 + \sum_{k=1}^{K} \left(\sum_{i=1}^{n} C_i(P_{G,i}^m(k)) + 2c_d u_{d,n}^m(k)\right)\right] \tag{3.4a}$$

subject to

$$x^m(k+1) = Ax^m(k) + Bu^m(k) + Gw^m(k) \qquad \forall k \; \forall m \tag{3.4b}$$

$$0 = Cx^m(k) + Du^m(k) + Ew^m(k) \qquad \forall k \; \forall m \tag{3.4c}$$

$$H \cdot P_{net}^m(k) \leq F \qquad \forall k \; \forall m \tag{3.4d}$$

$$u^m(k) \in U(k) \qquad \forall k \; \forall m \tag{3.4e}$$

$$\mathbf{Pr}[x^m(k) \in X(k), \; \forall m] \geq 1 - \varepsilon \qquad \forall k \tag{3.4f}$$

where $A, B, C, D, E$, and $G$ are the state-space system matrices and fixed. $F$ is the vector

of the transmission line flow limits, and $H$ is the PTDF matrix. $P_{net}$ is the vector storing intermediate calculation of the net generation for buses. $X$ and $U$ are the feasible regions for the state trajectory and control inputs, respectively. The cost function (3.4a) consists of (i) the penalty on the deviations from daily energy consumption of the plug-in EVs, (ii) the quadratic generation cost of conventional units, and (iii) the battery degradation cost reflecting the frequent discharge of the BSS power to the grid. We assume the degradation cost for charging the EV batteries are paid by the customers and, hence, the total cost in the objective function only captures the extra cycles of the BSS. Constraint (3.4b) represents the state equation describing dynamics of the energy resources. Constraint (3.4c) enforces the power balance. Power loss is ignored in the model but can be considered by modifying the loads based on the estimate of the total system losses. Transmission line constraints are expressed in (3.4d). In (3.4e), the input variables are restricted to ramp rate limits of generating units, charging capacity of plug-in EVs and BSSs. Chance constraint (3.4f) ensures that the probability of scenarios in which the state variables meet the enforced limits is equal to or larger than $1-\varepsilon$. Hence, the operation constraints are considered to be satisfied in most scenarios. A few operation scenarios may violate the chance constraints. For example, when the load demand at a time is very high while the renewables output is very low, it will then call for power generation from other units. If the online generation capacity is not enough to provide the requisite power, the generation upper constraint will be violated. The system will use either generation reserve to meet the load demand or has to shed some loads.

Formulation (3.4) will result in a different solution in each scenario $m$ at time $t$. The average values of state variables at time $t+L_2$ are calculated, and the operating points of controllable loads and energy storage units are used as the final state targets of the second-stage OPF engine, while the initial state is considered the same in all generated scenarios. The charging state of the plug-in EVs is set to 0 so that the next 24-hours charging demand $E_C$ keeps constant. The residual between the estimated and actual power allocated to the

plug-in EVs is measured and compensated at the next time step. Specifically, we add the penalty on the deviations between $L_c$ at the last time step of the day and the actual remaining energy need to be charged during that day.

### 3.3.3 Convex Approximations of the Chance Constraints

The chance constraint (3.4f) is generally a non-convex formulation and in need of a safe convex approximation to derive a computationally efficient solution. Taking the convex function $\phi(u) = (u+1)_+$, where $(x)_+ = max\{x, 0\}$, gives the Markov chance constraint bound [78, 79]. Convex approximation of the generic $\mathbf{Pr}(f(x,w) \leq 0) \geq 1-\varepsilon$ is expressed as

$$\mathbf{E}(f(x,w)+\alpha)_+ \leq \alpha\varepsilon \tag{3.5}$$

where $\alpha$ is a scalar. The parameter $\varepsilon$ is fixed to 0.05, so a 5% violation of the probabilistic constraints is allowed in the optimization process. The convex approximation of (3.4f) employing the above relaxation approach is given by

$$max(x^m(k) - x^{max})) \leq TU^m \qquad \forall k \; \forall m \tag{3.6a}$$

$$max(x^{min} - x^m(k)) \leq TU^m \qquad \forall k \; \forall m \tag{3.6b}$$

$$\frac{1}{M}\sum_{m=1}^{M}(TU^m + \alpha)_+ \leq \alpha\varepsilon \tag{3.6c}$$

where $TU$ is also a scalar. Therefore, with the convex approximation of the chance constraint, the relaxation formulation of the SED problem remains a convex problem.

### 3.3.4 Distributed Stochastic ED Optimization via ADMM

The ADMM approach is employed in this chapter to speed up the computation of the chance-constrained optimization problem. The state variables in (3.4) are $x_i(k) \in \mathbf{R}^{n\times K}$. We gather $x$ values in all the generated scenarios and form a 3-dimensional matrix $z$ where

$z_i^m(k) \in \mathbf{R}^{n\times K\times M}$. We define $\lambda$ as the scaled dual variable of the ADMM with the same dimension as $x$. The problem can be then rewritten as the global consensus problem [80] with the common global variable $z$. The steps to implement the ADMM procedure are summarized in Algorithm 1.

In step 2, a warm start is realized by solving the certainty equivalent MPC problem of the optimization formulation in (3.4). The suggested warm start can significantly reduce the number of ADMM iterations. In step 4, the problem (3.4a) to (3.4e) is split to a number of smaller MPC problems where scenarios can be solved in parallel. In step 5, the local variables are aggregated to consider the coupling information (3.4f) which is converted to convex constraints (3.6) and the ADMM iterations include solving small convex optimization problems. The MPC problems in $x$-update can be accelerated by customized solvers. The computation time of $z$-updates depends on the total number of samples $M$ and can be solved in only one CPU. 3-dimensional variables were converted to 2 dimensions to solve the optimization problem in this step, in order to further reduce the computation time.

**Algorithm 1** ADMM-enabled SED Optimization.

1: **Inputs:**

system data and operation constraints.

2: **Initialize:**

warm start.

local variables $x^m \leftarrow$ warm start value.

global variable $z \leftarrow x^{1:M}$.

scaled dual variables $\lambda^m \leftarrow 0$.

3: **Repeat:**

4: x-update, each processor solves the MPC problem.

5: z-update, compute $z$ based on coupled constraints.

6: $\lambda$-update, each processor updates scaled multipliers.

7: check the termination criterion, break when satisfied.

## 3.4 The Second-Stage EV Charging Strategy and Signal Communication

The second-stage optimization solves a short-term deterministic DCOPF and enables a two-way communication. Here, the convex DCOPF-based optimization formulation is preferred, since DCOPF is reliable and has a lower computation burden compared to the OPF in AC setting. The DCOPF optimization followed by an AC-feasibility check can ensure that the solutions are feasible in real-world operation of transmission system. The second-stage optimization results in the total power dispatched to all generation resources and the total loads allocated to all EV aggregators at the distribution level. The total aggregated load to all EV aggregators will be proportionally distributed based on the charging capacity upper and lower limits. Distribution line limits can be considered as constraints for the charging stations. The upper bound limits of the aggregator charging constraint—i.e., based on the number of available EVs— can be enforced as the distribution line limit minus the forecasted feeder load.

Following the second-stage dispatch and utility communications with EV aggregators, the reactive power dispatch signal can be sent to charging stations and voltage magnitudes can be compensated locally, combined with regulating transformers in the distribution system. Alternatively, the voltage-reactive power mode can be activated and charging stations can facilitate maintaining the voltage at each node autonomously with lower level control. The IEEE Std. 1547-2018 also requires the DERs to provide a capacity to inject and absorb the reactive power. Hence, the proposed architecture is in line with the current operation and standardized visions, and can be applied directly to the legacy systems in practice. Note that as the proposed model can keep the distribution system active power within the distribution line thermal limits and node voltages within the desired thresholds, only the communication and power flow between the utility and plug-in EVs are modeled (Fig. 3.3). The EV loads are aggregated to the associated bus as additive load and OPF is run at the transmission level. The downstream dispatch signals and the upstream estimation

of the EV charging constraints are transmitted simultaneously. The EMS system and utilities communicate through the wide area network (WAN), the utilities and charging stations communicate through local area networks (LANs), and the charging stations and plug-in EVs communicate through the neighborhood area networks (NANs). Note that the LAN-level signals can be transmitted via the proposed AMI. The NAN level required EV signal collection and direct load control implementation has been validated by the EVCS in [45]. The EV customer privacy is preserved as only the aggregated information is uploaded to the EMS (Fig. 3.3).

### 3.4.1 Control Strategy for EVs under Plug-in Operation Mode

A multi-agent framework is suggested to manage the EVs charging demand under the plug-in mode. The customers only need to set the EV departure time $t_{dep}$ and minimum state of charge (SOC) requirement $E_{dep}$ when they plug in their vehicles, or such information can be populated automatically using a default weekly driving profile. The aggregators receive the above information and SOC data $E_{ini}$ from the smart meters connected to each EV. Aggregators also control the EV charging energy demand at each time interval $k$. The second-stage communication and controls for EVs under plug-in mode are illustrated in Fig. 3.3. It details the signal and data flow among the OPF, EV aggregators and EVs in Fig. 3.1. The following procedure is proposed to charge the plugged-in EVs:

1. *Initialization*:

   (a) Import the EV charging capacity vectors $u_l^{min}$, $u_l^{max}$ based on the EV availability.

   (b) Import the system parameters and forecasts into the EMS and evaluate the first-stage charging vectors.

2. *Main Procedure*:

   At each time interval $k$, the system parameters and the EV model will be updated as follows:

(a) The EMS calculates the total power allocated to the utility $u_l(k+1)$, and the power allocated to the EV group $s$ that is managed by the corresponding aggregator, $u_{l,s}(k+1)$.

(b) The vehicle information $t_{dep}$, $E_{dep}$ and $E_{ini}$ are uploaded from the smart meters to the aggregator database, via which it calculates the charging capacity $u_{l,s}^{min}(k)$ and $u_{l,s}^{max}(k)$ of the EV group $s$.

(c) The aggregator evaluates the charging vector $u_{p,j}(k+1)$ and downloads the control variables to smart meters for EV charging in the next interval.

(d) The EMS replaces $u_l^{min}(k+1)$ to $u_l^{min}(k+4)$ with aggregated $u_l^{min}(k)$, and also $u_l^{max}(k+1)$ to $u_l^{max}(k+4)$ with the aggregated $u_l^{max}(k)$ uploaded from the aggregator database.

(e) Update the SOC of connected EV $j$ with $u_{p,j}(k)$.

In the main procedure above, step pairs (a)-(b) and (c)-(d) can run in parallel. In step (a), $u_l(k+1)$ is allocated proportionally to each EV group $s$. The ratio is actually the mean charging capacity $u_{l,s}^{min}(k-1)$ and $u_{l,s}^{max}(k-1)$ of the EV group $s$ to the mean total charging capacity $u_l^{min}(k-1)$ and $u_l^{max}(k-1)$. We limit the $u_{l,s}(k+1)$ within the range of $u_{l,s}^{min}(k)$ to $u_{l,s}^{max}(k)$ at step (c), so the implementation delay of the proposed charging strategy is 5 minutes (equal to the time-step in Stage 2). We assume that the charging capacity for a large number of EVs does not change drastically within a short time interval, thus the charging capacity at the next 20 minutes is updated with that in step (d). We assume the sliding time window of the EV aggregator is 24 hours starting from the current time interval $k_1$, and $k_{2,j}$ is the departure interval for each EV $j$ at time $t_{dep,j}$. The charging schedule for each aggregator $s$ considering the EVs' departure time and battery SOC is found in an optimization model formulated below:

$$\text{minimize} \quad \sum_j \left(\frac{E_{p,j}(k_1+1) - E_{dep,j}}{k_{2,j} - k_1}\right)^2 \tag{3.7a}$$

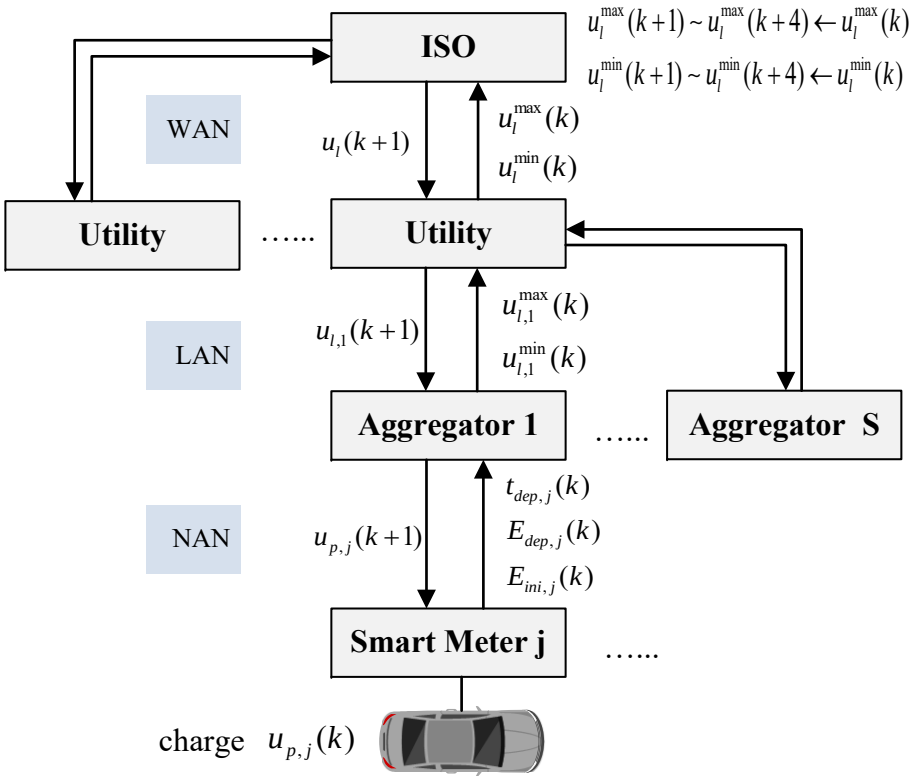


Figure 3.3: EMS communication with plug-in EVs through AMI.

subject to

$$E_{p,j}(k+1) = E_{p,j}(k) + \Delta t \cdot \alpha_c u_{p,j}(k) \qquad \forall k \; \forall j \tag{3.7b}$$

$$\sum_j u_{p,j}(k_1+1) = u_{l,s}(k_1+1) \tag{3.7c}$$

$$E_{p,j}(k_{2,j}) \geq E_{dep,j} \qquad \forall j \tag{3.7d}$$

$$0 \leq E_{p,j}(k) \leq E_{cap,j} \qquad \forall k \; \forall j \tag{3.7e}$$

$$0 \leq u_{p,j}(k) \leq u_{p,j}^{max} \qquad \forall k \; \forall j \tag{3.7f}$$

The optimization model prioritizes the EV charging schedules in (3.7a). Constraint (3.7b) represents the stage functions of EV batteries. Constraint (3.7c) enforces the total charging capacity of the aggregator equal to the power signal sent by the utility. Constraint (3.7d) requires the SOC of the EVs to be higher than the customer minimum requirement upon

departure. Constraints (3.7e) and (3.7f) restrict the EV battery capacity and power, respectively. The $E_{dep,j}$ is set to be 1.2 of the minimum requirement but limited to its capacity. As the EVs' charging capacity and vector are calculated by each aggregator, the problem turns into a moderate size optimization, intact, and can be parallelized. Only the aggregated EV information will be communicated between the EMS and the aggregators. When the batteries of the plug-in EVs are depleted, the customers are assumed to swap their batteries with fully charged batteries at the BSS.

It is worth mentioning that the proportional allocation of the total load $u_l(k)$ to each charging station within its limits ensures that each charging station has a certain level of flexibility. A few EV owners may prefer to minimize the total charging time instead of charging their EV batteries to the required SOC upon departure and enjoy a lower price to charge their EVs. Once the customer sets the EV charging target as to minimize the charging time, from the EV charging station perspective, the upper bound charging constraint remains the same while the lower bound charging demand increases. Through the suggested two-way communication platform, the utility will allocate the power within the charging capacity upper and lower limits to the charging station. The EVs owned by such class of customers with customized preferences will be charged during that time period based on the EV charging priority model listed in equation (3.7). Hence, our proposed EV charging strategy does not rely on strong assumptions of customer behaviors, and can be employed to satisfy different EV customer demands simultaneously.

### 3.4.2 BSS Model for EVs in Battery Exchange Mode

The aggregated BSS model in (3.2) is based on the detailed model presented in [56] in which a single BSS is modeled as a queuing network: the EVs form an open queue and the batteries circulating in a closed queue. It is assumed that the BSS reserves enough number of fully-charged batteries for EVs to exchange as needed, there are enough number of swapping servers and the batteries can be swapped when the EVs arrive. So, the queuing network

Table 3.1: Generator Parameters of the 12-Bus Test System

| Unit $i$ | $a_i$ ($/MW$^2$) | $b_i$ ($/MW) | $c_i$ ($) | $P_{G,i}^{min}$ (MW) | $P_{G,i}^{max}$ (MW) | $\Delta P_{G,i}^{min}$ (MW-h) | $\Delta P_{G,i}^{max}$ (MW-h) |
|---|---|---|---|---|---|---|---|
| $G_1$ | 0.0015 | 5.063 | 66.338 | 450 | 900 | -250 | 250 |
| $G_2$ | 0.0038 | 10.725 | 48.713 | 50 | 500 | -1200 | 1200 |
| $G_3$ | 0.0081 | 10.248 | 81.659 | 50 | 300 | -2400 | 2400 |

characteristic is maintained by the proposed aggregated model. The battery swapping load does not have a direct impact on the power flow balance, and the difference between the forecasted and actual battery swapping load can be considered in the next time interval by the EMS.

### 3.5 Numerical Case Studies

A modified 12-bus test system in [81] is utilized to verify the performance of the proposed EMS architecture. As illustrated in Fig. 3.4, the system consists of 3 conventional generating units: one coal-fired ($G_1$) and two natural gas units ($G_2, G_3$), parameters of which are presented in Table 3.1. The aggregated charging demand for EVs under the plug-in mode is modeled as a controllable load ($L_{c,4}$) and the BSS is regarded as a special energy storage resource ($B_{s,5}$). All the five resources are considered dispatchable. This test system hosts two DER units: a wind farm ($R_1$) and a photovoltaic (PV) power plant ($R_2$) with the total capacity of 200 MW and 120 MW, respectively. Hence, the total capacity of the solar and wind power is 320 MW and features nearly 16% penetration in terms of the total generation capacity. The predicted and actual data for renewable and load forecasts are taken from ERCOT in [82] and the weekly data captured in the week of December 18, 2017 in Texas is utilized in our simulations. The scale factor for wind farm, PV plant, and the load are 1/100, 1/10, and 1/32, respectively. The day-ahead forecasts are replaced by the current-day forecasts in an hour-ahead manner. A Gaussian probability distribution truncated at $\pm 2\delta$ is utilized to represent the load and renewable forecast errors, where $\delta$ denotes the standard

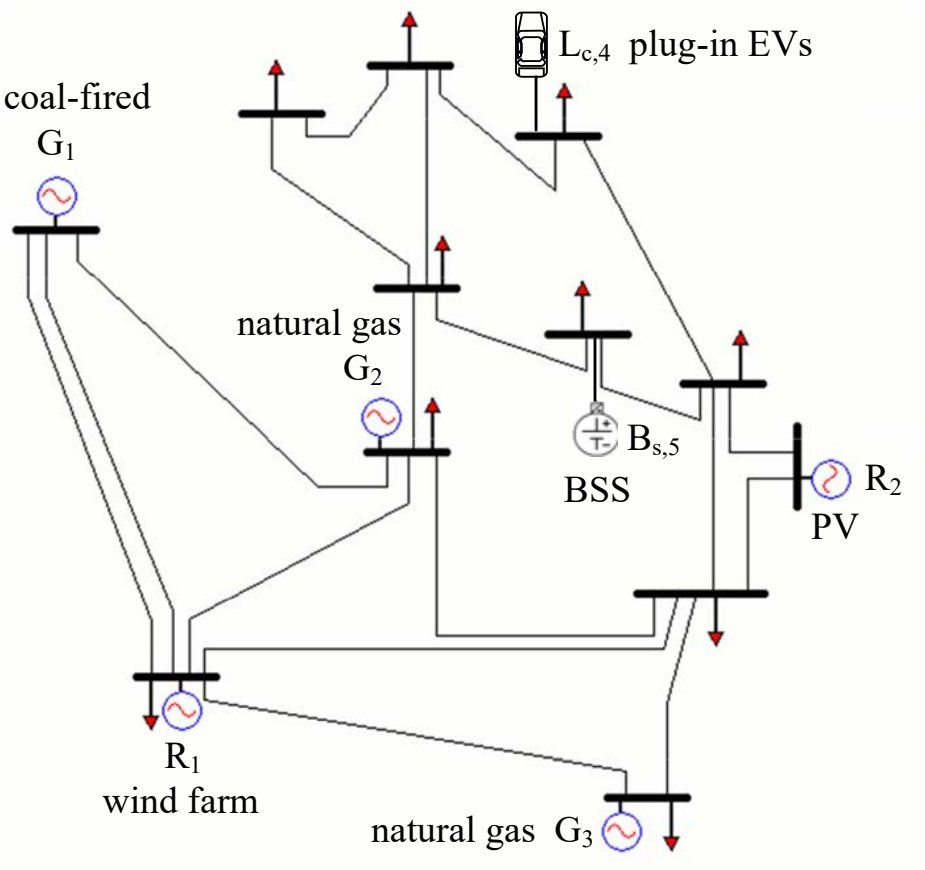


Figure 3.4: The studied testbed: a modified 12-bus test system.

deviation. Uncertainty levels larger than $\pm 2\delta$ is assumed to be handled by load curtailments and generation reserves.

The target area is assumed to be hosting 100,000 EVs accounting for 30% of the total vehicles. The charging/discharging efficiencies are 90%. The EV battery capacity is 70 kWh and $c_d$ is set to 21.4 \$/MWh. There are 70,000 EVs under plug-in mode and the remaining are operated under the battery swapping mode. Driving profiles for EVs under plug-in mode were obtained from the NHTS database [83, 84]. 1000 driving profiles in Texas are randomly selected to account for the customer behaviors of plug-in EVs. The initial SOC of the EVs is uniformly distributed between 0 to 80% of the battery capacity. The charging power is set to 10.2 kW. We also assume that the customers will plug-in their EVs to charge when the parking time is longer than half an hour. Each aggregator is assumed to manage 100 to 200

connected EVs. The BSS capacity is set to 525 MWh. We reserve 20% of BSS capacity for battery swapping, so a penalty will be added when the SOC of the BSS is lower than 20%. The SOC of the BSS could not be lower than 5% in order to protect the batteries. The charge/discharge rate of the BSS is 121 MW. The estimated energy consumption of battery swapping is derived from [85] based on the EV arrival rates. The actual energy consumption of the battery swapping is randomly generated using Poisson probability distribution.

### 3.5.1 Simulation Results

7 days of system operation are examined in the simulations. $L_1$ is equal to 24 hours, and $L_2$ is equal to 3 hours. We evaluate several different test cases (TC): (TC1) the base case, where the optimal solution with complete knowledge of renewables and load curves is found and the EV customers behavior exactly match that of the general estimations; (TC2) the certainty equivalent MPC, in which the uncertain parameters are substituted by the forecasts mean values; (TC3) the SMPC, in which the SED is calculated as one large optimization problem; (TC4) the SMPC, in which the SED is distributed using the ADMM method where $x$-update and $z$-update are solved using CVXGEN and SeDuMi solvers, respectively. Using CVXGEN [86], the $x$-updates can be managed very fast, even executed in series, as each MPC problem can be solved in milliseconds. All test cases are simulated with CVX optimizer in MATLAB 2017a on a Dual 8-Core 2.6GHz Intel Xeon machine.

Comparison results are summarized in Table 3.2. The cost values found in TC2, TC3, and TC4 match the base case (TC1) as the proposed EMS architecture intelligently utilizes both the macro (system-wide) and micro (AMI-recorded) information to dispatch the available resources. The ADMM-enabled SED in TC4 runs 2 times faster than that in TC3. The approximate chance constraints in TC3 and TC4 provide conservative operating points for the plug-in EVs and the BSS. Fig. 3.5 demonstrates that the MPC problem in TC2 requires the BSS to operate at its lower capacity during weekly peak-load intervals, still not as conservative as that in TC3 and TC4. The difference between the operating points and

Table 3.2: System Operation Costs in Different Test Cases

| TC | Total Cost ($) | Execution Time (h) |
|---|---|---|
| 1 | 1,431,438 | 0.1 |
| 2 | 1,459,430 | 34.8 |
| 3 | 1,457,545 | 46.2 |
| 4 | 1,457,391 | 39.8 |

the simulation results in TC3 and TC4 is primarily driven by the ADMM method which ensures an optimal convergence, even with sub-optimal solutions that may vary.

Note that the base case scenario in TC1 assumes a complete knowledge of renewable power outputs, customer load curves and battery swapping curves of BSSs. However, the availability of EVs under plug-in operation mode is modeled as the charging upper constraint, the charging lower constraint is assumed to be 0, and the aggregated EV demand is assumed to be flexible which can be scheduled during the day. Hence, the constraints and the EV demand under plug-in operation mode are the relaxation formulation to the actual EV charging optimization problem. Therefore, the simulation result in TC1 is a computationally tractable lower bound compared with the intractable 'optimal' solution for large-scale EV charging problems caused by the curse of dimensionality. The operation cost difference between TC1 and TC4 is 1.81%, so the optimality gap between the 'optimal' solution and that found in TC4 is less than 1.8%. Note that the optimality gap is primarily driven by the forecast errors.

### 3.5.2 EV Dynamics and Impacts on Grid Operations

The EVs' charging schedules and the aggregated charging constraints evaluated under the plug-in mode are demonstrated in Fig. 3.6. The EVs parking duration less than half an hour is ignored, thus the real-time upper charging constraint is less than that estimated using the EV availability data from the NHTS dataset. It, however, revealed a small impact on the EVs' charging schedules since the maximum charging power sent from the EMS to

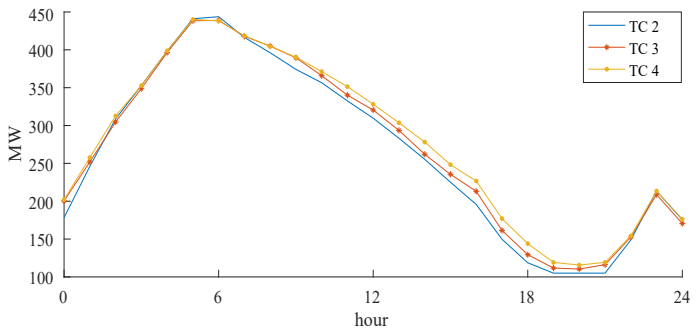


Figure 3.5: 3-hour-ahead SOC operation targets of the BSS: The first-stage SED outcome on Friday, 22 December 2017.

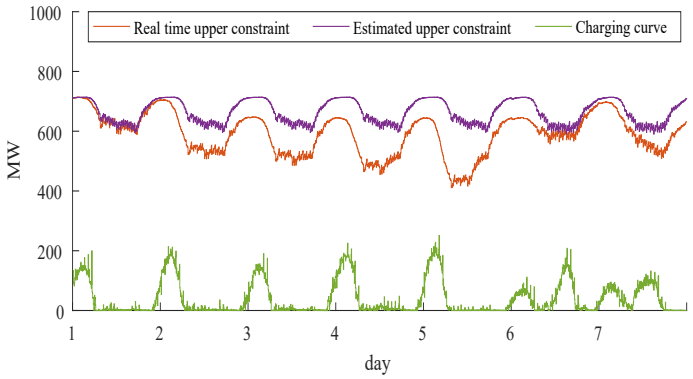


Figure 3.6: The charging curve and upper/lower charging constraints of the aggregated EVs under plug-in mode.

aggregators is less than 250 MW. EVs under plug-in mode will charge mostly during the night load valley and a few charge the minimum required energy during the day-time peak hours. The real-time lower charging constraint is nearly 0 which is not included in Fig. 3.6.

Penetration of EVs and DERs will significantly affect the SED solutions. According to Fig. 3.7, the impact of EVs alone on the load profile is not significant with no obvious super off-peak EV charging hours. If both EVs and DERs are considered, the modified net load profile can be characterized as the difference between the original load plus the EV demand and the DER power generation plus the BSS discharge. Hence, the load profile will then change sharply as demonstrated in Fig. 3.8. The system minimizes the total operation cost which reduces the load variations. The increased noise in the load profile is primarily driven by the system uncertainties and communication delays.

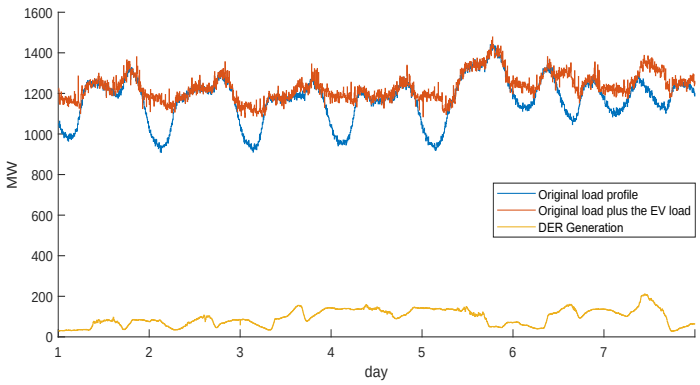


Figure 3.7: Comparison of the original and the modified load profiles with 16% renewable and 30% EV penetration, when only EV load impact is considered.

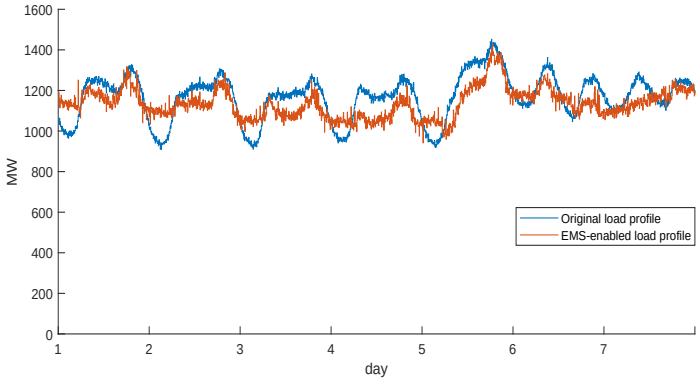


Figure 3.8: Comparison of the original and the EMS-enabled load profiles with 16% renewable and 30% EV penetration.

### 3.5.3 Solution Robustness

The estimated energy consumption of the EVs under plug-in mode in the next 24 hours may be different from the real energy demand, or in some cases depending on the weekly loading conditions and weather variations, the utility may desire to adjust the $E_C$ to increase the daily energy charged by the plug-in EVs when the next-week forecasts are available. Although the real-time upper constraint for the plug-in EVs will decrease and is different from the estimated value, the system will still stably operate within the operating limits as the OPF acquires the real-time maximum and minimum charging constraints of the plug-in EVs. The aggregated SOC of the connected EVs and the difference between the charging demand and the actual energy charged can be uploaded to the SED engine routinely, through

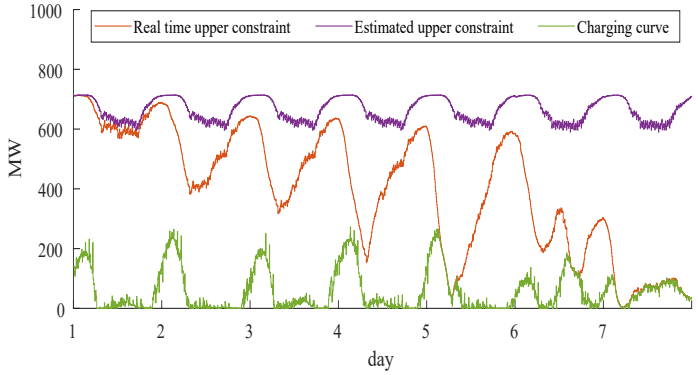


Figure 3.9: The charging curve and charging constraints of the aggregated EVs with 1.5 $E_C$ in TC4.

Table 3.3: Computation Time vs. Different Number of Samples

| M | 50 | 100 | 200 | 300 | 400 | 500 |
|---|---|---|---|---|---|---|
| TC3 (s) | 108 | 252 | 712 | 1265 | 2015 | 3027 |
| TC4 (s) | 42 | 74 | 180 | 318 | 561 | 751 |
| time ratio | 2.58 | 3.39 | 3.96 | 3.98 | 3.59 | 4.03 |

which the SED can adjust the charging demand accordingly. Fig. 3.9 illustrates the charging curve with 1.5 $E_C$ in TC4 where the system is observed to be robust. We reduce 60 MW in $E_C$ when the aggregated SOC reaches its 80% capacity. But the aggregated SOC of the plug-in EVs will still reach to 99.1% at the end of the 7th day and there is 148.1 MWh unfulfilled charging demand. The $E_C$ can be then adjusted back to the original value or less at the beginning of the next week.

### 3.5.4 Sensitivity Analysis and Role of Uncertain Parameters

#### 3.5.4.1 Performance of the ADMM-Enabled SED

The execution time reported in Table 3.2 reflects the system simulation run time in 7 days and includes the time of solving hourly SED optimization, 5-minute DCOPF optimization, and dynamic simulations of the driving profiles for EV customers under plug-in mode. The number of samples $M$ in the first-stage SED problem—which was set 100 in the simulations—

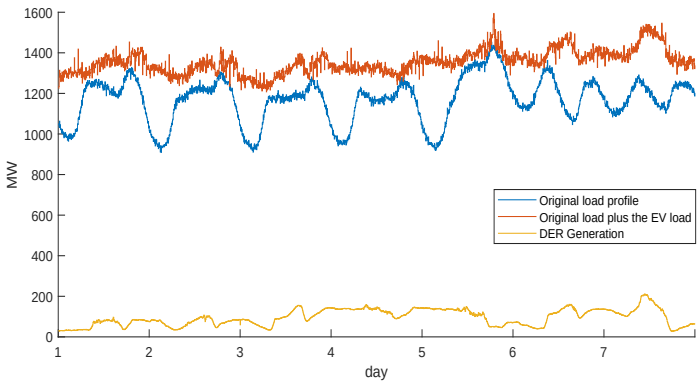


Figure 3.10: Comparison of the original and the modified load profiles with 16% renewable and 90% EV penetration when only EV load impact is considered.

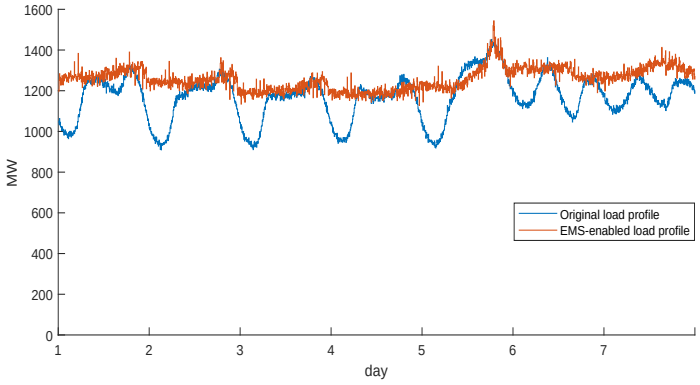


Figure 3.11: Comparison of the original and the EMS-enabled load profiles with 16% renewable and 90% EV penetration.

has a significant impact on the performance of the SED problem as the total number of variables is $269 * M$. The sample-based SMPC method is robust to any distribution of uncertainties as the suggested approach is based only on samples that are generated from the distributions, and does not rely on certain types of distributions. But the computation time increase exponentially as the number of samples increases. The sensitivity of the average computation time of the first-stage SED problem with variations in $M$ is shown in Table 3.3. With the same samples, ADMM-enabled SED in TC4 has a better performance than the large-scale SED optimization in TC 3 and the difference in computation time can be further highlighted as $M$ increases. Deterministic sampling can be applied to keep a medium number of samples, while ensuring the SMPC convergence.

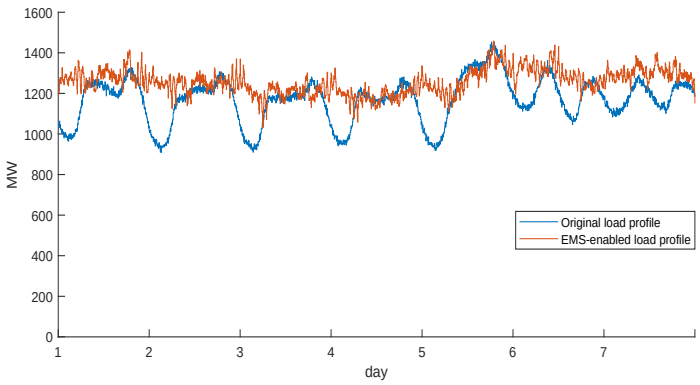


Figure 3.12: Comparison of the original and the EMS-enabled load profiles with 16% renewable and 90% EV penetration, and with additive battery swapping demand forecast.

#### 3.5.4.2 Massive Penetration of EVs

The weekly peak load is realized at 7 p.m. on Fridays as shown in Fig. 3.7. With 30% EV penetration in the grid, the SOC of the BSS reaches 20% of its capacity at 8 p.m., thus even if the forecast of the additive battery swapping consumption of the unsubscribed EV customers is not considered, the BSS charging to avoid the penalty of its SOC below 20% will not create a new weekly peak. However, when the EV penetration level exceeds 60% to 90%, the BSS reaches 20% of its capacity at or before 7 p.m. even with the SED approach applied. The BSS will charge during weekly peak loads to avoid the penalties and creation of a new peak. If only the EV load impact is considered, Fig. 3.10 shows that the new peak is 1594 MW at 7 p.m. on Friday night with 90% EV penetration. If both EV load and DER generation impacts are considered, Fig. 3.11 shows that the new peak at that time is 1544 MW, and there will be no obvious peak and off-peak time for the EMS-enabled load profiles except the weekly peak time periods. One could realize that the additive battery swapping demand could not be ignored in cases with high EV proliferation. If the actual $u_s$ (from the simulation results with 90% EV penetration in Section 3.5.1) is considered as the predicted $u_s$, the updated results reveal that it can avoid the simultaneous occurrence of the peak and the BSS minimum SOC by setting the BSS reaching 20% of the capacity at 8 p.m. again. The new EMS-enabled load profiles with additive battery swapping demand forecast

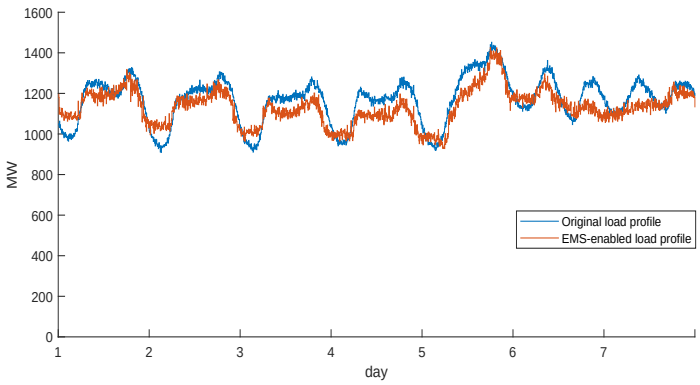


Figure 3.13: Comparison of the original and the EMS-enabled load profiles with 16% renewable and 30% EV penetration, with increased BSS customers from 30% to 70%.

is shown in Fig. 3.12.

#### 3.5.4.3 High Rate of EV Customers Subscribing the BSS Service

We assume that a sufficient number of charging facilities for the plug-in EVs exists in all scenarios and the BSS capacity does not change. With high percentage of customers subscribing the BSS service, the BSS could not fully fill the off-peak load valleys due to the capacity limits and very low battery swapping rate during the night. The BSS will charge the remaining demand during daytime off-peak hours to meet the swapping peak during 4 p.m. to 6 p.m. and avoid the minimum SOC at the peak time 7 p.m. The new EMS-enabled load profiles with 30% EV penetration and 70% subscription to the BSS service can be seen in Fig. 3.13, where the load variation is larger compared with that in Fig. 3.8. In practice, PVs can be good companions for the BSS with limited capacity. It is worth mentioning that even the BSSs are assumed to reserve a 20% capacity for battery swapping, one BSS with limited capacity may still occasionally run out of fully-charged batteries. The BSS may swap a not-fully-charged battery to the EV customer. From a system prospective, it can be regarded as a source of uncertainty for the battery swapping consumption, and will be managed in the next time interval by the EMS since it does not directly affect the power flow balance. Future research with detailed models should be devoted to the impact of BSSs

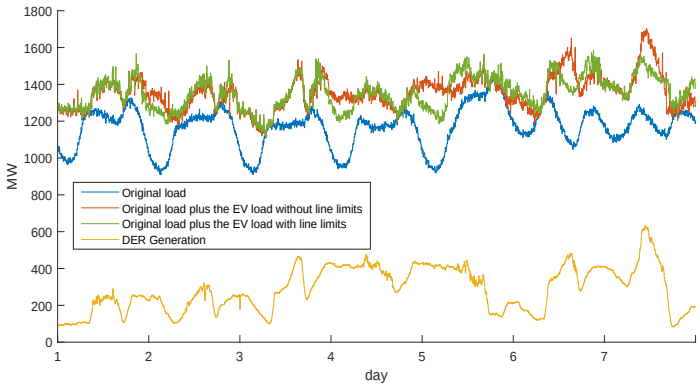


Figure 3.14: Comparison of the original and the modified load profiles with 36% renewable penetration and 90% EV penetration when only EV load impact is considered.

capacity on the grid operation.

#### 3.5.4.4 Increasing Penetration of Renewables

The renewable output with 16% renewable penetration and 90% EV penetration in the grid can be seen in Fig. 3.10, where EV load shows a characteristic of valley filling most of the time. The 12-bus test system in the case study is actually a modified IEEE 14-bus test system where no transmission line constraints are provided. Neglecting the transmission line thermal limits and when the power output of the wind and solar resources becomes 3 times larger than original, the EV load represented by the red line in Fig. 3.14 will present a characteristic of renewable-follower instead of valley-filler. However, the new proposed EMS engine will still try to reduce the daily variation of peak and off-peak load (see Fig. 3.15), as similarly observed in Fig. 3.11. This is because the optimization objective is to minimize the system total operation cost by dispatching both generation and EV loads.

The transmission line thermal limits can be added when congestion needs to be considered. If we assume the thermal limit for both transmission lines connected to the bus with plug-in EV load is 150 MW, Fig. 3.14 demonstrates that the renewable-follower characteristic of the plug-in EV load with line thermal limits is degraded compared to the case where the thermal limits are neglected, especially during the 7th day with high renewable

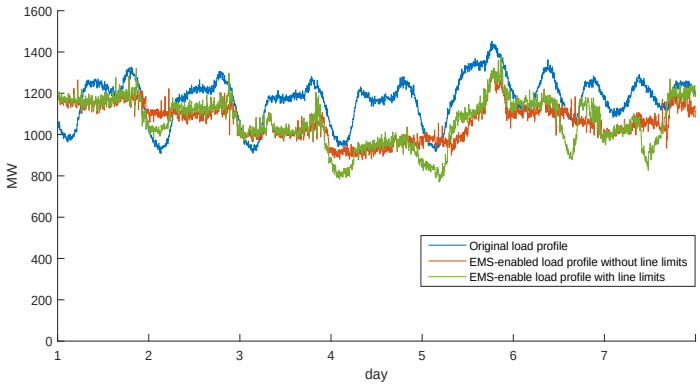


Figure 3.15: Comparison of the original and the EMS-enabled load profiles with 36% renewable and 90% EV penetration.

generation. This is because the transmission line limits can affect the system capability in dispatching EV loads to minimize cost. As a result, the reduction in daily peak and off-peak load variation in EMS-enabled load profile when the transmission line limits and congestion are considered is not as obvious as the case when such limits are ignored (see Fig. 3.15). The operation cost in TC1 for this scenario is found $ 1,297,491, while it is observed $1,323,796 in TC4 (the optimality gap in this case is less than 2.0%).

### 3.6 Discussion on Scalability and Optimality

In this section, the IEEE 118-bus test system is employed to evaluate the scalability of the proposed framework and the optimality of the suggested models. The test system specifications are taken from [87] with the following modifications: Two wind farms with rated power of 750 MW and 500 MW are placed at bus 25. One solar farm with a rated power of 650 MW is placed at bus 33. Hence, the total power capacity of the renewable sources is 1900 MW which features nearly 16% penetration in terms of the system total generation capacity. While the predicted and actual data for renewable and load forecasts are taken the same as those in Section 3.5, scale factors of 1/16, 1/1.85, and 1/12.8 are applied for wind farms, PV plant, and the load, respectively. Truncated Gaussian probability distributions are used to represent the load and renewable forecast errors. 60 Sobol quasi-random samples

Table 3.4: System Operation Costs in Different Test Cases for the IEEE 118-Bus Test System

| TC | Total Cost ($) | Execution Time (h) |
|---|---|---|
| 1 | 10,847,324 | – |
| 2 | 10,985,851 | 35.2 |
| 3 | 10,970,532 | 44.9 |
| 4 | 10,979,744 | 44.6 |

are employed in order to reduce the number of samples and enhance the computational efficiency of the sample-based SMPC optimization. The system is assumed to have 300,000 EVs accounting for 30% of the total vehicles. There are 210,000 EVs under plug-in mode and the remaining are operated under the battery swapping mode. The controllable load for EVs under the plug-in mode is placed at bus 115, and the BSS is placed at bus 117. Other assumptions for plug-in EVs and BSSs are the same as those presented in Section 3.5. The same simulation configuration in Section 3.5.1 is also used except that the CVXGEN solver is not used in the $x$-update of TC4, as this solver is only suitable to solve small and moderate-size MPC problems rather than large MPC problems [86].

### 3.6.1 Scalability

Computation comparison results of different test cases on the IEEE 118-bus test system are summarized in Table 3.4. Similar to those presented in Section 3.5.1 on the 12-bus test system, the cost values found in TC2, TC3, and TC4 match that of the base case scenario (TC1). However, due to the curse of dimensionality, the programming platform (MATLAB) failed to compute TC1 with a time step of 5 minutes. We, instead, used the hourly data to compute the results in TC1. Each first-stage SED problem in TC3 which is calculated as one large optimization problem can still be computed within 5 minutes since deterministic samples are used and computation time of each SED problem is $\sim$240 seconds. The total computation time of the ADMM-enabled SED in TC4 achieves only

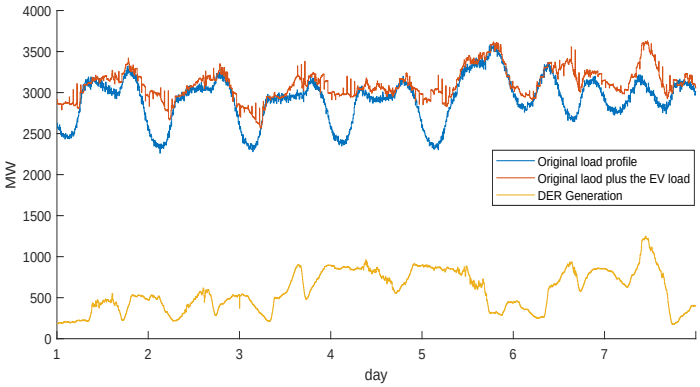


Figure 3.16: Comparison of the original and the modified load profiles with 16% renewable and 30% EV penetration in the IEEE 118-bus test system when only EV load impact is considered.

a little faster performance than that in TC3. The degraded performance in TC4 is caused by the non-customized solver for MPC problems and also the limited available CPU cores (16 cores) to solve the $x$-update (which has 60 samples and results in 60 MPC problems) of ADMM method in parallel. One can conclude, from the comparison results, that the proposed chance-constrained EMS is scalable to large power grids. Note that the ADMM method to accelerate the computation speed of the first-stage sample-based SED problem in large-scale power grids requires additional CPU cores if customized MPC solvers are not used. One needs to note that the proposed second-stage EV charging strategy is also scalable in terms of the number of EVs. This is because EV aggregators are employed to monitor and manage the charging schedules under the plug-in mode. The charging priority of EVs is calculated in parallel (simultaneously) for each EVCS during each charging period. Hence, the computation and communication requirements for the second-stage EV scheduling problem are not burdensome, and the network size will not play a significant role.

### 3.6.2 Optimality

The penetration levels (in percentage) of renewables and EVs in this case are kept the same as in Section 3.5.1. The total generation capacity of the IEEE 118-bus test system is, however, much higher than its original load compared with the 12-bus test system; as

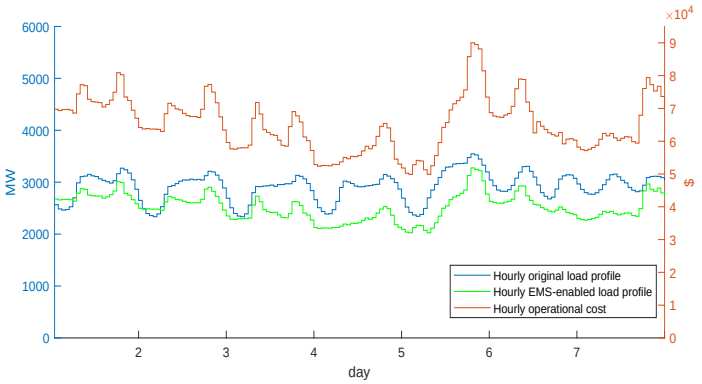


Figure 3.17: Comparison of the original and the EMS-enabled hourly load profiles with 16% renewable and 30% EV penetration in the modified IEEE 118-bus test system, and the system hourly operation costs. The y axis corresponding to the EV load is located on the left, and that of the system operation cost is on the right.

a result, the renewables in this case will supply more load in percentage than that in the 12-bus test system. As shown in Fig. 3.16, the flexibility of the EV load is utilized to either fill the super off-peak of the original load during the night, or follow the renewable output when the renewable generation is high. Similar to Fig. 3.8, Fig. 3.11, and Fig. 3.15, the proposed EMS engine minimizes the total operation cost and reduces the load variation (see Fig. 3.17).

The operation cost difference between TC4 and TC1 is evaluated 1.2% (i.e., the optimality gap of less than 1.2%). Overall and during all simulations, the optimality gap of the proposed approach is found less than or equal to 2% under different penetration levels of renewables and EVs and on different test systems. The numerical results demonstrate that the proposed method achieves a nearly-optimal solution based on the forecast accuracy available in the utility industry practices. In particular, the performance of the proposed method is mainly dependent on that of the first-stage SED problem, i.e., the second-stage DCOPF is the deterministic optimization problem based on the first-stage calculations, and the EV charging scheduling model in equation (3.7) only tries to maintain the EV flexibility and prioritize the EV charging schedule. The first-stage SED problem is formulated as an SMPC problem which can achieve a nearly-optimal solution when a good forecast is available.

The good forecast and system state estimation can be obtained by the proposed two-stage architecture through system level prediction and two-way communications. The optimality is maintained when using the convex relaxation of the chance-constraint optimization to solve the SMPC problem. Hence, the proposed model guarantees a nearly-optimal solution during most of the scenarios.

## 3.7 Conclusion

With the growing penetration of renewables and EVs in modern electrified power grids, advanced EMS designs are required to address the intensified system uncertainties and high-demand flexibility requirements. A two-stage chance constrained EMS architecture is proposed in this chapter [88], where in the first stage, the system-level forecast information embedded in an stochastic MPC algorithm is utilized to optimize the short-term (next 24-hour) energy dispatch of flexible loads and storage units, while the second stage implements the dispatch signals with respect to system security and real-time requirements. The proposed EMS architecture successfully captures the real-time heterogeneous randomness in the grid and of customer behaviors—harnessing a full advantage of both macro (system-wide) and micro (AMI-captured) data—to model and dispatch the time-dependent controllable sources (e.g., EVs and storage units). Different EV charging modes and their impacts on the grid operation were extensively analyzed through which the suggested control mechanism was proven robust as it tries to meet the first-stage targets without violating the motion constraints of the individual objects. With the AMI and BSS in place, EV charging management is done via aggregators and EVs under plug-in mode were able to fill the off-peak load valleys with no large load spikes. Promising a low computational burden with an embedded distributed algorithm (ADMM) and parallel computing, the proposed EMS architecture only communicates the aggregated data and can be effectively utilized for dispatch optimization in large-scale integrated transmission and distribution models.

# Chapter 4: Aggregated EV Load Modeling and Associated Flexibility

## 4.1 Abstract

Different EV charging methods and charging levels result in different load characteristics in the power grid, that if aggregated, influence the power grid operation. The existing EV charging demand models are either based on the charging status upon EV arrival or smart charging algorithms reinforced with particular charging methods and/or charging levels. The coordination of low level control and high level energy management system in previous chapters can ensure the safe and secure operation of the power grids under both transient dynamics and steady-state conditions. This chapter proposes a new data-driven approach for EV charging load modeling. The multi-timescale flexibility of aggregated EV load is also quantified in the chapter using the proposed control and energy management scheme.

The suggested EV load models and associated flexibility metrics is first presented. Then we introduce the mathematical model formulated to consider different charging mechanisms and communication delay scenarios between EVs and the power system. The interactions between the EV charging loads and the power grid are then simulated through a two-stage energy management system (EMS), where the model parameter identification is accomplished through simulations. Several aspects of the proposed models are discussed along with the numerical case studies and simulation results.

## 4.2 Aggregated EV Load Modeling

In this section and in order to accomplish the aggregated EV load modeling, several assumptions are made: (i) there exist sufficient number of EV charging infrastructure in the grid, (ii) the EV customer can select the charging mechanism based on his/her priorities and preferences. The supply and demand interactions in the market enforce the need for a

certain level of adequacy in EV charging infrastructure. The plug-in EVs (PEVs) including battery EVs (BEVs) and plug-in hybrid EVs (PHEV) using conductive charging with level 1 and level 2 charging mechanisms are assumed to deploy smart charging algorithms; that is the energy demand of such EVs needs to be met upon EV departure. Furthermore, the PHEV load can be curtailed and gasoline can be used instead when necessary. The BSSs are assumed to have routine BEV customers who subscribe to the battery swapping services; also, the BEV customers who prefer to use the plug-in charging mode can still swap their batteries when the EV batteries are depleted and plug-in charging mode could not satisfy the next trip energy demand requirement. The BEV customers can alternatively use FC mechanisms. The aggregated EV load of the FC stations (FCSs) are assumed to be inelastic with no flexibility. Thus, the flexibility of aggregated EV load is largely driven by the EV load characteristic of the EVCSs and the BSSs.

### 4.2.1 Steady-State EV Load Characteristics

Many EV customers charge their EVs in the EVCS with level 1 and level 2 charging mechanisms. Equation (3.1) can be modified to (4.1) to consider PHEVs. Equation (4.1a) states that the $L_c(k+1)$ during the next time step $k+1$ is the sum of $L_c(k)$, the actual charging power $u_l$ allocated to PEVs, and the power curtailed from the PHEVs but met by the gas stations $u_{ls}$ at the current time step $k$. Equation (4.1b) restricts the PEV demand, and $\varsigma$ reflects the maximum flexibility of the PEV demand. $u_l$ and $u_{ls}$ are limited to the lower and upper bound capacities in (4.1c) and (4.1d), respectively.

$$L_c(k+1) = L_c(k) + \alpha_c \Delta t (u_l(k) + u_{ls}(k)) \qquad \forall k \tag{4.1a}$$

$$0 \;\leq\; L_c(k) \;\leq (1+\varsigma) E_C \qquad \forall k \tag{4.1b}$$

$$u_l^{min}(k) \;\leq\; u_l(k) \;\leq u_l^{max}(k) \qquad \forall k \tag{4.1c}$$

$$u_{ls}^{min}(k) \leq u_{ls}(k) \leq u_{ls}^{max}(k) \qquad \forall k \tag{4.1d}$$

It is assumed that the customers with PHEVs prefer to charge their vehicles in the EVCS, as the electricity cost is normally 2 or 3 times less than gas. However, when the cost of electricity is higher than that for the gas, e.g., during the peak hours of a year, both customers and the system operators are willing to let the PHEVs to fill the gas. The PHEV charging requests will be declined by the EVCS and the energy demand will be met by gas stations. So, the actual $u_{ls}$ can be recorded by the smart meter. The estimated values of $L_c$ and $u_{ls}$ do not include the gas use for routine PHEV travels.

Based on (4.1), the aggregated EVCS load at each bus can be regarded as virtual batteries, where the battery energy of the PEV load increases gradually, and the charging constraints vary with time. When the uncontrolled charging strategy is employed, it will render little load flexibility to the grid. The EV load will be then modeled as inelastic load. This can be reflected in (3.1c) since the upper bound and lower bound charging constraints are equal. However, since it is assumed that there is sufficient number of charging infrastructure available in the system, there will be a large number of EVs connected to the grid as vehicles are not moving most of the time during a day. Some EVs only have a few miles of trip during a day and the EV can be charged even in the next day. The flexibility of individual EV loads is dependent on the daily driving miles and EV idle time. If the EV load is flexible and the required charging demand that needs to be met is longer than 24 hours, it is defined as a *fully controllable* EV load. The EV load that can offer some flexibility in time, but has to be charged within 24 hours, is defined as *deferrable* EV load. A few PEV load needs to be charged immediately once plugged-in as they are heavy-duty inelastic loads. With the proper charging priority and charging power schedules, a certain level of flexibility provided by the aggregated PEV loads could be maintained in the power grid. Some power system operating conditions that influence the daily total energy allocated to PEVs, e.g., during outages, would also affect the EV load flexibility. Fig. 4.1 shows the state transition of PEV


Figure 4.1: Transition of EV load flexibility.

loads in terms of system flexibility. It is worth mentioning that some of the customers may charge their EVs at private places not observable by the system operator. Hence, these EV loads could not be controlled and can be regarded as inelastic loads. They can be aggregated to traditional loads and forecasted using load forecasting algorithms. Hence, the EVCS load model can still be effectively represented by (4.1) when the smart charging and private charging networks are not strongly coupled.

Focusing on BSSs, the aggregated EV load model of the BSS in (4.2) remains the same as (3.2). The aggregated BSS load at each bus can also be regarded as virtual batteries. Similar to regular batteries, the BSS has fixed energy and power capacity. Moreover, its flexibility is also affected by the battery swapping load. The BSSs typically reserve some fully-charged batteries for EVs to swap. When a large number of EVs need to swap the batteries, and at the same time, the BSS has minimum number of batteries in reserve, the BSS will charge the batteries even during the peak load period to satisfy the demand, and the BSS is regarded as inelastic load. Otherwise, with enough energy and power capacity, the BSS can meet the daily battery swapping load economically and also increase or decrease the daily charging demand flexibly. Hence, Fig. 4.1 could also represent the state transitions of BSSs.

$$B_s(k+1) = B_s(k) + (\alpha_c u_c(k) - (\alpha_d)^{-1} u_d(k))\Delta t - E_s(k) \qquad \forall k \tag{4.2a}$$

$$B_s^{min} \leq B_s(k) \leq B_s^{max} \qquad \forall k \tag{4.2b}$$

$$0 \leq u_c(k) \leq u_c^{max} \qquad \forall k \tag{4.2c}$$

$$0 \leq u_d(k) \leq u_d^{max} \qquad \forall k \tag{4.2d}$$

Focusing on high power FCSs, the aggregated FC load is modeled as inelastic load and it can be forecasted directly using load forecasting algorithms. Note that reference [57] shows that the charging sessions for fast charging over the day follows a distribution where the charging sessions are mainly concentrated around the center of the day. The practical FCS operation data in [89] also indicates that the aggregated FC demand follows a certain curve and is predictable. Hence, the uncertainty of the FC EV load can be treated similar to that for traditional loads.

### 4.2.2 Dynamic EV Load Characteristics

EV loads can be regarded as constant power or constant current loads during the transient operating states; the dynamic behavior of the aggregated EV loads is, however, mainly decided by the EVCS controllers. If the EVCS design in [73] is used, both PEVs and BSSs can respond to system disturbances and try to ride-through during the system abnormal operating conditions automatically. Note that this is achieved through a decentralized architecture, where real-time communication between the EVSE and the EVCS or BSSs is available.

The dead band for the frequency response provided by the inverter-based loads is typically set as $\pm 0.2$ Hz [73, 90], and the EV load can provide frequency regulation services during the system normal operating conditions. The Automatic Generation Control (AGC) signals are sent from the system operator every 2 to 4 seconds, so the real-time communication between the EVCS and the utility is also required. The EVCS and BSS loads can respond to the frequency signals, e.g., the *RegD* signal from the Pennsylvania-New Jersey-Maryland Interconnection (PJM) market, where PJM is a regional transmission organization (RTO) in the northeastern United States that coordinates the movement of wholesale electricity in all or parts of 13 states and the District of Columbia. The actual power for EVSEs

is, hence, the sum of the dispatch and regulation power. As *RegD* signals are conditional neutrality signals, the EVCS can detect the actual EV SOC when the regulation signal is back to the neutrality; therefore, it will have little impacts on the dispatch during system normal operating conditions. The EVCSs and BSSs reveal a high performance in following the *RegD* signal, so the revenue achieved by providing this ancillary service is mainly dependent on the regulation capacity that the EV load could offer. Once the economic operation base-point of the EVCS is decided by the economic dispatch optimization, the EVCS can follow the regulation signals based on the operation base-point. The high and low regulation limits must fall within the EV charging and discharging power constraints, and the regulation limits are the sum of the PEV and BSS regulation bands as enforced in (4.3a). It is here assumed that the ratio of regulation capacity to the regulation limits is $\alpha_r$. We also assume that the frequency regulation capacity needed for the system is $f_c^{max}$ and the regulation up and down capacities are symmetric. The frequency regulation capacity ratio that all storage units can provide in the system is $\beta_r$. The actual frequency regulation capacity that the aggregated EV load can provide can be then represented in (4.3b).

$$\begin{aligned} f_l(k) \; &= min(u_l(k) - u_l^{min}, u_l^{max} - u_l(k)) \; + min(u_c(k) - u_c^{min}, u_c^{max} - u_c(k)) \; + \\ &\quad min(u_d(k) - u_d^{min}, u_d^{max} - u_d(k)) \end{aligned} \tag{4.3a}$$

$$f_c(k) \; = \; min(\alpha_r f_l(k), \beta_r f_c^{max}) \tag{4.3b}$$

Note that the two dynamic characteristics can be realized simultaneously during grid transient state. If a frequency event occurs and the disturbance is higher than the predefined threshold, EVCSs and BSSs which enable real-time communication only with EVSEs will activate the frequency-droop control to facilitate the grid to ride-through the disturbance. The EVCSs and BSSs which enable real-time communication with EVSE and the utility will also follow the AGC signals and provide frequency regulation services.

### 4.2.3 Flexibility of the Aggregated EV Loads

We define the *day-ahead flexibility* of PEVs in EVCSs as the SOC range of the aggregated EVs and the daily EV load demand variation that do not affect the charging capabilities. If the PEVs are scheduled to prioritize the charging schedule based on both the departure time and the energy needed for charging, the individual PEVs can meet their charging demands and a certain level of flexibility can be maintained by the aggregated PEV load. While the PEV charging includes individual EV charging schedules, and the virtual battery model constraints are time-dependent, the BSSs are featured with fixed capacity and charging constraints. The flexibility of BSS is affected by the aggregated battery swapping load curve. The day-ahead flexibility can be then defined as the SOC range of the aggregated BSSs that has little impacts on the charging and discharging schedules and the battery swapping demand. Different from PEVs, the day-ahead flexibility of which needs to be obtained by simulations including individual PEVs, the day-ahead flexibility of BSSs can be explicitly obtained by the economic dispatch simulation, where the aggregated model can be used and it can be treated as a large battery storage.

The *intra-day flexibility* of the aggregated EV load including different EV charging mechanisms can be defined as the ability to improve the system load factor. With a given daily charging demand of PEVs and a forecasted battery swapping curve of the BSSs, the EVCS and BSS loads can be dispatched to meet the charging demand during the off-peak hours so as to minimize the load variations. This will result in significant improvements in the energy delivery efficiency and an increase in the system load factor. If the aggregated EV loads are assumed to participate in the ancillary service (AS) market and contribute to the frequency regulation, the *real-time flexibility* of the aggregated EV load can be then represented by $f_c$. Hence, we here limit the discussion of aggregated EV load models to system normal operating conditions.

## 4.3 Parameter Identification of the Aggregated EV Load Models

With the multi-timescale flexibility that the aggregated EV loads can offer to the system, the flexibility of the EV loads can be quantified and utilized by the system operator during daily operations. As we here study the cases with significant EV penetration, the aggregated EV load will impact the market price; hence, a production cost modeling approach has to be implemented. The economic dispatch model is used in this chapter to take into account both dispatch and AS market (frequency regulation and spinning reserve), and the system daily normal operation is then studied.

### 4.3.1 Economic Dispatch Model for Parameter Identification

If the communication network latency is high and the AMI only supports the 5-minute bi-directional communication, the aggregated EV load could not provide the frequency regulation services to the system. The proposed economic dispatch model for the system operator considering the EV load with different charging mechanisms is presented in (4.4).

$$\text{minimize} \quad \gamma(L_c(K+1)-E_C)^2+\sum_{k=1}^{K}(V_S u_{ls}(k)+V_C P_C(k)) + \sum_{k=1}^{K}(\sum_{i=1}^{n} C_i(P_{G,i}(k))+2c_d u_d(k)) \tag{4.4a}$$

subject to

$$\sum_{i=1}^{n}(P_{R,i}(k)+P_{G,i}(k))+u_d(k)-u_c(k)-u_l(k)=L_O(k)+L_F(k) \qquad \forall k \tag{4.4b}$$

$$P_{G,i}(k+1)=P_{G,i}(k)+\Delta P_{G,i}(k) \qquad \forall k\ \forall i \tag{4.4c}$$

$$P_{G,i}^{min} \le P_{G,i}(k) \le P_{G,i}^{max} \qquad \forall k\ \forall i \tag{4.4d}$$

$$\Delta P_{G,i}^{min} \le \Delta P_{G,i}(k) \le \Delta P_{G,i}^{max} \qquad \forall k\ \forall i \tag{4.4e}$$

$$P_{C,i}(k) + P_{R,i}(k) = \Lambda_{R,i}(k) \qquad \forall k \; \forall i \tag{4.4f}$$

$$0 \; \leq \; P_{R,i}(k) \; \leq \Lambda_{R,i}(k) \qquad \forall k \; \forall i \tag{4.4g}$$

$$\boldsymbol{H} \cdot \boldsymbol{P}_{net}(k) \leq \boldsymbol{F} \qquad \forall k \tag{4.4h}$$

$$(4.1), (4.2)$$

where the objective function (4.4a) minimizes the total dispatch cost by allocating both generation and EV loads. The objective function (4.4a) consists of (i) the penalty cost for the deviations from daily energy consumption of the PEVs, (ii) the shedding cost of PHEVs and the curtailment cost of renewable power, (iii) the quadratic generation cost of conventional generating units, and (iv) the cost for discharging EVs—the degradation cost of EVs is considered when the V2G operating mode results in extra battery cycles to EV customers. Equations (4.1) and (4.2) represent the state and input constraints of EVCS and BSS, respectively. Equation (4.4b) enforces the power balance constraint. Equations (4.4c)–(4.4e) are the state equations for the conventional generating units. Equations (4.4f) and (4.4g) represent the intermittent renewable power output. Transmission line constraints are expressed in (3.4d). $\boldsymbol{F}$ is the vector of the transmission line flow limits. $\boldsymbol{H}$ is the power transfer distribution factor (PTDF) matrix. $\boldsymbol{P}_{net}$ is the vector storing intermediate calculation of the net generation at the network buses.

### 4.3.2 Co-Optimization of Energy and Ancillary Services

If the real-time communication between the EVCS and EVSEs is enabled, and EVCS and the utility can also interact in real-time, the aggregated EV loads can participate in the frequency regulation market. Compared with the sequential optimization in which energy and reserves were cleared sequentially, the co-optimization with a single dispatch solution for energy and AS market every five minutes results in a more optimal energy dispatch and AS reserve schedules. If $OF_{ED}$ represents the objective function introduced in (4.4a), the

joint optimization model considering both energy dispatch and AS can be then represented by (4.5).

$$\text{minimize} \quad OF_{ED} - \sum_{k=1}^{K} (V_F f_c(k)) \tag{4.5a}$$

subject to

$$R_{G,i}(k) \leq P_{G,i}^{max} - P_{G,i}(k) \qquad \forall k \; \forall i \tag{4.5b}$$

$$\sum_{i=1}^{n} R_{G,i}(k) \geq \rho L_O(k) \qquad \forall k \tag{4.5c}$$

$$(4.1) - (4.3), (4.4b) - (4.4h).$$

where the objective function (4.5a) is to minimize the total dispatch cost minus the revenue of the frequency regulation provided by EVs. The regulation capacity provided by EVs is stated in (4.3). $R_{G,i}$ in (4.5b) is the reserve provided by the online conventional generating unit $i$, $\rho$ in (4.5c) is the percentage of demand which specifies the reserve requirement. Other equations are the same as those previously introduced in the economic dispatch model. Note that the joint optimization model in the PJM market is defined as a single dispatch solution for energy, regulation, synch reserves and non-synch reserves every five minutes [91]. We only model the energy dispatch and frequency regulation provided by the aggregated EV loads in the objective function to demonstrate the role of the aggregated EV load in the joint optimization. The benefits of the frequency regulation that EVs can provide are modeled as the negative cost to the system. In practice, other objective and constraints can be added to the co-optimization model, e.g., the frequency regulation provided by the conventional generating units [92].

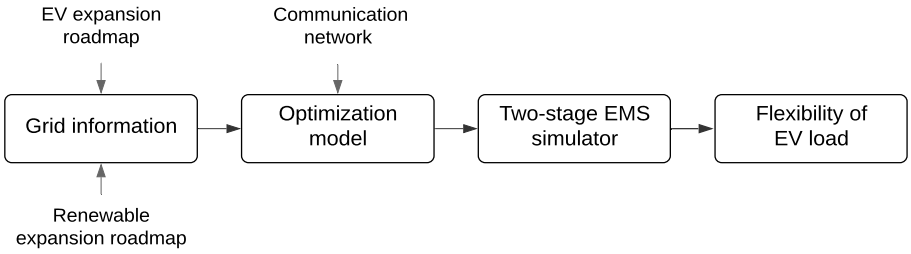


Figure 4.2: The flowchart of the suggested parameter identification procedure.

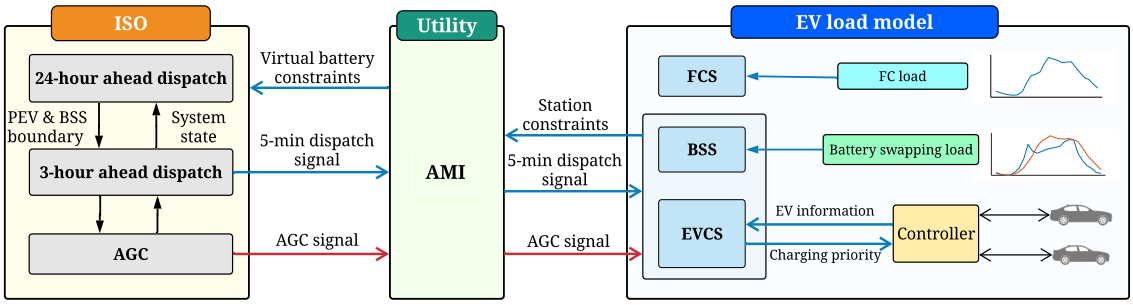


Figure 4.3: The proposed framework to simulate the aggregated EV load models.

### 4.3.3 Parameter Identification Procedure

The steps to simulate the EV charging load is illustrated in Fig. 4.2. The following procedure is proposed to simulate the EV charging loads:

1. Assuming a certain penetration level of BEVs, PHEVs, and EV charging infrastructure under a given market mechanism, the power grid operation data is imported by the regional independent system operator (ISO). Note that the market mechanism is driven by the customer demand and energy policy, and should include other information such as the EV and power sector expansion road-maps.

2. Based on the market information, e.g., the type of ancillary service that the EV load provides, initial parameters for the proposed mathematical model are determined.

3. EV charging demand based on the proposed optimization model is simulated. The simulation is realized through a two-stage EMS architecture, where AMI is employed to achieve the communication between the system and EV customers.

4. Requisite parameters in the proposed mathematical model are calibrated through multiple simulations. As the simulator enables the interactions between the system operator and EV customers, both EV customer and power system objectives are considered.

The two-stage EMS utilized to identify the aggregated load model parameters either uses the economic dispatch model in Section 4.3.1 or the co-optimization model in section 4.3.2 based on the communication delays and EV market participation. The EMS model is a modified version of the one [88] presented in Chapter 3, and the entire simulation system is demonstrated in Fig. 4.3. Specifically, in Stage 1, as the BSS and PEV operation schedules are time-dependent, the 24 hour-ahead optimization problem is solved using the model predictive control (MPC) in a receding-horizon manner, where the time step is set to 1 hour, and the load, renewable, and EV load forecasts are updated hourly. The 3-hour-ahead $L_c$ and $B_s$ are employed as the boundary conditions in Stage 2. In Stage 2, the same optimization problem is solved with a 3-hour look-ahead time window, but the time step is 5 minutes and the look-ahead time window shrinks as time progresses until the next hour to recover back to 3 hours. While the first stage includes the system-level forecasts and the 24-hour-ahead optimization problem at each hour, the second stage uses short-time forecasts and the uploaded EV virtual battery model constraints to calculate the 5-minute dispatch schedules. Furthermore, the second stage EMS involves the interactions between the EVs and the ISOs. Bi-directional communications are achieved through the utility AMI. The priority of EV charging in EVCS has to meet the individual EV constraints; therefore, the EV information such as the SOC, departure time, and the minimum charging demand need to be collected from the connected EVs. The ISO receives the uploaded aggregated EV constraints, and at the same time, downloads the dispatch signals accordingly. So, the communication delay for the PEV dispatch is 5 minutes. AGC signals can also be sent to the BSSs and EVCSs, and are distributed proportionally if the real-time communication is enabled. The controller in BSSs and EVCSs can implement the integrated dispatch and

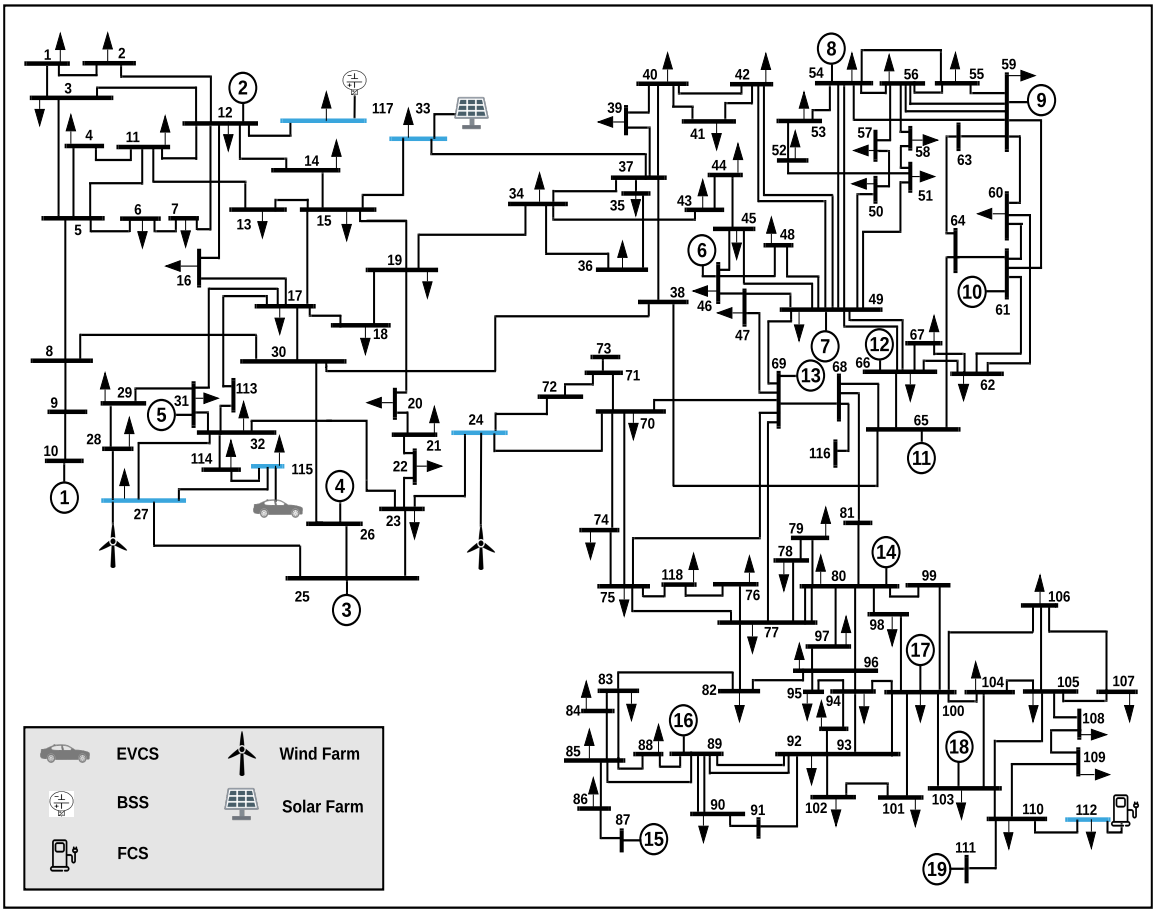


Figure 4.4: The modified 118-bus test system with EV loads and renewables.

AGC signals by (i) using priority-stack-based control which turns on and turns off the EV load based on the charging priority or (ii) adjusting the duty cycle of the charging EVs proportionally. As FC EVs do not offer the flexibility to the system, only the aggregated load is forecasted and added to the associated bus during the parameter identification procedure.

## 4.4 Numerical Case Studies

In this section, a test system is built to simulate the proposed aggregated EV load model. Then the parameter identification procedure in Section 4.3.3 is applied to quantify the flexibility of the aggregated EV loads in the system.

### 4.4.1 The Modified IEEE 118-Bus Test System with EV Loads

A modified IEEE 118-bus test system is utilized to simulate the aggregated EV load. As illustrated in Fig. 4.4, the system consists of 19 online conventional generating units. The test system specifications are taken from [87] with the following modifications: two wind farms with the total capacities of 500 MW and 750 MW are placed at bus 24 and bus 27, respectively. A photovoltaic (PV) power plant with a rated power of 650 MW is placed at bus 33. Hence, the total power capacity of the renewable sources is 1900 MW and features nearly 16% penetration in terms of the system generation capacity (23% penetration to the total online generation capacity). The predicted and actual data for renewables and load forecasts are taken from ERCOT and the weekly data captured in the week of December 18, 2017 in Texas is utilized in our simulations [82]. Scale factors of 1/16, 1/1.85, and 1/12.8 are applied for wind farms, PV plant, and the load, respectively. The day-ahead forecasts are replaced by the current-day forecasts in an hour-ahead manner. Both the renewable curtailment and PHEV shedding price are set to 40 \$/MWh. The spinning reserve requirement is set to 73 MW. $\alpha_r$ is assumed to be 0.7, and $\beta_r$ is assumed to be 0.9 in the frequency regulation. $f_c^{max}$ is set to 54.75 MW. The reserve and frequency regulation capacities are also scaled based on the ERCOT market [93].

The system is assumed to have 800,000 EVs accounting for 80% of the total vehicles. The charging and discharging efficiency is assumed 90%. The EV battery capacity (in linear SOC region) is 70 kWh and $c_d$ is set to 21.4 \$/MWh. There are 100,000 EVs using FC, the aggregated FCS charging demand is modeled as an inelastic load at bus 112, and the forecasted load curve is derived from the distribution of daily FC loads in [53]. The actual energy consumption of the FC load is randomly generated using the Poisson probability distribution. There are 600,000 EVs using plug-in charging methods with the charging power of 10.2 kW, where 100,000 of them are PHEVs, and the aggregated EVCS load is placed at bus 115 as a virtual battery. The customers are assumed to plug-in their EVs to charge when the parking time is longer than half an hour and BEV customers will swap the

depleted battery in BSS if the plug-in mode could not satisfy their next trip. Each aggregator is assumed to manage 100 to 200 connected EVs. Driving profiles for PEVs were obtained from the National Household Travel Survey (NHTS) 2017 database [83]. The estimated upper charging constraint is based on the availability of the aggregated EVs. The estimated total charging load is derived from the aggregated EV load demand. 1000 driving profiles in Texas are randomly selected to account for the customer behaviors of the PEVs during the simulations. The initial SOC of the EVs is uniformly distributed between 0 to 80% of the battery capacity. The remaining 100,000 EVs are assumed to use battery swapping, the aggregated BSS is placed at bus 117, and the virtual battery capacity is set to 1050 MWh. The charge/discharge rate of the BSS is 242 MW. So, the BSS is able to be charged and discharged several cycles a day when necessary. We reserve 20% of the BSS capacity for battery swapping, and a penalty will be applied when the SOC of the BSS is lower than 20%. The SOC of the BSS could not be lower than 5%. The estimated energy consumption of battery swapping from customers who subscribe the service is derived from [85] based on the EV arrival rates. The actual battery swapping load from these customers is also generated using the Poisson probability distribution. The estimated energy consumption of PEV customers who use battery swapping services is assumed to be 0, and the actual battery swapping load from these customers is obtained from the simulations. Note that transmission line limits are not provided in the test system [87]. We assume that there is no congestion in transmission system, and hence, the EV loads are aggregated in one bus. When the congestion in the system needs to be considered, the EV loads need to be modeled in each bus. However, the optimization formulation will remain the same and the optimization model is still a convex problem.

### 4.4.2 Simulation Results

We run the 7-day economic dispatch simulations in the test system using the proposed framework. The CVX optimizer in MATLAB 2017a is employed to run all the test case

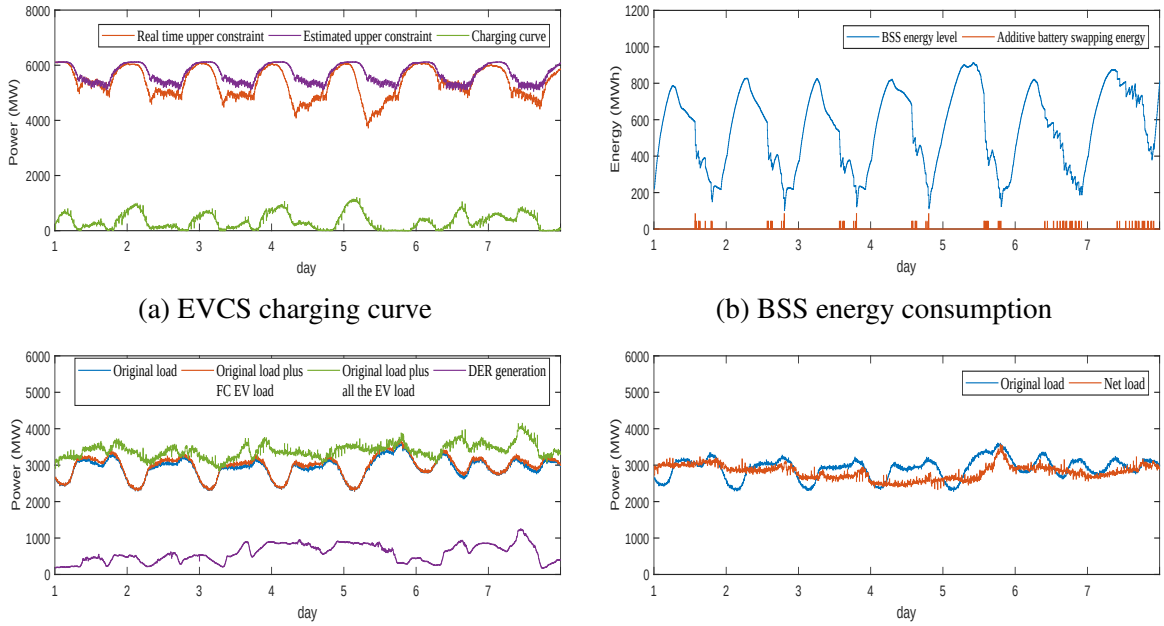


(a) EVCS charging curve

(b) BSS energy consumption

(c) EV load impact

(d) Net load

Figure 4.5: Different aggregated EV loads and their impacts on the power system with 16% renewable penetration and 80% EV penetration.

scenarios. Figure 4.5a shows that the real-time upper charging constraint of the aggregated EVCS charging is close to the estimated upper constraint (number of EVs parked), and the lower charging constraint is nearly 0 which is not included in the figure. The flexibility of the aggregated EVCS load is maintained during the week. The maximum charging power is less than 1200 MW and it is mainly decided by the economic dispatch outcome. Hence, a certain level of over-subscription in the EVCSs should be allowed. The aggregated BSS energy increases during the night and then decreases in the daytime (see Fig. 4.5b) because customers will mainly swap their batteries in the daytime. The additive battery swapping from PEV customers will decrease the energy of the aggregated BSS loads to less than 210 MWh (20% of the reserved BSS energy). The FC load shown in Fig. 4.5c will increase the peak of the original load. FC load only has a small ratio to the total EV load, and the extensive flexibility is provided by the EVCS and BSS loads. Hence, the aggregated EV load is not impacted a lot by the FC load; the total EV load including all the three charging methods shows a characteristic of renewable follower. The EMS reduces the daily variation

Table 4.1: Comparison of the Load Factor and Fuel Cost in Different Cases

| Test Case | load factor | unit cost ($/MWh) |
|---|---|---|
| TC1 | 0.78 | 26.48 |
| TC2 | 0.74 | 26.57 |
| TC3 | 0.84 | 25.79 |

of the peak and off-peak load in order to minimize the system total operation cost (see Fig. 4.5d), where the net load can also be represented by the total power output of the conventional generators. The total operation cost is found $ 12,527,577, and it is close to the lower bound of the optimal cost ($ 12,337,347). The lower bound is calculated using hourly data by assuming the perfect knowledge of load, FC and battery swapping curves. Also, the upper and lower charging constraints of aggregated EVCSs are relaxed to estimated values; the daily aggregated EVCS load is also assumed to be flexible that can be controlled during the calculation. Load factor for the week in this base case (TC1) scenario is 0.78 and the fuel cost of generators is 26.48 $/MWh on average as shown in Table 4.1.

### 4.4.3 Parameter Identification Results for EV Flexibility

#### 4.4.3.1 Day-Ahead Flexibility of the Aggregated EVCS and BSS Virtual Batteries

With the estimated energy consumption ($E_C$) of the EVs under plug-in mode for the next 24 hours, the maximum and minimum charging demand do not significantly change during the week in the base case scenario. Figures 4.6a and 4.6b illustrate that when the daily charging target is changed to 1.5 $E_C$, the maximum charging capacity will decrease sharply after the SOC of the EVCS virtual battery reaches 70%. When the daily charging target is changed to 0.5 $E_C$, the minimum charging capacity does not increase significantly. However, when the SOC of the virtual battery in Fig. 4.6d is below 30%, the battery swapping load from PEVs will increase dramatically as illustrated in Fig. 4.7. Therefore, it is suggested to maintain the SOC of EVCS virtual battery at least within 30% to 70% to maintain the flexibility of the

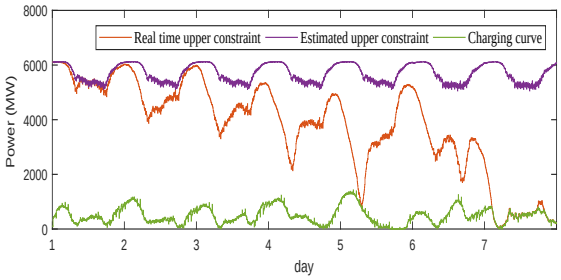


(a) PEV charging curve with 1.5 $E_C$

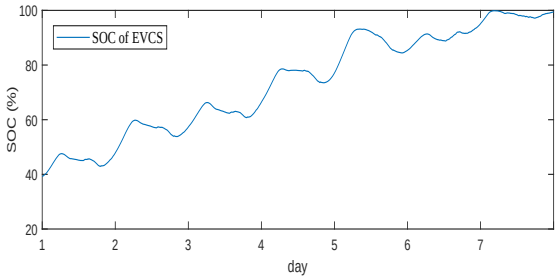


(b) SOC of EVCS with 1.5 $E_C$

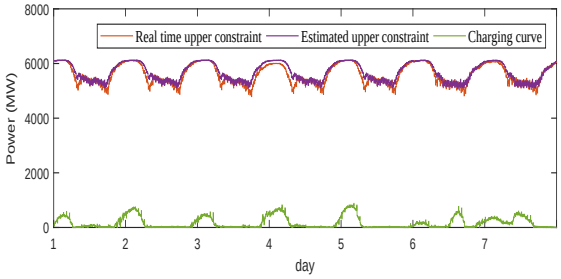


(c) PEV charging curve with 0.5 $E_C$

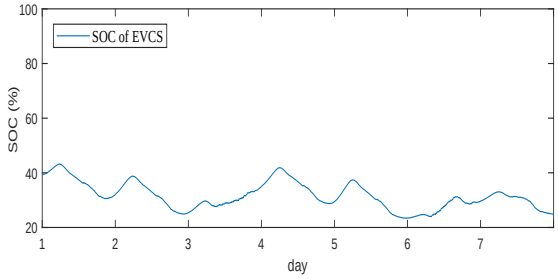


(d) SOC of EVCS with 0.5 $E_C$

Figure 4.6: The day-ahead flexibility of the aggregated PEV loads.

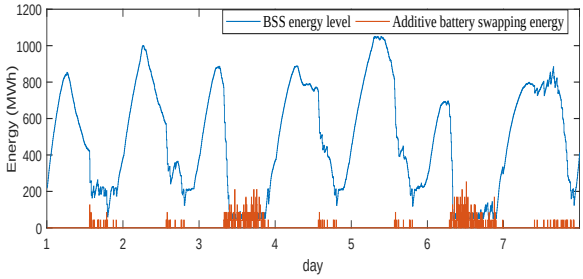


Figure 4.7: Impact of additive BSS load from PEVs on the aggregated BSS virtual battery under 0.5 $E_C$.

PEV loads in the system. Keeping the range of SOC between 40% to 60% can ensure that the increase or decrease of 0.5 daily PEV demand will have little impacts on the charging constraints. While the charging constraints of EVCS virtual battery are time-dependent, BSSs have a fixed number of batteries; hence, the charging and discharging power capacity of the aggregated BSS virtual battery will not be affected by the number of EVs under battery swapping mode in most cases. The flexibility of the BSS virtual battery can be evaluated by the economic dispatch optimization explicitly as storage units. Specifically,

based on Fig. 4.5b, the daily peak of the BSS is around 800 to 850 MWh except the 5th day with weekly peak reaching to 900 MWh. Hence, the fully controllable load is about 150 to 200 MWh and less than 100 MWh during the day with the weekly peak as the capacity of the BSS is 1050 MWh. Other parts are deferrable loads except that when the BSS reaches to the reserved capacity of 210 MWh. The BSS will charge from the grid to avoid the penalty of below 210 MWh, and the BSS load becomes inelastic when the stored energy in BSS is below 210 MWh.

#### 4.4.3.2 Intra-Day Flexibility of the Aggregated EV Loads

The aggregated EV load in the base case scenario provides a large flexibility to the system, where the load factor is 0.78. If the EV penetration level changes to 20% of the total vehicles and the charging mechanism remains the same, the aggregated EV load will then mainly offer the valley filling during the off-peak hours (see Fig. 4.8a). According to Fig. 4.8b, although the net load decreases compared to that in the base case condition, the load factor decreases from 0.78 to 0.72. Hence, the lower the EV penetration, the lower the flexibility that the aggregated EV load can offer to the system. Under the same EV penetration and with the same number of battery swapping EVs compared to the base case condition, as the number of PEVs decreases to 200,000, then the number of FC EVs will increase to 500,000 that accounts for 50% of the vehicles. The FC load will increase the peak load significantly, and the EVCS and BSS virtual batteries will mainly achieve the valley filling so that there are no obvious super off-peak hours for EV charging (see Fig. 4.8c). As shown in Table 4.1, the load factor decreases to 0.74 and the average fuel cost of the system generators increases to 26.57 $/MWh in this case (TC2). It can also be seen from Fig. 4.8d that high penetration of FC EV loads will affect the flexibility of the aggregated EV load and may result in a higher peak of the net load compared to the original load. Note that this case is studied as the proposed model aims at simulating different EV charging levels and customer participation, and as neutral as possible to the technology types providing the charging

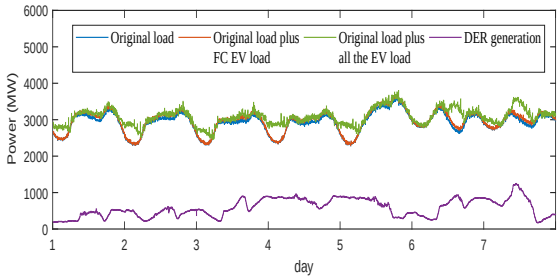


(a) EV load impact with 20% EV penetration level

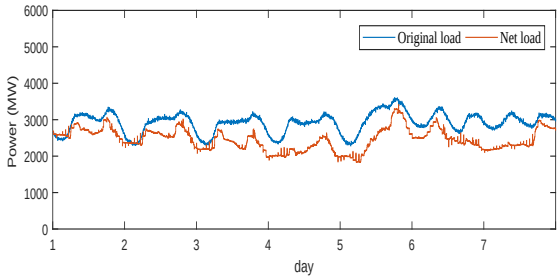


(b) Net load with 20% EV penetration level

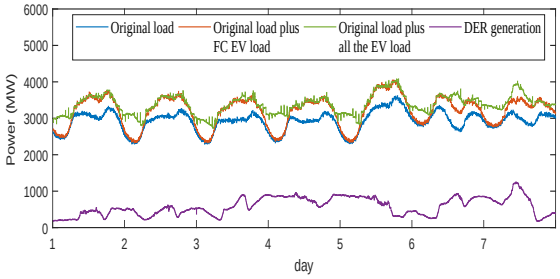


(c) EV load impact with 50% FC EV

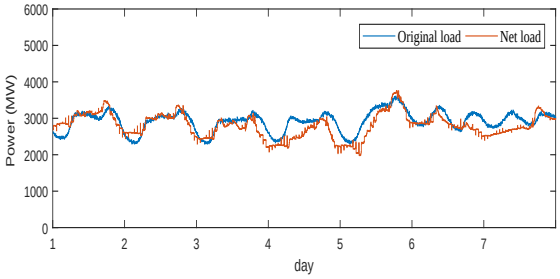


(d) Net load with 50% FC EV

Figure 4.8: Comparison of the intra-day flexibility for aggregated EV loads.

services. In practice, if the home charging is not available to many customers and more FCSs have been built than the regular charging mechanisms in a region, there will be more FC EV load. However, the results indicate that the large FC EV load has negative impacts on the system; i.e., FCSs should not be the main charging method unless there are plenty of solar power to match the FC EV load and the flexibility needs are met by other energy resources in the grid.

#### 4.4.3.3 Real-Time Flexibility of the Aggregated BSS and EVCS Virtual Batteries

With the real-time communication in the system and frequency regulation service provided by EV loads, the aggregated EV load can be simulated through the framework using the joint optimization model. We here employ the same simulation configuration in Section 4.4.2 except that the joint optimization model is used instead of the economic dispatch model. With the first simulation conducted, the additive battery swapping load from PEVs can be achieved. If one replaces the estimated values (originally assumed as 0) with the

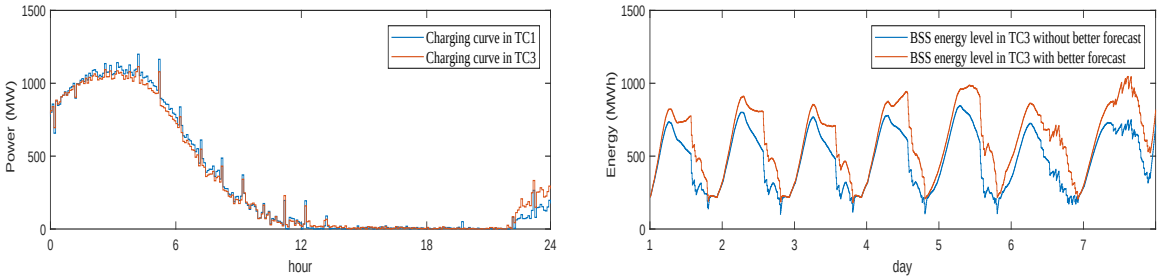


(a) PEV charging curve in the 5th day

(b) BSS energy consumption

Figure 4.9: Comparison between the economic dispatch model and the joint dispatch model.

simulation results obtained from the first simulation and run the simulation again, then the simulation results are demonstrated in Fig. 4.9. Compared to the economic dispatch model in the base case scenario, the EV charging schedules for EVCSs when the joint optimization model is applied are similar except for a few hours as shown in Fig. 4.9a. This is because the frequency regulation capacity needed by the system is much smaller than the EV load needed to be dispatched. But the fuel cost decreases to 25.79 $/MWh because the joint optimization results in revenues on the frequency regulation provided by the aggregated EV loads. With better forecasts (considering the daily additive battery swapping load), Fig. 4.9b shows that the BSSs will also maintain their energy level higher than the reserved values and will avoid charging during peak hours to meet the EV demand of these customers. The load factor is then improved to 0.84 in this test case (TC3) as shown in Table 4.1. Hence, the frequency regulation service provided by the EV loads can reduce the operation cost significantly, and only some EVCSs and BSSs with advanced design need to enable the real-time communication; this is because the needed frequency regulation capacity in such scenarios is much smaller than the load that needs to be dispatched. Also, if the additive battery swapping load is forecasted and considered by the ISO under high penetration of EVs, the system performance and its load factor will be improved. One needs to note that with better forecast results, the stored energy in the BSS is mostly higher than the reserved energy; hence, there is no inelastic BSS load. However, as illustrated in Fig. 4.9b, a better charging schedule of BSS is achieved at the cost of reducing the portion of fully controllable

load that the BSS can provide. The intrinsic flexibility that the BSS provides to the system is the same, as it depends only on the physical constraints, e.g., BSS capacity and battery swapping profiles.

## 4.5 Discussions

As an initial work to characterize the flexibility of the aggregated EV load models in large-scale electric power system, this Section discusses the generality, precision, and applicability of the proposed model.

### 4.5.1 Parameter Calibrations and Generality of the Aggregated EV Load Model

While we simulated the aggregated EV load model in a modified IEEE 118-bus test system, the parameter identification procedure in Section 4.3.3 can be used to simulate aggregated EV load in any particular regions of interest, given that the data on the system typology, power gird operation, a certain penetration level of EVs and different mixes of EV charging methods are available. FC and battery swapping loads can be generated or imported from the regional databases, the PEV customer behaviors can also be imported from local customer surveys as the proposed method is a data-driven approach. Simulation results in the base case condition can be followed by multiple simulations to quantify the flexibility of the aggregated EV loads. Thus, the proposed data-driven approach can be used as an effective tool for EV planning purposes at the system level to analyze the EV load impacts on the power grid. Note that in the case studies, it is assumed that whenever the EVs are parked for more than half an hour, the customers can connect their EVs to EVCSs. Most customers can swap their batteries immediately at the BSS, or charge their EVs via FCS whenever necessary. Hence, the proposed model can be universally used to simulate the aggregated EV load model when there are sufficient charging infrastructure, which means that enough number of charging infrastructure is available (charging capacity higher than forecasted EV load demand) to meet the customer charging demand and a certain level of infrastructure

adequacy is maintained by the utility.

### 4.5.2 Impacts of Renewable Penetration Level on the Model Precision

In order to test the performance of the aggregated EV load under low renewable penetration level, the capacity of renewables is reduced from 1900 MW to 36 MW, while other parameters are kept the same as in the base case. The renewable capacity is then less than 0.6 % of the online generation capacity in the system and the impact of DERs on the system can be ignored as illustrated in Fig. 4.10a. The EV load can reduce the daily variation of the peak and off-peak load effectively with the flexibility it can offer to the system; i.e., there are no load spikes compared with when the pricing-based EV load models are employed under high penetration of EVs. The net load in Fig. 4.10b is also similar as the original load plus the EV load in Fig. 4.10a as the DERs generation is small. Fig. 4.10b also indicates that the EV load will increase the total load and the net load profiles will not have obvious peak and off-peaks during most of the days in a week. The observation that the EV load contributes to a significant increase in the total load under high EV penetration levels is in line with the practical utility operation, e.g., 23% EV penetration in the California independent system operator (CAISO) market causes an obvious increase of the load [42]. Hence, the aggregated EV load models can effectively represent steady-state characteristics of aggregated EV load using smart charging.

The aggregated EV load can provide not only frequency regulation service but also load damping. New variable can be introduced to clearly model the frequency regulation, and the load damping that the aggregated EV load provides can be considered by modifying the joint optimization model. For instance, 270 MW EV load can be set to provide nearly 48 MW primary frequency response in the case studies. However, the ratio of the frequency regulation capacity to the frequency regulation limit, and the ratio of the load damping capacity to the load damping limit should be small so that the ancillary service provided by the aggregated EV load does not significantly impact the distribution system voltage and be

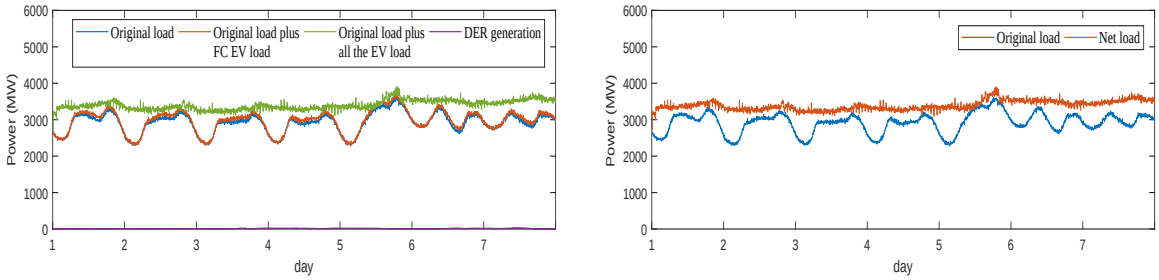


(a) EV load impact

(b) Net load

Figure 4.10: Impact of aggregated EV loads on the power system with very low renewable penetration and 80% EV penetration.

less affected by the uncertainty in customer behaviors. It is also worth mentioning that under scenarios where VREs provide the main power and the system lacks large synchronous generators to maintain the grid stability, even the joint optimization model considering the above ancillary services provided by the EV load could not precisely characterize the grid flexibility requirements. Applying the proposed model to identify the aggregated EV load under such scenarios is oversimplification of the problem that may lead to significant errors.

### 4.5.3 Applicability of the Proposed EV Load Modeling Method

The proposed model is suitable to identify the aggregated EV load models for large-scale centralized power grids under higher EV penetration levels, in which the aggregated EV loads are predictable and the system dynamics do not vary sharply within a short time interval. Hence, a large number of EVs are preferred, as the corresponding load is better predictable and less affected by the randomness of the customer behaviors based on the load aggregation effect. Also, the dispatch of the EV load could impact the market prices, and thus, a production cost modeling approach must be implemented [94]. The performance of the EMS will drop when the number of EVs is low, since the aggregated EV loads are less predictable in such circumstances. In contrast, the pricing-based EV charging strategies can be used when there are only a small number of EVs; these methods require little communication and the aggregated EV loads under these charging strategies do not

have an obvious impact on the market prices. This is in line with practical system operation policies: large-scale storage units have to be modeled in the transmission system, while small storage units can follow the price signals and participate in energy arbitrage. It is also worth mentioning that the EV load can mitigate the impacts of the feeder-level interruptions and facilitate the feeder restoration process under interruptions. But the control and energy management schemes under these scenarios are not explored in this chapter. Hence, the proposed model could not fully characterize the reliability evaluation of the gird considering the EV loads.

## 4.6 Conclusion

Virtual battery models for aggregated EVCSs with level 1 and level 2 charging mechanisms and aggregated BSSs are proposed in this chapter [95]. A data-driven approach is also introduced to simulate the impacts of the aggregated EV loads on the system considering the two virtual battery models and FC EV loads. The proposed method can quantify the demand-side flexibility that the aggregated EV load can provide to the system. The proposed EV load modeling approach and associated test platform can also be used as a benchmark to (i) simulate different EV penetration levels and market patterns and (ii) assess the impacts of different EV charging infrastructure expansion plans on the power grid operation.

# Chapter 5: Flexible EV Loads for Enhancing Power System Resilience

## 5.1 Abstract

The impacts of EVs and renewables on the power grid performance requirements vary depending on the penetration levels, spatio-temporal characteristics, and the imposed stochasticity. Very low penetration of EVs and renewables in a distribution feeder will not significantly impact the grid and, hence, uncoordinated EV charging algorithms can be employed in such circumstances where there will be no renewable curtailments. The increasing penetration of EVs and renewables in the feeder will have a significant impact on the load curves and economic operation of the feeder. Smart charging algorithms should be employed that can account for the renewable curtailments, compatible with the communication networks with smart meters. Hence, solutions and strategies facilitating the adaptive operation of EVCSs to meet the grid performance requirements under different operating conditions and different EV penetration levels are needed to address this emerging transformation in power grids.

We first presents the charging strategies of EVCSs under normal operating conditions. Then the different restoration processes for EVCSs considering various interruptions are introduced. The numerical case studies and simulation results are also presented, followed by the conclusions.

## 5.2 Economic Dispatch Models for EVCSs under Normal Operating Conditions

### 5.2.1 Cost-based Economic Dispatch of EVCSs under Massive Penetration of Utility-Scale EVs

The previous chapters studied control and energy management schemes in the current regulated electricity markets with independent system operators (ISOs) under power grid

normal operating conditions, where multi-agents system is employed to manage the EV charging locally and communicate with the ISOs, as the optimization problem with thousands and millions of EVs is very large and hard to solve directly as one optimization problem. Only the aggregated EV information is considered by a central station and the optimization problem becomes a moderate-size problem to solve. We here define the above cost-based transmission-level economic dispatch of EVs as the *EVCS Operation Strategy 2*. In a deregulated electricity market with virtual power plants, the optimization problem can be distributed to all nodes. Each station or node solves its own optimization problem, considering coupling information from the neighboring nodes or the globally coupled information.

### 5.2.2 Price-based Optimization of EVCSs under Low Penetration of Utility-Scale EVs

The price-based economic dispatch is suitable for operating microgrids with DERs such as EVCSs and PVs, when the utility-scale DER penetration is low. The pricing signals, i.e., the locational marginal prices (LMPs), are generated by the transmission level economic dispatch. The penetration level of DERs in the microgrid can be high in such cases, as long as the percentage of controllable loads and power generation remains relatively low in the utility with little impacts on the LMPs. In other words, the ratio of the dispatchable DERs to the total load in the utility should remain small so that the DERs' operation strategies do not significantly affect the transmission-level economic dispatch results. EV charging can be scheduled during the lower price time intervals, and the EVs' flexibility can be used to avoid the renewable curtailments.

The joint optimization problem to dispatch both EVCS and PV systems is formulated in equation (5.1). The objective function of the price-based economic dispatch is to minimize the operational costs of the combined EVCS and PV systems based on the acquired pricing

signals.

$$\text{minimize} \quad \sum_{k=1}^{K} (\lambda_p(k)u_c(k) + (2c_d - \lambda_p(k))u_d(k) + V_C P_C(k)) + OF_{EV} + OF_{PV} \tag{5.1a}$$

subject to

$$L_c(k+1) = L_c(k) + \alpha_c u_c(k) - (\alpha_d)^{-1} u_d(k) \qquad \forall k \tag{5.1b}$$

$$\sum_{k_1}^{k_2} \alpha_c u_c(k) - (\alpha_d)^{-1} u_d(k) \geq \beta_p E_C \tag{5.1c}$$

$$0 \leq u_c(k) \leq u_c^{max} \qquad \forall k \tag{5.1d}$$

$$0 \leq u_d(k) \leq u_d^{max} \qquad \forall k \tag{5.1e}$$

$$P_C(k) + P_R(k) = \Lambda_R(k) \qquad \forall k \tag{5.1f}$$

$$0 \leq P_R(k) \leq \Lambda_R(k) \qquad \forall k \tag{5.1g}$$

$$P_R(k) + P_E(k) - u_c(k) + u_d(k) = L_O(k) \qquad \forall k \tag{5.1h}$$

$$P_E^{min} \leq P_E(k) \leq P_E^{max} \qquad \forall k \tag{5.1i}$$

$$\begin{aligned} -P_L \leq\ & P_R(k+1) - u_c(k+1) + u_d(k+1) - (P_R(k) \\ & - u_c(k) + u_d(k)) \leq P_L \qquad \forall k \in [1, K-1] \end{aligned} \tag{5.1j}$$

$$OF_{EV} = \gamma(L_c(K+1) - E_C)^2 \tag{5.1k}$$

$$OF_{PV} = -\sum_{k=1}^{K} \lambda_p(k) P_R(k) \tag{5.1l}$$

The objective function (5.1a) consists of (i) the cost for charging EVs, (ii) the revenue for discharging EVs—the degradation cost of EVs are considered when the vehicle to grid (V2G) operating mode results in extra battery cycles to EV customers, (iii) the curtailment

cost of PV power, (iv) the penalty cost for deviations from daily energy consumption of the PEVs reflected in (5.1k), and (v) the revenue for PV systems to follow the dispatch signals presented in (5.1l). Constraint (5.1b) represents the state equation describing dynamics of the EV batteries, where self-discharge is ignored. Constraint (5.1c) describes the required charging demand of the EVCS during a certain time interval. Multiple levels of charging demand during different time intervals can be described in (5.1c) with different selections of $k_1$, $k_2$ and $\beta_p$, the values of which can be obtained though historical datasets. Constraints (5.1d) and (5.1e) enforce the EVCS power to the charge and discharge capacity limits. Constraints (5.1f) and (5.1g) represent the effective PV power output and curtailment, limited above by the total power output of the PV system. Constraint (5.1h) enforces the power balance requirements. Constraint (5.1i) specifies the exchange power limits of the feeder. In (5.1j), the DER power variation in two consecutive time-steps is restricted to a pre-specified value. We define the joint dispatch of EVCSs and PV system through the proposed optimization problem (5.1) as the *EVCS Operation Strategy 1*. Note that while DCOPF is used in the economic dispatch formulation, other models, e.g., convex relaxations of ACOPF, can also be used and integrated with the optimization problem.

## 5.3 Restoration Strategies for EVCSs under Interruptions and Emergency Operating Conditions

We utilize the EVs' flexibility to reduce the system operational costs during normal operating conditions, while mitigating the impacts of the *feeder-level* interruptions during emergencies. If there is an outage in the feeder, the unused EVs can serve as a grid-support resource: EVs can discharge some energy to support the interrupted load during interruptions, and EVs can charge or swap the batteries in other feeders during the recovery process or during their travels. This potential for EVs and PVs can be further highlighted for feeder resilience support when considering the rapid deployment of such technologies in modern power distribution systems; furthermore, as more charging facilities are available in other

feeders, EVs can be regarded as mobile energy batteries to support the loads in the feeder when necessary, thereby exchanging their flexibilities spatiotemporally across a network of multiple feeders [96].

The system-level blackouts or other high-impact low-probability (HILP) events driven by extreme weather conditions may result in the majority of the feeders in the system being interrupted [97]. We regard the conventional restoration mechanisms with load pick-up and crew dispatch [98] as the primary restoration strategy. We here define and investigate a restoration approach focusing on the EVs and distributed generators as the *ancillary restoration* mechanisms. The proposed framework for ancillary restoration can be seen in Fig. 5.1. It is a complementary restoration approach that facilitates the primary restoration process, and it can be used under both low and high penetration levels of DERs. The restoration steps are described as follows:

1. The EVCSs will charge the EV batteries to high SOCs during the normal operating conditions several hours ahead when the HILP event hits the grid with available or projected weather forecasts.

2. During the interruption, the EV and PV systems can form a microgrid to supply the feeder or the residential homes depending on the scale of the DERs.

3. During the Recovery Action stage

   (a) The communication between the EVCS and the utility should be connected first so that the EV load can be estimated and scheduled along with the primary restoration practices. The EV load scheduling and EV load recovery methods under low EV and high EV penetration levels are different.

   (b) With low EV penetration in the utility, the EVCS can maximize the power recovery of connected EVs within the feeder constraints. Other survived or recovered feeders with battery swapping stations can help swap the batteries for the EVs that could not be charged to the desired SOC for the trip.

(c) The utility needs to seek a trade-off between the amount of recovery power and increased EV load demand under high EV penetrations. This is because the EV load demand is high at the beginning of the recovery stage due to the EV battery energy supply during the disruption. Only the critical EV loads should be charged once the feeder is energized, and EV load curtailment should be considered when necessary. The EV load should be restored gradually to meet the EV customer trip demand after the inelastic load in the system is restored. The average SOC of EVs in the utility can be increased using cost-based economics dispatch after the majority of the generators and the system original loads are recovered.

The above Steps 1, 2, 3.a and 3.b can be employed as the operation strategy for EVCSs during restoration processes under low utility-scale penetration of EVs and we here define it as the *EVCS Operation Strategy 3*. If $k_3$ is the start time during normal operating conditions to increase the EV load, and $k_4$ is the start time of the disruption, the optimization problem to schedule the EV charging during the time period starting from $k_3$ to $k_4$ can be represented by (5.1a) – (5.1j), (5.1l) and (5.2). Equation (5.2) is a soft constraint enforcing the EVCS to charge the EVs with maximum power capacity.

$$OF_{EV} = \gamma(L_c(k_4) - u_c^{max}(k_4 - k_3))^2 \tag{5.2}$$

The Steps 1, 2, 3.a and 3.c are employed as the operation strategy of EVCSs during the restoration interval under high utility-scale penetration of EVs and we here define it as the *EVCS Operation Strategy 4*. The transition of EV load flexibility in Chapter 4 can be utilized here. The charging target of the aggregated EV load can be increased during the grid normal operating state so that the portion of fully controllable and deferrable EV loads increase. During the recovery stage, the portion of inelastic EV load can be recovered firstly, followed by the other EV loads. However, future work needs to be done to investigate the

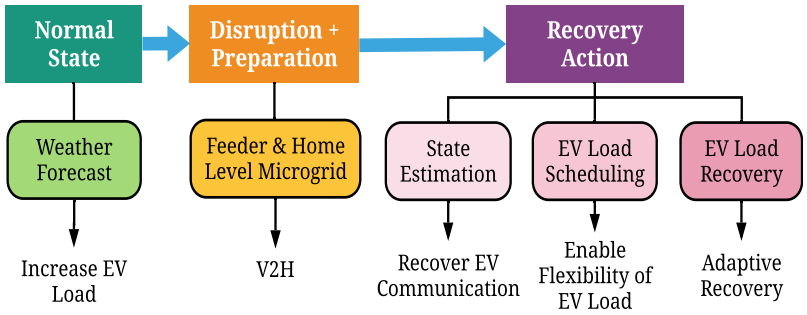


Figure 5.1: The ancillary restoration process by flexible loads such as EVs.

EV customer behaviors under interruptions and detailed algorithms to facility the recovery using EVs with different EV customer behaviours.

## 5.4 The Proposed Framework for Adaptive Operation of EVCSs

The EVCSs need to adjust the charging algorithms with different EV penetration levels under normal operating conditions. They also have to consider the EV charging algorithm and restoration processes when interruptions occur. Hence, the EVCS operator should consider all the conditions and effectively employ a suite of adaptive operation strategies to manage the EVs as different scenarios unfold. The overall architecture of a holistic solution proposed for EVCS adaptive operation is demonstrated in Fig. 5.2. It requires the communication system to be built, the EVs to be connected with smart meters, and the interaction between the utility and the EVCSs to be enabled. According to Fig. 5.2, only the operation strategies need to be adjusted as different grid conditions unfold once the communication system is established. This is achieved at minimum effort for the EVCS operators in order to meet the system requirements when transitioning through different operating states over time.

## 5.5 Numerical Case Studies

Real-life data is imported to simulate and evaluate the effectiveness of the proposed algorithms under low utility-scale penetration of EVs. The historical load profile of a feeder in

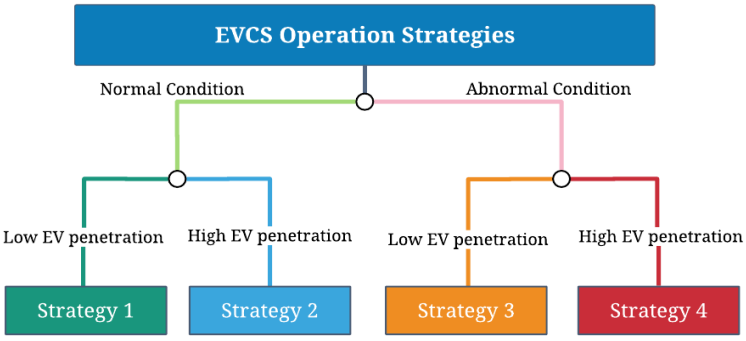


Figure 5.2: The holistic framework of adaptive operation of EVCSs.

year 2015 is utilized. The feeder supplies 549 customers in the US District of Columbia (DC), with the average feeder load of 1.52 MW and yearly peak load of 3.28 MW. It is corresponding to an overhead line feeder supplying majorly the residential customers and a few commercial customers. The modified IEEE 13-node test feeder is employed as the typology for the test system, the one-line diagram of which is illustrated in Fig. 5.3. We here assume the all loads are balanced three-phase loads. The total load of the feeder is proportionally distributed to the nodes. We also assume that the transformer connected to the feeder is of 5 MVA capacity, and reverse power flow is not allowed. The minimum net-load of the feeder is 0.3 MW. The integrated EVCS and PV system is located at node 635 (see Fig. 5.3), and connected to the grid through a transformer. The weather data is taken from the National Solar Radiation Database around Washington DC area [99]. The global horizontal irradiance data in year 2015 is used and the overall PV system efficiency is assumed to be 20%. $V_C$ is set to 25 \$/MWh. A PV system with a total capacity of 9 MW can generate the equivalent electricity satisfying yearly energy demand in the feeder. The penetration level of PV in the feeder is defined as the percentage of PV capacity to 9 MW PV system. The hourly LMPs in year 2015 from the PJM market are used as the pricing signals [100]. The uncoordinated PEV load is acquired from [101] to assess the daily EV demand and make a comparison with the coordinated EV charging strategies. The scale factor for the EV load is 7. We assume there are 2400 vehicles in the feeder based on the

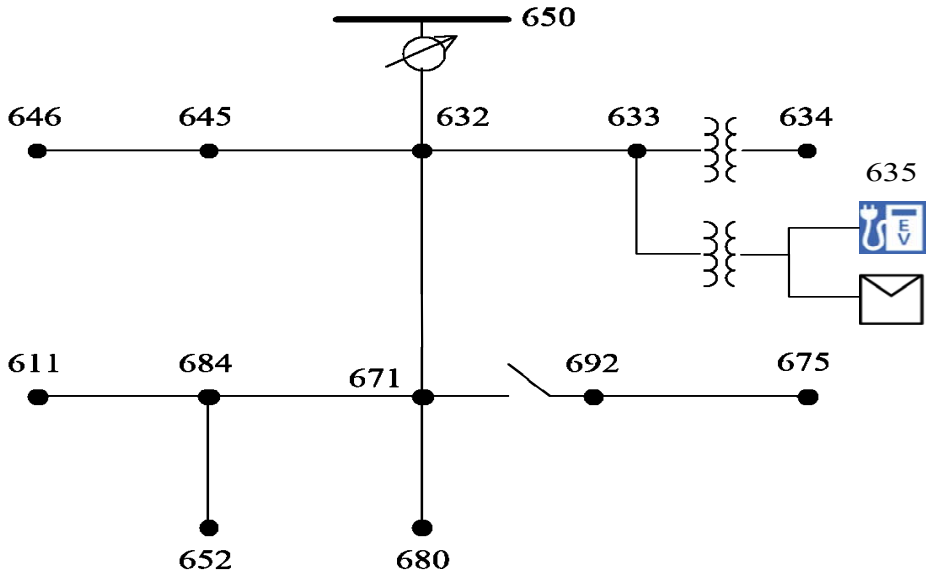


Figure 5.3: The modified IEEE 13-node test feeder with EVCS and PV system located at node 635.

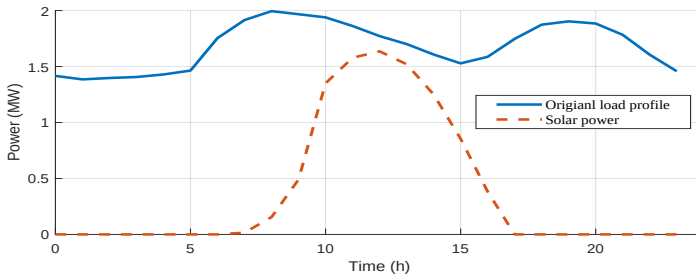


Figure 5.4: The feeder load profile and solar power output during a winter day.

daily EV demand. The EVCS in the feeder is assumed to charge at least 10% of the EV daily energy demand during the time period of 9 a.m. to 9 p.m., and charge at least 30% during other time intervals of the day. Then $\beta_{p1} = 0.1$ and $\beta_{p2} = 0.3$. The charge/discharge rate of the EVCS is 6 MW with the efficiency of 95%. $c_d$ is set to 20 \$/MWh.

### 5.5.1 Uncoordinated vs. Smart Charging Strategies

We assume a 2.7 MW PV system and 1440 EVs in the feeder. Hence, the PV and EV penetration levels are 30% and 60%, respectively. The PV output and the feeder load profile of a typical winter day in year 2015 is illustrated in Fig. 5.4. Compared with the

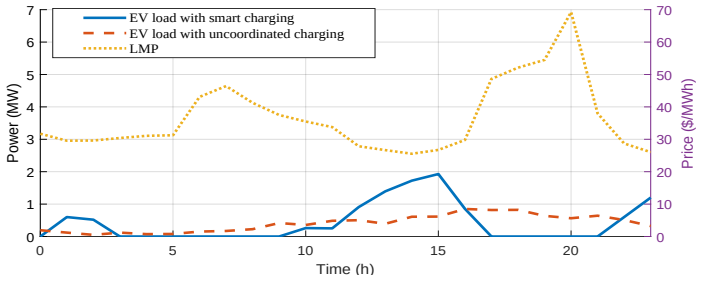


Figure 5.5: Different EV load profiles under different charging algorithms in the feeder, and the LMP profile of the feeder. The y axis corresponding to EV load is on the left, and that of the LMP is on the right.

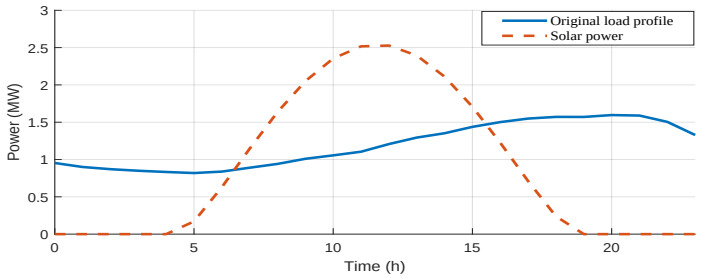


Figure 5.6: The feeder load profile and solar power output during a summer day.

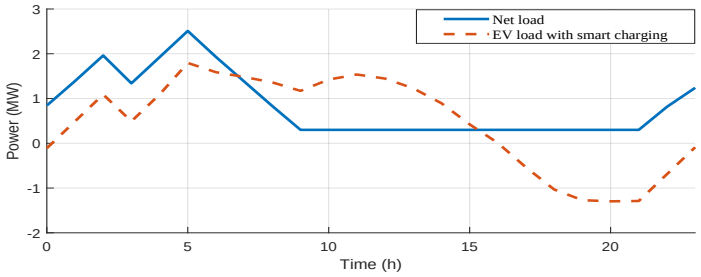


Figure 5.7: The net load profile and the EV load profile of the feeder.

uncoordinated charging strategies in Fig. 5.5, the smart charging could follow the LMP and charge during low-price time periods.

In a summer day when the PV power is nearly its output capacity (see Fig. 5.6), the PV output is higher than the original load demand. The uncoordinated charging of EVs will cause a significant curtailment of PV generation during the day. However, the proposed joint optimization mechanism will schedule the EV loads by taking into account the LMP and to decline the PV curtailment by following the PV output power. The V2G is also used

to minimize the cost of the integrated EV-PV system without violating the grid constraints. The results are illustrated in Fig. 5.7. The net-load is the aggregated load of the feeder, and is equal to the total load including the original load and the EV loads minus the PV output.

Considering the transformer upper constraint, the maximum EV penetration in the case of an uncoordinated charging is 87.5% if one assumes no PV system in the feeder. With smart charging mechanisms, the maximum EV penetration can be 100% and the EVs will be charging during low LMP time intervals to meet the customer trip demand.

### 5.5.2 PV Curtailment under Different Levels of EV Penetration in the Feeder

Without EVs, a 8.6% PV penetration level in the system results in the minimum load of 0.3 MW in the feeder without curtailment. The PV penetration level can increase to 16.6% when there is 100% EV penetration with uncoordinated charging, if a 2-hour slightly overload of the transformer is allowed. A small percentage of PV curtailment should be allowed and smart charging algorithms should be employed by the EVCS operators to increase the PV system integration capacity.

EVCSs with smart charging mechanisms can improve the PV penetration significantly. The PV power curtailment and the operation cost of the integrated EV-PV system in the feeder are demonstrated in Fig. 5.8 and Fig. 5.9. The PV power curtailment under different EV and PV penetration levels is illustrated in Fig. 5.8. The intersection points between 2% PV curtailment (dashed curve) and PV power curtailment curves under different EV penetration levels indicate the marginal conditions—the percentage of PV penetration level—to economically invest on PV systems. The operational cost of the combined system decreases almost linearly until more than 2% of PV curtailment happens in Fig. 5.9. Hence, the PV penetration level with 2% PV curtailment in Fig. 5.8 can be regarded as the upper bound when seeking an economic investment under a certain level of EV penetration.

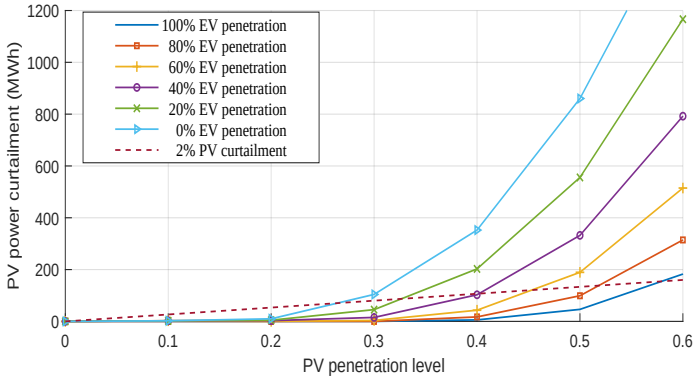


Figure 5.8: PV energy curtailment against the penetration level of PV systems. Each line represents the EV penetration level.

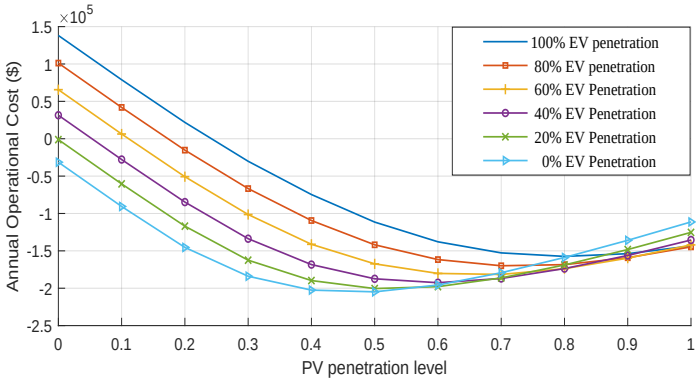


Figure 5.9: The operational cost of the integrated EV-PV system in the feeder during 2015 vs. the penetration level of PV systems. Each line represents the EV penetration level.

### 5.5.3 Restoration Strategy of EVCSs under Low Utility-Scale Penetration of EVs

With the same penetration level of PV and EVs as in Section 5.5.1, we apply the Strategy 3 to manage the operation of the EVCSs under interruptions and in emergency operating conditions. The PV output and load profile of a typical spring or fall day in year 2015 is illustrated in Fig. 5.10. We assume that the EVs have the battery capacities of 70 kWh. At 12 a.m., all the EVs are assumed to be in the EVCSs and the EVCSs have 40% aggregated SOC. At 1:00 a.m. the EVCS receives the weather information reflecting a HILP storm that is approaching the system during the day with a strong wind profile, and the overhead distribution line connected to the feeder is vulnerable to be broken. We assume that the main grid fails to supply the feeder from 6:00 a.m. to 3:00 p.m. during the day due to the

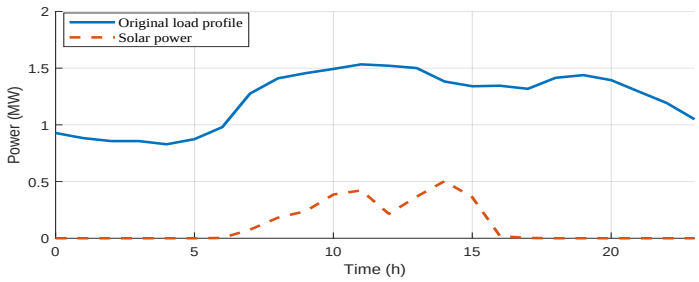


Figure 5.10: Feeder load profile and solar power output during a fall season day.

Table 5.1: Energy Consumption and Supply of the EVCS During Each Stage of the Restoration Process

| Stage | schedule (MWh) | actual (MWh) |
|---|---|---|
| Normal State | 30 | 20.25 |
| Disruption & Preparation | -20.15 | -10.16 |
| Recovery Action | 6 | 0 |

inclement weather.

Table 5.1 presents the implementation results when Strategy 3 is applied during each stage of restoration. The EVCS wish to charge as much energy to the EVs in Strategy 3 before the interruption occurs so as to avoid the penalty of energy interruption (during outages) in the feeder. The actual energy charged to the EVs in the EVCSs, 20.25 MWh, is observed less than the expected value due to the grid constraints. As the repair time of the outage elements, i.e., the interruption duration, depends on many factors, the actual energy supplied by the EVCS may be more or less than the energy stored in the EVs during the first stage. The EVCS needs to acquire the SOC of EVs and reschedule the EV charging during the Recovery Action stage. Following the interruption, there is a 13.15 MWh energy that remains unused, which is higher than the EVCS daily demand of 9.85 MWh. Hence, no EV demand should be scheduled at the immediate hour following the restoration process is accomplished.

The EV charging curve with and without Strategy 3 applied is shown in Fig. 5.11. The operation strategy without considering the interruptions will only follow the electricity

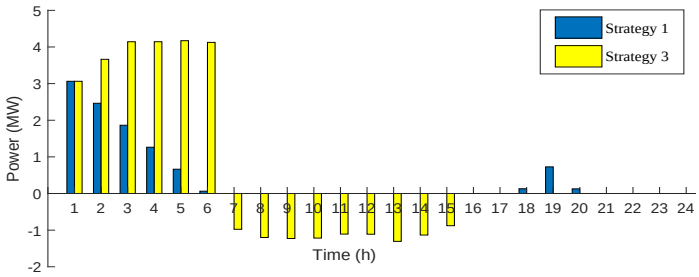


Figure 5.11: Different EV charging strategies during the ancillary restoration process in the feeder. Positive values are the EV loads, and negative values are the energy supplied by the EVCS to the load.

pricing signals before the interruption occurs, and then charge the other part of EV demand following the interruption. The charging Strategy 3, however, will charge more energy to the battery before the interruption occurs, and supply the feeder during the interruption.

## 5.6 Conclusion

The increasing penetration of EVs will bring about potentials to improve the maximum capacity of intermittent renewable energies that the feeders can accommodate cost-effectively. With the increasing penetration of EVs, the adaptive EVCS operation strategies enable the EVCSs to safely operate in the modern distribution systems [102]. The proposed ancillary restoration framework utilizes the EVs as the grid support resources to harnesses the EVs' flexibility in providing additional energy before the interruptions, provide energy to customers during interruptions, and facilitate recovery of EV loads following the interruptions. The proposed framework requires smart communication platforms that can help the EVCS operator make effective decisions as different grid operating conditions unfold over time.

# Chapter 6: Conclusion and Future Work

## 6.1 Conclusion

This dissertation presents new control and energy management schemes for power systems to smoothly integrate the emerging energy resources and loads at large-scale, i.e., VREs and EV load. The coordination of low level control and high level energy management system can ensure the safe and secure operation of the power grids under both transient dynamics and steady-state conditions. The multi-timescale flexibility of aggregated EV load is quantified using the proposed control and energy management schemes. The flexibility of aggregated EV load can also be harnessed by the system operator to not only satisfy the supply-demand balance during day-to-day normal operating conditions, but also ensure resilience services during interruptions.

In **Chapter 2**, detailed EVCS control scheme was proposed to address the EVCS safety considerations, which depends on how well the risk management and control mechanisms are implemented within the design processes to prevent the hazardous conditions and catastrophic consequences. We also proposed a systematic approach to evaluate the electrical safety of EVCSs, centered on the hierarchy of risk control measures that are widely used in safety management systems. The approach is generic enough to be applied, with minimum modifications, to other DERs.

In **Chapter 3**, a centralized two-stage EMS architecture was proposed to be used in power systems with high proliferation of renewables and EVs. We formulated the EV scheduling problem as a global optimization problem to minimize the economic dispatch cost at the transmission level by dispatching both generators and EV load. Formulation of a global optimization problem allows the model to compute the globally optimal solution contingent on oracle forecasting. The solution of the proposed model was found sub-optimal primarily due to the applied SMPC algorithm and limited observations of the EV

driving profiles. However, the system uncertainties were handled by the rolling-horizon control of the SMPC algorithm and a decision making mechanism that enables statistical estimation of the system and parameters control via two-way communications. The results indicated that the proposed two-stage EV scheduling framework can improve power system performance via a nearly-optimal solution, and at the same time, coordinates the system-level EV charging without strong assumptions of the EV customer behaviors. Furthermore, the existing communication system can be utilized with minimum required investments.

In **Chapter 4**, a framework is proposed to model the aggregated EV load considering different EV charging mechanisms. With the steady-state time-varying characteristics of the aggregated EV load model, the system operators can have a better state estimation and energy management scheme to reduce the system operation cost. With the dynamic characteristics of the aggregated EV load model, the system operator can simulate and test the impacts of EVs and renewables on the system stability performance. With the multi-timescale flexibility that the aggregated EV load can provide, the system operators can avoid unnecessary expensive investments in the EV charging infrastructure (e.g. transformer upgrade) and alleviate the system flexibility enhancements needed to integrate higher penetration of VRE. The proposed model can also be used as a benchmark system to simulate the impacts of aggregated EV loads on the power grid.

In **Chapter 5**, restoration approaches for EVCSs are proposed to enhance the power grid resilience against extremes. Adaptive operation strategies are suggested to facilitate the EVCSs to meet the grid performance requirements under different operating conditions and different EV penetration levels.

## 6.2 Publications

Publications directly related to dissertation:

- **B. Wang**, D. Zhao, P. Dehghanian, Y. Tian and T. Hong, "Aggregated Electric Vehicle Load Modeling in Large-Scale Electric Power Systems," *IEEE Transactions on*

*Industry Applications*, Accepted for Publication, in Press, 2020.

- **B. Wang**, P. Dehghanian, and D. Zhao, "Chance-Constrained Energy Management System for Power Grids with High Proliferation of Renewables and Electric Vehicles," *IEEE Transactions on Smart Grid*, vol. 11, no. 3, pp. 2324-2336, May 2020.

- **B. Wang**, P. Dehghanian, S. Wang, and M. Mitolo, "Electrical Safety Considerations in Large-Scale Electric Vehicle Charging Stations," *IEEE Transactions on Industry Applications*, vol. 55, no. 6, pp. 6603-6612, Nov./Dec. 2019.

- **B. Wang**, J. A. Camacho, G. M. Pulliam, A. H. Etemadi, and P. Dehghanian, "New Reward and Penalty Scheme for Electric Distribution Utilities Employing Load-Based Reliability Indices," *IET Generation, Transmission, and Distribution*, vol. 12, no. 15, pp. 3647-3654, 2018

- **B. Wang**, P. Dehghanian, D. Hu, S. Wang, and F. Wang, "Adaptive Operation Strategies for Electric Vehicle Charging Stations," *IEEE Industry Applications Society (IAS) Annual Meeting*, Sept.-Oct. 2019, Baltimore, Maryland, USA.

Other publications:

- S. Wang, P. Dehghanian, L. Li, and **B. Wang**, "A Machine Learning Approach to Detection of Geomagnetically-Induced Currents in Power Grids," *IEEE Transactions on Industry Applications*, vol. 56, no. 2, pp. 1098-1106, March-April 2020.

- P. Dehghanian, **B. Wang**, and M. Tasdighi, "New Protection Schemes in Smarter Power Grids with Higher Penetration of Renewable Energy Systems," *Pathways to A Smarter Power System*, pp. 317-342, 2019, ISBN: 978-0-081-02592-5.

- J. Su, P. Dehghanian, M. Nazemi, and **B. Wang**, "Distributed Wind Power Resources for Enhanced Power Grid Resilience," *The 51th North American Power Symposium (NAPS)*, Oct. 2019, Wichita, Kansas, USA.

- S. Wang, P. Dehghanian, L. Li, and **B. Wang**, "A Machine Learning Approach to Detection of Geomagnetically-Induced Currents in Power Grids," *IEEE Industry Applications Society (IAS) Annual Meeting*, Sept.-Oct. 2019, Baltimore, Maryland, USA.

- M. S. Misaghian, M. Safari, A. Heidari, M. Kia, P. Dehghanian, and **B. Wang**, "Electric Vehicles Contributions to Voltage Improvement and Loss Reduction in Microgrids," *The 50th North American Power Symposium (NAPS)*, Sept. 2018, Fargo, North Dakota, USA.

## 6.3 Future Work

Future research could be directed toward the following:

- To utilize other customized solvers for MPC problems with more CPU cores, facilitating the ADMM method to speed up the implementation of the first-stage SED problem in large-scale power systems with guaranteed convergence; and to investigate the solvability of practical algorithms to solve the chance-constrained SED with look-ahead features in AC settings.

- To study customer behaviors under the scenarios with insufficient EV charging infrastructure in the system and characterize how the flexibility of the aggregated EV load is affected by insufficient charging infrastructure.

- Having plenty of EV charging infrastructure may be favorable to EV customers motivating many customers to switch from the combustion vehicles to EVs without the anxiety of EV travel distance. However, the simulation results indicate that the actual maximum charging power is mainly decided by the economic dispatch outcome. Moreover, maintaining a high adequacy of EV charging facilities may be costly to stakeholders and hard to pursue a timely investment return. Further research

is needed to address the issue on how "sufficient" the EV charging infrastructure need to be to meet the customers charging demand, power system flexibility needs, and stakeholder's return on investment expectation. Regulatory mechanisms can be explored so that EVs can be charged based on the flexibility that individual EVs can provide.

- The load damping provided by the demand side is fading fast as electronically controlled load are taking over as the predominant component of the system load [103]. The stakeholders and customers are also pursuing a target that the majority of the power supply come from VREs such as solar and wind [104]. Such trends impose significant challenges on the power grid frequency control. How the system operator can use the emerging load such as the aggregated EVs and DERs to maintain the stability of the future inverter-based power systems and reformulate the joint dispatch model require both theoretical studies on the system stability (e.g. boundary conditions, frequency thresholds setting) and validations using hardware-in-loop simulations.

- Detailed restoration strategies under interruption scenarios considering the EV loads should be studied. The system operator can also use the control and energy management schemes adaptively when different grid operating conditions unfold over time [102]. Then, the associated EV load models could be utilized for EV charging infrastructure expansion planning considering both reliability and economic evaluation [96, 105, 106].

- The proposed model studied the system-level EV charging impacts, while the regional numbers of EVs is stable and mobility of EVs does not significantly affect the power grid; the mobility and location of EVs are important factors for utility-level EV charging infrastructure planning. Coordination of transmission and distribution-level EV charging infrastructure expansion will result in more optimal decisions. Furthermore, the actual EV charging infrastructure expansion needs to consider other

critical factors such as customer preferences, cost of different charging mechanisms, etc. The EV charging infrastructure expansion should consider the increasing rate of EV charging demand and all the above factors to achieve the dynamic equilibrium of the market.

## Bibliography


[1] M. Islam and H. Gabbar, "Study of micro grid safety & protection strategies with control system infrastructures," *Smart Grid and Renewable Energy*, vol. 3, no. 1, pp. 1–9, 2012.

[2] (2019, April) Monthly energy review. U.S. Energy Information Administration. [Online]. Available: https://www.eia.gov/totalenergy/data/monthly/archive/00351904.pdf

[3] (2019) U.S. energy facts explained. U.S. Energy Information Administration. [Online]. Available: https://www.eia.gov/energyexplained/us-energy-facts/

[4] Non-renewable energy. National Geographic. [Online]. Available: https://www.nationalgeographic.org/encyclopedia/non-renewable-energy/

[5] (2016) Paris agreement. United Nations. [Online]. Available: https://unfccc.int/process-and-meetings/the-paris-agreement/what-is-the-paris-agreement

[6] J. Helveston and J. Nahm, "China's key role in scaling low-carbon energy technologies," *Science*, vol. 366, no. 6467, pp. 794–796, 2019. [Online]. Available: https://science.sciencemag.org/content/366/6467/794

[7] (2019) Global energy transformation: A roadmap to 2050 (2019 edition). International Renewable Energy Agency. [Online]. Available: https://www.irena.org/publications/2019/Apr/Global-energy-transformation-A-roadmap-to-2050-2019Edition

[8] (2019) Annual energy outlook for 2018. U.S. Energy Information Administration. [Online]. Available: https://www.eia.gov/energyexplained/use-of-energy/transportation-in-depth.php

[9] A. Ahmad, Z. A. Khan, M. S. Alam, and S. Khateeb, "A review of the electric vehicle charging techniques, standards, progression and evolution of ev technologies in germany," *Smart Science*, vol. 6, no. 1, pp. 36–53, 2018.

[10] T. Bohn and H. Glenn, "A real world technology testbed for electric vehicle smart charging systems and pev-evse interoperability evaluation," in *2016 IEEE Energy Conversion Congress and Exposition (ECCE)*, Sep. 2016, pp. 1–8.

[11] Z. J. Lee, D. Chang, C. Jin, G. S. Lee, R. Lee, T. Lee, and S. H. Low, "Large-scale adaptive electric vehicle charging," in *2018 IEEE International Conference on Communications, Control, and Computing Technologies for Smart Grids (SmartGridComm)*, Oct 2018, pp. 1–7.

[12] "SAE electric vehicle and plug in hybrid electric vehicle conductive charge coupler," *SAE Int. Std J1772-2017*, pp. 1–116, Oct. 2017. [Online]. Available: https://www.sae.org/standards/content/j1772_201710/

[13] "Electric vehicle power transfer system using a three-phase capable coupler," *SAE Int. Std J3068-2018*, pp. 1–100, April 2018. [Online]. Available: https://www.sae.org/standards/content/j3068_201804/

[14] J. M. Green, B. Hartman, and P. F. Glowacki, "A system-based view of the standards and certification landscape for electric vehicles," *World Electric Vehicle Journal*, vol. 8, no. 2, pp. 564–575, 2016. [Online]. Available: http://www.mdpi.com/2032-6653/8/2/564

[15] K. Zhang, Z. Yin, X. Yang, Z. Yan, and Y. Huang, "Quantitative assessment of electric safety protection for electric vehicle charging equipment," in *2017 International Conference on Circuits, Devices and Systems (ICCDS)*, Sep. 2017, pp. 89–94.

[16] M. Wogan. (2016) Electric vehicle charging safety guidelines. WorkSafe New Zealand. [Online]. Available: https://worksafe.govt.nz/laws-and-regulations/regulations/electrical-regulations/regulatory-guidance-notes/electric-vehicle-charging-safety-guidelines/

[17] Risk control - fire safety when charging electric vehicles. UK Fire Protection Association.

[18] C. M. Affonso, Q. Yan, and M. Kezunovic, "Risk assessment of transformer loss-of-life due to pev charging in a parking garage with pv generation," in *2018 IEEE Power Energy Society General Meeting (PESGM)*, Aug 2018, pp. 1–5.

[19] G. Naveen, T. H. Yip, and Y. Xie, "Modeling and protection of electric vehicle charging station," in *2014 6th IEEE Power India International Conference (PIICON)*, Dec 2014, pp. 1–6.

[20] X. Nie, J. Liu, L. Xuan, H. Liang, S. Pu, Q. Wang, and N. Zhou, "Online monitoring and integrated analysis system for ev charging station," in *IEEE PES Asia-Pacific Power and Energy Engineering Conference*, Dec 2013, pp. 1–6.

[21] "IEEE standard for interconnection and interoperability of distributed energy resources with associated electric power systems interfaces," *IEEE Std 1547-2018 (Rev. of IEEE Std 1547-2003)*, pp. 1–138, 2018.

[22] S. Wang, P. Dehghanian, L. Li, and B. Wang, "A machine learning approach to detection of geomagnetically induced currents in power grids," *IEEE Transactions on Industry Applications*, vol. 56, no. 2, pp. 1098–1106, 2020.

[23] Z. Yi, X. Zhao, D. Shi, J. Duan, Y. Xiang, and Z. Wang, "Accurate power sharing and synthetic inertia control for dc building microgrids with guaranteed performance," *IEEE Access*, vol. 7, pp. 63 698–63 708, 2019.

[24] L. Li, M. Doroslovački, and M. H. Loew, "Discriminant analysis deep neural networks," in *2019 53rd Annual Conference on Information Sciences and Systems (CISS)*, 2019, pp. 1–6.

[25] Blames wind farm settings for state-wide power failure. [Online]. Available: https://www.abc.net.au/news/2017-03-28/wind-farm-settings-to-blame-for-sa-blackout-aemo-says/8389920

[26] M. Li, M. Lenzen, F. Keck, B. McBain, O. Rey-Lescure, B. Li, and C. Jiang, "GIS-based probabilistic modeling of BEV charging load for australia," *IEEE Transactions on Smart Grid*, vol. 10, no. 4, pp. 3525–3534, July 2019.

[27] M. Ban, M. Shahidehpour, J. Yu, and Z. Li, "A cyber-physical energy management system and optimal sizing of networked nanogrids with battery swapping stations," *IEEE Trans. Sust. Energy*, 2017.

[28] M. R. Sarker, H. Pandzic, and M. A. Ortega-Vazquez, "Optimal operation and services scheduling for an electric vehicle battery swapping station," *IEEE Trans. Power Syst.*, vol. 30, no. 2, pp. 901–910, 2015.

[29] Maigha and M. L. Crow, "Electric vehicle scheduling considering co-optimized customer and system objectives," *IEEE Transactions on Sustainable Energy*, vol. 9, no. 1, pp. 410–419, Jan 2018.

[30] S. S. Amiri, S. Jadid, and H. Saboori, "Multi-objective optimum charging management of electric vehicles through battery swapping stations," *Energy*, vol. 165, pp. 549 – 562, 2018.

[31] Q. Yan, B. Zhang, and M. Kezunovic, "Optimized operational cost reduction for an ev charging station integrated with battery energy storage and pv generation," *IEEE Trans. Smart Grid*, 2018.

[32] M. Moeini-Aghtaie, A. Abbaspour, M. Fotuhi-Firuzabad, and P. Dehghanian, "Phev's centralized/decentralized charging control mechanisms: Requirements and impacts," in *The 45th North American Power Symposium (NAPS)*, 2013, pp. 1–6.

[33] Z. Liu, Q. Wu, M. Shahidehpour, C. Li, S. Huang, and W. Wei, "Transactive real-time electric vehicle charging management for commercial buildings with pv on-site generation," *IEEE Trans. Smart Grid*, 2018.

[34] A. Ravichandran, S. Sirouspour, P. Malysz, and A. Emadi, "A chance-constraints-based control strategy for microgrids with energy storage and integrated electric vehicles," *IEEE Transactions on Smart Grid*, vol. 9, no. 1, pp. 346–359, Jan 2018.

[35] H. Zhang, Z. Hu, Z. Xu, and Y. Song, "Evaluation of achievable vehicle-to-grid capacity using aggregate pev model," *IEEE Transactions on Power Systems*, vol. 32, no. 1, pp. 784–794, Jan 2017.

[36] J. Zhao, J. Wang, Z. Xu, C. Wang, C. Wan, and C. Chen, "Distribution network electric vehicle hosting capacity maximization: A chargeable region optimization model," *IEEE Transactions on Power Systems*, vol. 32, no. 5, pp. 4119–4130, Sept 2017.

[37] A. Nikoobakht, J. Aghaei, R. Khatami, E. Mahboubi-Moghaddam, and M. Parvania, "Stochastic flexible transmission operation for coordinated integration of plug-in electric vehicles and renewable energy sources," *Applied Energy*, vol. 238, pp. 225 – 238, 2019.

[38] M. Eagar. (2017) What is the difference between decentralized and distributed systems. [Online]. Available: https://medium.com/distributed-economy/what-is-the-difference-between-decentralized-and-distributed-systems-f4190a5c6462

[39] F. Marra, G. Y. Yang, C. Træholt, E. Larsen, C. N. Rasmussen, and S. You, "Demand profile study of battery electric vehicle under different charging options," in *2012 IEEE Power and Energy Society General Meeting*, July 2012, pp. 1–7.

[40] A. Shukla, K. Verma, and R. Kumar, "Multi-stage voltage dependent load modelling of fast charging electric vehicle," in *2017 6th International Conference on Computer Applications In Electrical Engineering-Recent Advances (CERA)*, Oct 2017, pp. 86–91.

[41] O. Tremblay and L. Dessaint, "Experimental validation of a battery dynamic model for EV applications," *World Electric Vehicle Journal*, vol. 3, no. 2, pp. 289–298, 2009.

[42] G. Fitzgerald, C. Nelder, and J. Newcomb. Electric vehicles as distributed energy resources. Rocky Mountain Institute. [Online]. Available: https://rmi.org/wp-content/uploads/2017/04/RMI_Electric_Vehicles_as_DERs_Final_V2.pdf

[43] D. S. Callaway and I. A. Hiskens, "Achieving controllability of electric loads," *Proceedings of the IEEE*, vol. 99, no. 1, pp. 184–199, Jan 2011.

[44] B. Wang, J. A. Camacho, G. M. Pulliam, A. H. Etemadi, and P. Dehghanian, "New reward and penalty scheme for electric distribution utilities employing load-based reliability indices," *IET Generation, Transmission Distribution*, vol. 12, no. 15, pp. 3647–3654, 2018.

[45] T. Bohn, C. Cortes, and H. Glenn, "Local automatic load control for electric vehicle smart charging systems extensible via ocpp using compact submeters," in *2017 IEEE Transportation Electrification Conference and Expo (ITEC)*, June 2017, pp. 724–731.

[46] J. Cochran, M. Miller, Zinaman *et al.*, "Flexibility in 21st century power systems," 5 2014.

[47] F. Pourahmadi, H. Heidarabadi, S. H. Hosseini, and P. Dehghanian, "Dynamic uncertainty set characterization for bulk power grid flexibility assessment," *IEEE Systems Journal*, vol. 14, no. 1, pp. 718–728, March 2020.

[48] M. Rothleder and C. Loutan, "Chapter 6 - case study–renewable integration: Flexibility requirement, potential overgeneration, and frequency response challenges," in *Renewable Energy Integration (Second Edition)*, L. E. Jones, Ed. Boston: Academic Press, 2017, pp. 69 – 81.

[49] A. Ulbig and G. Andersson, "Analyzing operational flexibility of electric power systems," *International Journal of Electrical Power & Energy Systems*, vol. 72, pp. 155 – 164, 2015, the Special Issue for 18th Power Systems Computation Conference.

[50] M. A. Saffari, M. S. Misaghian, M. Kia, A. Heidari, D. Zhang, P. Dehghanian, and J. Aghaei, "Stochastic robust optimization for smart grid considering various arbitrage opportunities," *Electric Power Systems Research*, vol. 174, pp. 1–14, September 2019.

[51] M. Moeini-Aghtaie, A. Abbaspour, M. Fotuhi-Firuzabad, and P. Dehghanian, "Optimized probabilistic PHEV demand management in the context of energy hubs," *IEEE Transactions on Power Delivery*, vol. 30, no. 2, pp. 996–1006, 2015.

[52] M. S. Misaghian, M. Saffari, M. Kia, A. Heidari, P. Dehghanian, and B. Wang, "Electric vehicles contributions to voltage improvement and loss reduction in microgrids," in *North American Power Symposium (NAPS)*, 2018, pp. 1–6.

[53] R. Wolbertus and R. Van den Hoed, "Electric vehicle fast charging needs in cities and along corridors," *World Electric Vehicle Journal*, vol. 10, no. 2, 2019.

[54] Z. Ding, Y. Lu, L. Zhang, W. Lee, and D. Chen, "A stochastic resource-planning scheme for PHEV charging station considering energy portfolio optimization and price-responsive demand," *IEEE Transactions on Industry Applications*, vol. 54, no. 6, pp. 5590–5598, Nov 2018.

[55] Z. Yi, D. Scoffield, J. Smart, A. Meintz, M. Jun, M. Mohanpurkar, and A. Medam, "A highly efficient control framework for centralized residential charging coordination of large electric vehicle populations," *International Journal of Electrical Power & Energy Systems*, vol. 117, p. 105661, 2020. [Online]. Available: http://www.sciencedirect.com/science/article/pii/S0142061519321775

[56] B. Sun, X. Tan, and D. H. K. Tsang, "Optimal charging operation of battery swapping and charging stations with qos guarantee," *IEEE Transactions on Smart Grid*, vol. 9, no. 5, pp. 4689–4701, Sep. 2018.

[57] T. Gnann, S. Funke, N. Jakobsson, P. Plötz, F. Sprei, and A. Bennehag, "Fast charging infrastructure for electric vehicles: Today's situation and future needs," *Transportation Research Part D: Transport and Environment*, vol. 62, pp. 314 – 329, 2018.

[58] Y. He, B. Venkatesh, and L. Guan, "Optimal scheduling for charging and discharging of electric vehicles," *IEEE Transactions on Smart Grid*, vol. 3, no. 3, pp. 1095–1105, Sept 2012.

[59] M. Latifi, A. Rastegarnia, A. Khalili, and S. Sanei, "Agent-based decentralized optimal charging strategy for plug-in electric vehicles," *IEEE Transactions on Industrial Electronics*, 2018.

[60] Plug-in electric vehicle handbook for public charging station hosts. U.S. Department of Energy. [Online]. Available: https://afdc.energy.gov/files/pdfs/51227.pdf

[61] "Electric vehicle conductive charging system," *IEC Standard 61851*, 2014.

[62] I. Stoychev and J. Oehm, "Advanced electronic circuit breaker techniques for the use in electric vehicle charging stations," in *2016 IEEE International Conference on Electronics, Circuits and Systems (ICECS)*, Dec 2016, pp. 660–663.

[63] P. Dehghanian, Y. Guan, and M. Kezunovic, "Real-time life-cycle assessment of high-voltage circuit breakers for maintenance using online condition monitoring data," *IEEE Transactions on Industry Applications*, vol. 55, no. 2, pp. 1135–1146, March 2019.

[64] "IEEE guide for performing arc-flash hazard calculations," *IEEE Std 1584-2018 (Revision of IEEE Std 1584-2002)*, pp. 1–134, Nov 2018.

[65] L. B. Gordon, L. Cartelli, and N. Graham, "A complete electrical shock hazard classification system and its application," *IEEE Transactions on Industry Applications*, vol. 54, no. 6, pp. 6554–6565, Nov 2018.

[66] Electrical safety program. University of Pennsylvania. [Online]. Available: https://ehrs.upenn.edu/health-safety/general-safety/electrical-safety

[67] D. T. Roberts, "Applying risk assessment at the worker level: Applications to electrical safety," *IEEE Industry Applications Magazine*, vol. 25, no. 1, pp. 18–24, Jan 2019.

[68] P. Dehghanian, B. Zhang, T. Dokic, and M. Kezunovic, "Predictive risk analytics for weather-resilient operation of electric power systems," *IEEE Trans. on Sust. Energy*, vol. 10, no. 1, pp. 3–15, Jan 2019.

[69] L.-D. Radu, "Qualitative, semi-quantitative and, quantitative methods for risk assessment: Case of the financial audit," *Analele Stiintifice ale Universitatii "Alexandru Ioan Cuza" din Iasi - Stiinte Economice*, vol. 56, pp. 643–657, 2009. [Online]. Available: https://EconPapers.repec.org/RePEc:aic:journl:y:2009:v:56:p:643-657

[70] F. Freschi, M. Mitolo, and R. Tommasini, "Electrical safety of plug-in electric vehicles: Shielding the public from shock," *IEEE Industry Applications Magazine*, vol. 24, no. 3, pp. 58–63, May 2018.

[71] W. H. Kersting, "Radial distribution test feeders," in *2001 IEEE Power Engineering Society Winter Meeting. Conference Proceedings (Cat. No.01CH37194)*, vol. 2, Jan 2001, pp. 908–912 vol.2.

[72] Impact of IEEE 1547 standard on smart inverters. IEEE PES Industry Technical Support Task Force.

[73] B. Wang, P. Dehghanian, S. Wang, and M. Mitolo, "Electrical safety considerations in large-scale electric vehicle charging stations," *IEEE Transactions on Industry Applications*, vol. 55, no. 6, pp. 6603–6612, 2019.

[74] M. C. Falvo, D. Sbordone, I. S. Bayram, and M. Devetsikiotis, "Ev charging stations and modes: International standards," in *2014 International Symposium on Power Electronics, Electrical Drives, Automation and Motion*, June 2014, pp. 1134–1139.

[75] T. Branch, "Using CSA Z463 standard to build a foundation for electrical risk management (fferm)," in *2018 IEEE Electrical Power and Energy Conference (EPEC)*, Oct 2018, pp. 1–6.

[76] D. E. Olivares, J. D. Lara, C. A. Canizares, and M. Kazerani, "Stochastic-predictive energy management system for isolated microgrids," *IEEE Trans. Smart Grid*, vol. 6, no. 6, pp. 2681–2693, 2015.

[77] A. Mesbah, "Stochastic model predictive control: An overview and perspectives for future research," *IEEE Control Systems*, vol. 36, no. 6, pp. 30–44, Dec 2016.

[78] S. P. Boyd. Chance constrained optimization. [Online]. Available: http://ee364a.stanford.edu/lectures/chance_constr.pdf

[79] J. Duchi. (2018) Optimization with uncertain data. [Online]. Available: http://stanford.edu/class/ee364b/lectures/robust_notes.pdf

[80] S. Boyd, N. Parikh, E. Chu, B. Peleato, and J. Eckstein, "Distributed optimization and statistical learning via the alternating direction method of multipliers," *Foundations and Trends in Machine Learning*, vol. 3, no. 1, pp. 1–122, 2011.

[81] L. Xie and M. D. Ilic, "Model predictive economic/environmental dispatch of power systems with intermittent resources," in *2009 IEEE Power Energy Society General Meeting*, July 2009, pp. 1–6.

[82] ERCOT. [Online]. Available: http://www.ercot.com/gridinfo

[83] National Household Travel Survey. [Online]. Available: http://nhts.ornl.gov/download.shtml

[84] X. Fang, S. Jung, and H. Zhang. Smart microgrid with electric vehicles. [Online]. Available: https://github.com/seoho91/EV_Grid

[85] L. Cheng, Y. Chang, J. Lin, and C. Singh, "Power system reliability assessment with electric vehicle integration using battery exchange mode," *IEEE Transactions on Sustainable Energy*, vol. 4, no. 4, pp. 1034–1042, Oct 2013.

[86] J. Mattingley and S. Boyd, "CVXGEN: A code generator for embedded convex optimization," *Optimization and Engineering*, vol. 12, no. 1, pp. 1–27, 2012.

[87] R. D. Zimmerman, C. E. Murillo-Sanchez, and R. J. Thomas, "Matpower: Steady-state operations, planning, and analysis tools for power systems research and education," *IEEE Transactions on Power Systems*, vol. 26, no. 1, pp. 12–19, Feb 2011.

[88] B. Wang, P. Dehghanian, and D. Zhao, "Chance-constrained energy management system for power grids with high proliferation of renewables and electric vehicles," *IEEE Transactions on Smart Grid*, vol. 11, no. 3, pp. 2324–2336, 2020.

[89] Fastned. [Online]. Available: https://www.altenergymag.com/article/2018/07/why-fast-charging-stations-are-good-for-the-grid/29029

[90] U. Tamrakar, F. B. dos Reis, A. Luna, D. Shrestha, R. Fourney, and R. Tonkoski, "Virtual inertia emulation using commercial off-the-shelf inverters," in *2018 IEEE Energy Conversion Congress and Exposition (ECCE)*, Sep. 2018, pp. 1111–1116.

[91] A. Giacomoni, K. Patel, and C. M. Velasco. Price formation education 3: Reserves and co-optimization. PJM Interconnection. [Online]. Available: https://www.pjm.com/-/media/committees-groups/stakeholder-meetings/price-formation/20180117-am/20180117-price-formation-education-3-updated.ashx

[92] T. Ding, Z. Wu, J. Lv, Z. Bie, and X. Zhang, "Robust co-optimization to energy and ancillary service joint dispatch considering wind power uncertainties in real-time electricity markets," *IEEE Transactions on Sustainable Energy*, vol. 7, no. 4, pp. 1547–1557, Oct 2016.

[93] Future ancillary services in ERCOT. [Online]. Available: https://www.ferc.gov/CalendarFiles/20140421084800-ERCOT-ConceptPaper.pdf

[94] R. H. Byrne, R. J. Concepcion, and C. A. Silva-Monroy, "Estimating potential revenue from electrical energy storage in pjm," in *2016 IEEE Power and Energy Society General Meeting (PESGM)*, July 2016, pp. 1–5.

[95] B. Wang, D. Zhao, P. Dehghanian, Y. Tian, and T. Hong, "Aggregated electric vehicle load modeling in large-scale electric power systems," *IEEE Transactions on Industry Applications*, pp. 1–14, 2020.

[96] P. Jamborsalamati, M. Hossain, S. Taghizadeh, A. Sadu, G. Konstantinou, M. Manbachi, and P. Dehghanian, "Enhancing power grid resilience through an IEC61850-based ev-assisted load restoration," *IEEE Transactions on Industrial Informatics*, vol. 16, no. 3, pp. 1799–1810, March 2020.

[97] R. Yao and K. Sun, "Towards simulation and risk assessment of weather-related outages," *IEEE Transactions on Smart Grid*, pp. 1–1, 2018.

[98] P. Dehghanian, S. Aslan, and P. Dehghanian, "Maintaining electric system safety through an enhanced network resilience," *IEEE Transactions on Industry Applications*, vol. 54, no. 5, pp. 4927–4937, Sep. 2018.

[99] National solar radiation database. National Renewable Energy Laboratory. [Online]. Available: https://nsrdb.nrel.gov/nsrdb-viewer

[100] Real-time hourly lmps. PJM market. [Online]. Available: https://dataminer2.pjm.com/feed/rt_hrl_lmps/definition

[101] M. Muratori. (2017) Impact of uncoordinated plug-in electric vehicle charging on residential power demand - supplementary data. National Renewable Energy Laboratory. [Online]. Available: https://dx.doi.org/10.7799/1363870

[102] B. Wang, P. Dehghanian, D. Hu, S. Wang, and F. Wang, "Adaptive operation strategies for electric vehicle charging stations," in *2019 IEEE Industry Applications Society Annual Meeting*, Sep. 2019, pp. 1–7.

[103] J. Undrill. (2018) Primary frequency response and control of power system frequency. Lawrence Berkeley National Laboratory. [Online]. Available: https://www.ferc.gov/industries/electric/indus-act/reliability/frequency-control-requirements/primary-response.pdf

[104] M. Child, C. Kemfert, D. Bogdanov, and C. Breyer, "Flexible electricity generation, grid exchange and storage for the transition to a 100% renewable energy system in europe," *Renewable Energy*, vol. 139, pp. 80 – 101, 2019. [Online]. Available: http://www.sciencedirect.com/science/article/pii/S0960148119302319

[105] P. Zhou, R. Jin, and L. Fan, "Reliability and economic evaluation of power system with renewables: A review," *Renewable and Sustainable Energy Reviews*, vol. 58, pp. 537 – 547, 2016. [Online]. Available: http://www.sciencedirect.com/science/article/pii/S136403211501727X

[106] T. Adefarati, R. Bansal, and J. J. Justo, "Reliability and economic evaluation of a microgrid power system," *Energy Procedia*, vol. 142, pp. 43 – 48, 2017, proceedings of the 9th International Conference on Applied Energy. [Online]. Available: http://www.sciencedirect.com/science/article/pii/S1876610217357351